Radio observations of the host galaxies of short Gamma-Ray Bursts

DISSERTATION

zur Erlangung des akademischen Grades

doctor rerum naturalium (Dr. rer. nat.)

vorgelegt dem Rat der Physikalisch-Astronomischen Fakultät

der Friedrich-Schiller-Universität Jena

von

M. Sc. Ana Maria Nicuesa Guelbenzu

Gutachter

1. Prof. Dr. Katharina Schreyer, Friedrich-Schiller-Universität Jena, Germany
2. Prof. Dr. Ulrich Heber, Friedrich-Alexander-Universität Erlangen-Nürnberg, Germany
3. Prof. Dr. Giampaolo Piotto, University of Padua, Italy

Tag der Disputation: 13.03.2020

a mi madre Magdalena Guelbenzu Bandrés

.

Contents

1 Introduction **1**
1.1 GRBs, their afterglows and progenitors . . . 1
1.1.1 The bursts and their bimodal distribution . . . 1
1.1.2 The afterglows . . . 3
1.1.3 GRB progenitor models . . . 6
1.1.4 Short GRBs . . . 7
1.2 Long-GRB host galaxies . . . 9
1.2.1 Photometric studies . . . 9
1.2.2 Spectroscopic studies . . . 10
1.2.2.1 Star formation rates . . . 11
1.2.2.2 GRB environments, ISM metallicities . . . 11
1.2.3 Legacy samples . . . 14
1.2.4 Radio observations . . . 15
1.3 Short-GRB host galaxies . . . 18
1.3.1 Host galaxies as tracers of the nature of the short-GRB progenitors . . . 18
1.3.2 Identifying the host galaxies of short GRBs . . . 20
1.3.3 Previous radio studies of short-GRB host galaxies . . . 22
1.4 Immediative objective of this work . . . 24

2 Target selection, observations, and data reduction **25**
2.1 ATCA target selection . . . 25
2.1.1 Building the sample . . . 25
2.1.2 Adding more targets . . . 26
2.1.3 The final sample . . . 27
2.2 Observations and data reduction . . . 32
2.3 Radio-derived star formation rates . . . 35

3 Results I: Targets with radio detection **37**
3.1 The morphologically disturbed host of GRB 050709 . . . 37
3.1.1 The burst and its afterglow . . . 38
3.1.2 The host galaxy . . . 38
3.1.3 Was the GRB progenitor a collapsing massive star? . . . 41
3.1.4 *ATCA* radio observations of the host galaxy . . . 42
3.1.5 What is the nature of the radio source? . . . 43
3.1.6 Summary of Section 3.1 . . . 45
3.2 The starburst host galaxy of GRB 071227 . . . 46
3.2.1 Archival observations of the GRB and its host galaxy . . . 46
3.2.2 Radio-continuum detection of the GRB host galaxy . . . 48
3.2.3 Could GRB 071227 be a member of the long-GRB population? . . . 49

3.2.4 Was GRB 071227 due to a young NS-NS progenitor system? 51
3.2.5 Summary of Section 3.2 52
3.3 Identifying the host galaxy of GRB 100628A 52
3.3.1 Archival observations of the GRB and its host galaxy 52
3.3.2 VLT spectroscopy of the GRB field 54
3.3.3 Objects inside the *Swift*/XRT error circle 55
3.3.4 Star formation rate based on optical spectroscopy 57
3.3.5 *ATCA* radio observations 58
3.3.6 The radio source inside the XRT error circle 59
3.3.7 A second host-galaxy candidate 60
3.3.8 Summary of Section 3.3 62

4 Results II: Targets without radio detection 63
4.1 GRB 050724: a bulge-dominated host with a faint disk component 64
4.2 GRB 061006: an edge-on spiral host galaxy 65
4.3 GRB 061201: a very faint host galaxy 67
4.4 GRB 070729: three host-galaxy candidates 69
4.5 GRB 070809: two suspected host-galaxy candidates 72
4.6 GRB 080123: a relatively bright host-galaxy candidate 73
4.7 GRB 080905A: a cosmologically nearby, face-on spiral host galaxy 76
4.8 GRB 130515A: a galaxy close to the XRT error circle 78
4.9 GRB 150424A: a suspected bright and a suspected faint host 80
4.10 Summary of Chapter 4 83

5 Discussion 84
5.1 Data summary 84
5.2 Radio-derived star formation rates 85
5.3 Radio SFRs in long and short-GRB host galaxies 89
5.4 Radio vs. optical SFRs in long and short-GRB hosts 90
5.5 The most actively star-forming short-GRB hosts 93
5.6 Future radio observations 94

6 Summary and conclusions 97

7 Appendix 99
7.1 Supplementary tables and figures 99
7.2 The Australia Telescope Compact Array 105
7.3 Data reduction: *ATCA* radio data 106
7.3.1 General 106
7.3.2 Bandpass, flux and phase calibrations 107
7.3.3 Image reconstruction 108
7.4 Data reduction: optical photometry 109
7.5 Data reduction: optical spectroscopy 111

.

Zusammenfassung

Phänomenologisch werden Gamma-Ray-Bursts (GRBs) in lange und kurze unterteilt, mit der Grenzlinie bei 2 Sekunden. Während eine physikalische Verbindung zwischen langen GRBs und Ic-Supernovae seitens Beobachtung und Theorie gut bestätigt ist, ist die Situation bei den kurzen Bursts seitens der Beobachtung weit weniger klar. Theoretische Arbeiten lassen stark vermuten, dass die kurzen Bursts Folge der Verschmelzung von Neutronenstern (NS)-NS und NS-Black hole -Doppelsternen sind. Aktuelle Beobachtungsdaten sind nicht im Konflikt mit dieser Ansicht, aber ein direkter Beobachtungsnachweis dieses theoretischen Konzepts ist bisher nicht gelungen.

Einige Modellrechnungen zur Sternentwicklung sagen voraus, dass es eine Untergruppe von jungen NS-NS-Doppelsternen geben sollte, die bereits innerhalb von Millionen Jahren nach ihrer Entstehung verschmelzen. Sie unterscheiden sich dergestalt von der Mehrzahl dieser Objekte, die typischerweise erst nach Milliarden von Jahren verschmelzen. Wenn einige kurze GRBs ihren Ursprung in einer solchen Untergruppe von jungen, verschmelzenden NS-NS-Doppelsternen haben, dann sollten sich diese zum Zeitpunkt ihrer Explosion noch in oder nahe von Sternentstehungsgebieten befinden. Möglicherweise könnten sich gar deren komplette Muttergalaxien in einer intensiven Sternbildungsphase befinden.

Ich berichte hier über die Ergebnisse von Radio-Kontinuum-Beobachtungen mit dem Australia Telescope Compact Array (ATCA) im 5.5 und 9.0 GHz-Band mit dem Ziel, in 12 Muttergalaxien von kurzen Bursts mit Rotverschiebungen zwischen z= 0.1 und 0.5 nach optisch verborgener Sternentstehung zu suchen. Dies ist die bisher größte Stichprobe von GRB-Muttergalaxien von kurzen Bursts, welche dergestalt systematisch im Radioband studiert wird. Sie stellt ∼1/3 der gegenwärtig bekannten Gruppe solcher Muttergalaxien dar. Sieben der 12 GRBs hatten einen detektierten optischen Afterglow, d.h., sie konnten mit Subbogensekunden-Genauigkeit lokalisiert werden. Fünf GRBs haben nur eine Lokalisierung mit Bogensekunden-Genauigkeit, basierend auf der Röntgen-Detektion deren Afterglows. Ihnen können jedoch gut-definierte Muttergalaxie-Kandidaten zugeordnet werden.

Meine Radiobeobachtungen gehen sehr tief, in der Regel erreichen sie ein $1\sigma_{\rm rms}$ von 5 bis 7 μJy beam^{-1}. Ich detektiere Radioemission von drei der 12 untersuchten Galaxien. Im Falle der neun Nichtdetektionen kann ich die Sternbildungsrate (star formation rate; SFR) zu typischerweise kleiner als 1-5 $M_\odot$ yr^{-1} für jene Galaxien bei kleineren Rotverschiebungen z und zu kleiner

als 10-30 $M_\odot$ yr^{-1} für jene bei größeren Rotverschiebungen einschränken. Die drei detektierten Galaxien sind (i) die edge-on (linsenförmige) Muttergalaxie von GRB 071227 bei z=0.381 mit einer aus den Radiodaten abgeleiteten SFR von $\sim$ 30 $M_\odot$ yr^{-1}, (ii) die morphologisch gestörte, potentielle Muttergalaxie von GRB 100628A (z=0.102), welche eine Radioquelle in einem ihrer Gezeitenarme zeigt, und (iii) die unregelmäßig geformte, wechselwirkendende Muttergalaxie von GRB 050709 bei z=0.1606, welche eine ausgedehnte Radioemission in ihrem östlichen Teil aufweist, dort, wo der optische Afterglow lokalisiert war. Obwohl die drei Radio-Detektionen sehr vielversprechend sind, liefert letztlich keiner dieser Fälle einen schlüssigen Beweis für eine physikalische Verbindung des entsprechenden kurzen Bursts, sprich des entsprechenden verschmelzenden NS-NS-Doppelsterns, zu einer momentan andauernden Phase intensiver Sternbildung in der jeweiligen GRB-Muttergalaxie.

Abstract

Phenomenologically, Gamma-Ray Bursts (GRBs) divide into long and short, with the borderline at 2 seconds. While a physical link between long GRBs and type Ic supernovae is observationally and theoretically well established, for short bursts the observational situation is less clear. Theoretical work strongly suggests that short bursts are produced by merging neutron star (NS)-NS and NS-black hole binaries. Current observational data are not in conflict with this view but a direct observational proof of this theoretical concept has not yet been done.

Some stellar population synthesis models suggest that a subpopulation of young NS-NS binaries should exist which merges already within millions of years after their formation. This is different from the majority of these objects which typically merge after billions of years. If some short GRBs have their origin in a subpopulation of young merging NS-NS binaries, then their progenitors should still be located inside or close to their stellar birthplaces when they explode. Possibly, even their entire host galaxies could still be in the process of an intense star-formation episode when these NS-NS binaries merge and give rise to a short GRB.

Here I report about the results of radio-continuum observations in the 5.5 and 9.0 GHz band with the Australian Telescope Compact Array (*ATCA*) with the aim to search for optically hidden star-formation in a sample of 12 short-GRB host galaxies at redshifts between z=0.1 and 0.5. This is the so far largest sample of short-GRB hosts systematically studied in the radio band. It represents ∼1/3 of the presently known sample of short-GRB hosts. Seven of these short GRBs have a detected optical afterglow, i.e., a sub-arcsec localization accuracy. Five GRBs have only arcsec-sized X-ray afterglow error circles, but they have well-defined host-galaxy candidates.

My radio observations went very deep, typically reaching a $1\sigma_{\rm rms}$ of 5 to 7 μJy beam^{-1}. I detect radio emission from three of the 12 targeted galaxies. In the case of the nine non-detections the constraints I can set on the star formation rate (SFR) are deep, typically smaller than 1–5 $M_\odot$ yr^{-1} for the lower redshifts and 10–30 $M_\odot$ yr^{-1} for the higher redshifts. The three detected galaxies are (i) the edge-on (lenticular) host of GRB 071227 at a redshift of z=0.381 which revealed a radio-derived SFR of $\sim$ 30 $M_\odot$ yr^{-1}, (ii) the morphologically disturbed host-galaxy candidate of GRB 100628A (z=0.102) which shows a radio source in its tidal arm, and (iii) the irregularly shaped, interacting host of GRB 050709 at z=0.1606 which shows extended radio emission in its eastern part where the optical afterglow was placed. Although the three radio detections are very promising, finally none of these cases provides conclusive evidence for a physical association of the corresponding short-GRB progenitor to a recent intense star-formation episode.

.

Chapter 1

Introduction

1.1 GRBs, their afterglows and progenitors

1.1.1 The bursts and their bimodal distribution

Gamma-Ray Bursts (GRBs) are unpredictable transient events in the gamma-ray sky consisting of powerful flashes of gamma radiation, lasting from a few milliseconds to several thousands of seconds. The first event was recorded by the *Vela satellites 4A* and *4B* on the 2nd July 1967, fifty years ago (Klebesadel et al. 1973). There was a substantial observational and theoretical effort in the 1970s and 1980s to understand this phenomenon (for a summary see, e.g., Ruderman 1975; Nemiroff 1994), with very small success. In the early 1990s the Compton Gamma-Ray Observatory/Burst And Transient Source Experiment (CGRO/BATSE; Fishman et al. 1994) revealed that the bursts occur isotropically across the sky at a rate of about 1 per day.

The gamma radiation is highly variable and, therefore, the temporal profile of the bursts is a distinctive fingerprint. They show a wide diversity of temporal profile patterns, ranging from multiple peaks, single-spike events, a fast rise and exponential decay behavior (so-called FREDs), precursor events occurring hundreds of seconds before the main flash, or smooth emission lasting tens of seconds after the main event (for a historical review see, e.g., Klose 2000; van Paradijs et al. 2000; Hurley et al. 2011).

After several pioneering discoveries by the Italian-Dutch BeppoSAX satellite (e.g., Piro & BeppoSAX Team 1997) and the HETE II mission (e.g., Ricker et al. 2003), the present days are characterized by routine GRB detections by NASA's *Swift* satellite (Gehrels et al. 2004) and the *Fermi* gamma-ray observatory (e.g., Meegan et al. 2009), occasional GRB discoveries by the European satellite *Integral*, and by the 3rd InterPlanetary Network (IPN) consisting of satellites in orbit around Earth, Mars, and Sun (e.g., Hurley et al. 2011). From the point of

view of localization accuracy and optical counterpart detection, for more than 10 years the most productive GRB satellite is *Swift* (launched on November 20, 2004; Gehrels et al. 2004).

Swift is operated by a collaboration of various research facilities in Italy, UK, and the United States. Since 2005 it has been the work-horse to achieve many scientific breakthroughs. It is the first satellite which can start observing GRB afterglows within a minute after the GRB trigger. For this reason the satellite carries three different telescopes, the Burst Alert Telescope (BAT; Barthelmy et al. 2005a) which is a wide-field telescope operating in the 15–150 keV band, the X-ray Telescope (XRT; Burrows et al. 2005), operating in the soft X-ray regime between 0.2 and 10 keV, and the Ultraviolet/Optical Telescope (UVOT; Roming et al. 2005) for observations in the ultra-violet and visible domain (150–650 nm).

Swift detects about 100 GRBs per year with BAT. It localizes them with typically 3 arcmin accuracy (error circle radius) and in more than 90% of the cases it detects the X-ray afterglow within seconds or minutes after the onset of a burst (typically 3 to 5 arcsec error radius). This is supplemented by optical observations with UVOT. All this information is immediately send to the ground station and distributed world-wide.[1]

BATSE/CGRO revealed that GRBs show a bimodality in their duration distribution, suggesting two different populations of burst sources. Based on these data, the general phenomenological definition is that long and short bursts separate at T_{90} = 2 s, with the peak of the short-burst population at T_{90} ~0.5 s and the peak of long-burst population at ~30 s (Kouveliotou et al. 1993). Thereby, T_{90} stands for the interval (burst duration) between the observed times where the measured gamma-ray fluence has reached 5% and 95% of its total fluence (an illustrated example is given in Narayana Bhat et al. 2016).

The potential existence of an intermediate class of GRBs has been discussed by several authors (e.g., Horváth et al. 2008; Řípa et al. 2012; Kulkarni & Desai 2017), though phenomenologically its existence is less obvious (e.g., de Ugarte Postigo et al. 2011).

Since there is a substantial overlap between the long- and short-burst population around T_{90} = 2 s (Fig. 1.1), a division into long and short can only be a first guess about the true origin of a burst. Besides, the shape of the bimodal distribution is energy-sensitive and consequently detector-dependent (Sakamoto et al. 2011). Nevertheless, the classical long-short division according to the BATSE scheme is still the most appropriate procedure used in the literature. Its basic concept has been exported to all following GRB missions since it allows for a rapid burst classification. Statistically it has been found that a bona-fide short burst shows no arrival time difference between high and low-energy photons (the so called spectral lag), while bona-fide

[1] `http://gcn.gsfc.nasa.gov/gcn3_archive.html` and `http://www.mpe.mpg.de/~jcg/grbgen.html`

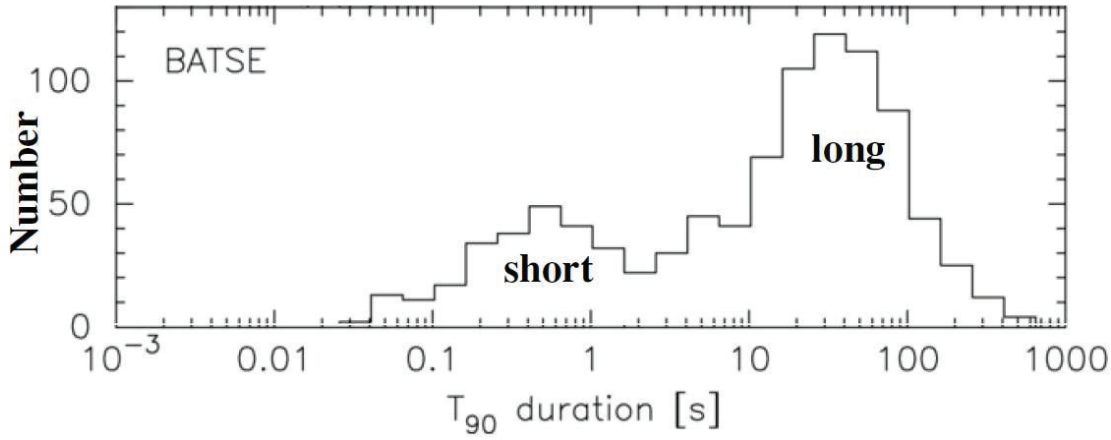

Fig. 1.1: The bimodal duration distribution of GRBs. The separation between short and long bursts is set at 2 s. Shown here are the data obtained by the *BATSE* experiment on the *Compton Gamma-Ray Observatory* between 1991 and 2000. Adapted from Sakamoto et al. (2011).

long bursts do (the high-energy emission peaks earlier or later than the low-energy emission; e.g., Bernardini et al. 2015). Understanding the physical reason for this phenomenon is still a matter of debate (e.g., Uhm & Zhang 2016).

1.1.2 The afterglows

The burst of gamma radiation is usually called the *prompt phase*, which is followed by a much less energetic but long-lasting *afterglow*. The afterglow phase can be observed from the X-ray band (Costa et al. 1997), via the optical/NIR bands (van Paradijs et al. 1997) up to the radio regime (Frail et al. 1997). The afterglow usually starts minutes after the prompt phase and can be detectable up to several days after the burst (in few cases even months [X-rays; e.g., GRB 060729, Grupe et al. 2007] or years [radio; e.g., GRB 030329, van der Horst et al. 2008]). Its spectral energy distribution (flux density vs. frequency) and temporal evolution (flux density vs. time) is described by a power law, $F_\nu(t) \sim t^{-\alpha}\nu^{-\beta}$. The constants α and β depend on the evolutionary phase of the afterglow (time after the burst) and on the spectral window. In the optical bands some minutes or hours after the burst α usually lies in range between about 0.5 and 2.5 and β between about 0.5 and 1 (see, e.g., Kann et al. 2006; Zeh et al. 2006).

The detection of an optical afterglow allows for a sub-arcsec precise GRB localization, a redshift measurement either directly via the afterglow light or via the suspected GRB host galaxy. In addition, afterglow light curves give insight into the circumburst density profile (e.g., Schulze et al. 2011), allow for a measurement of the afterglow physical parameters (e.g., Varela et al. 2016), and even reveal information about the opening angles of the explosion (e.g., Sari et al.

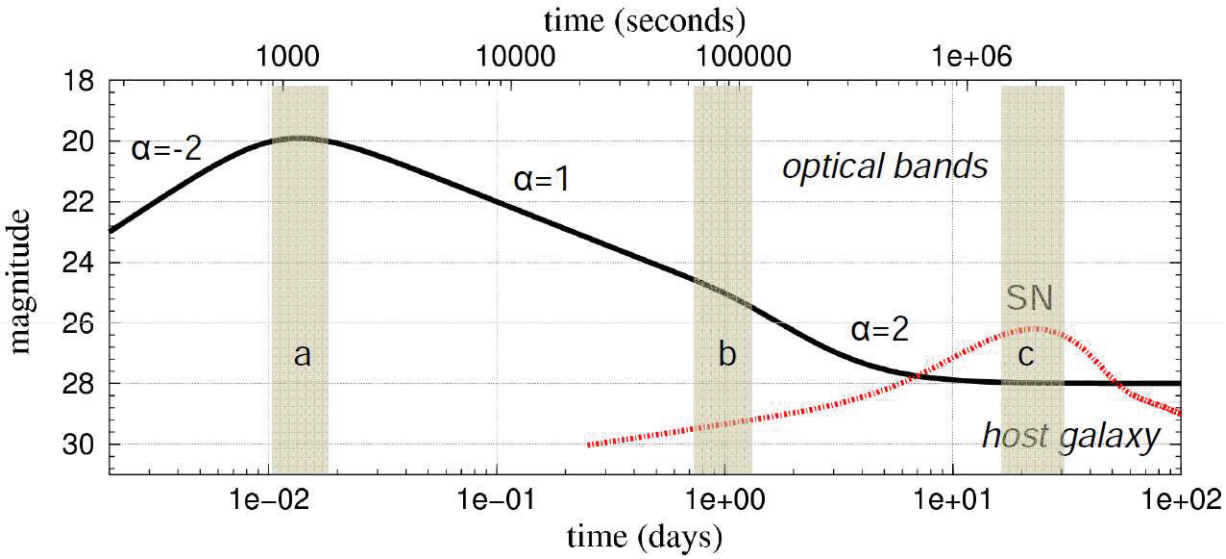

Fig. 1.2: Idealized light curve of an optical transient following a gamma-ray burst (long and short). After reaching maximum light (a), which is a measure of the initial Lorentz factor Γ of the outflow, the proper afterglow phase stars (Γ decreases). It might show evidence for a break due to a jetted explosion (b) and, for long GRBs, a rising supernova component (c). All evolutionary phases before the rise of the SN component (for long GRBs) can be described by a power law (flux density $F_\nu \sim t^{-\alpha}$, typical values for α are given).

1999; Zeh et al. 2006; Nicuesa Guelbenzu et al. 2012).

Rhoads (1999) predicted that if GRBs are due to a collimated explosion, then this should manifest as a break in the afterglow light curve, i.e., a steepening of its decay after some time. This was first observed in the afterglow of GRB 990123 (Castro-Tirado et al. 1999b; redshift z=1.609). Meanwhile it is known that probably all afterglow light curves show such a break in the optical/NIR bands and in X-rays. The break typically happens about one day after the burst when the power-law decay steepens from about $F_\nu(t) \sim t^{-1}$ to about $F_\nu(t) \sim t^{-2}$ (for observational data see, e.g., Zeh et al. 2006; Lu et al. 2012).

GRBs have been detected from z=0.0085 (GRB 980425: Galama et al. 1998; Tinney et al. 1998) to z=9.4 (GRB 090429B Cucchiara et al. 2011), showing that GRBs are the most energetic electromagnetic events in the universe with isotropic equivalent energies typically in the 10^{51-54} erg range. For a comprehensive review about the phenomenology of afterglow light curves in the optical bands see Kann et al. (2010, 2011) (Fig. 1.2).

According to the most accepted models, a GRB is released within a relativistic jet by the collision of outwards moving ultra-relativistic shells, while an afterglow is produced once the highly relativistic matter released by the explosion (Lorentz factor in the order of 10 to 100, or higher; Lithwick & Sari 2001) collides with the interstellar medium surrounding the exploding star, starts to decelerate and emits synchrotron radiation. This is the so-called fireball model

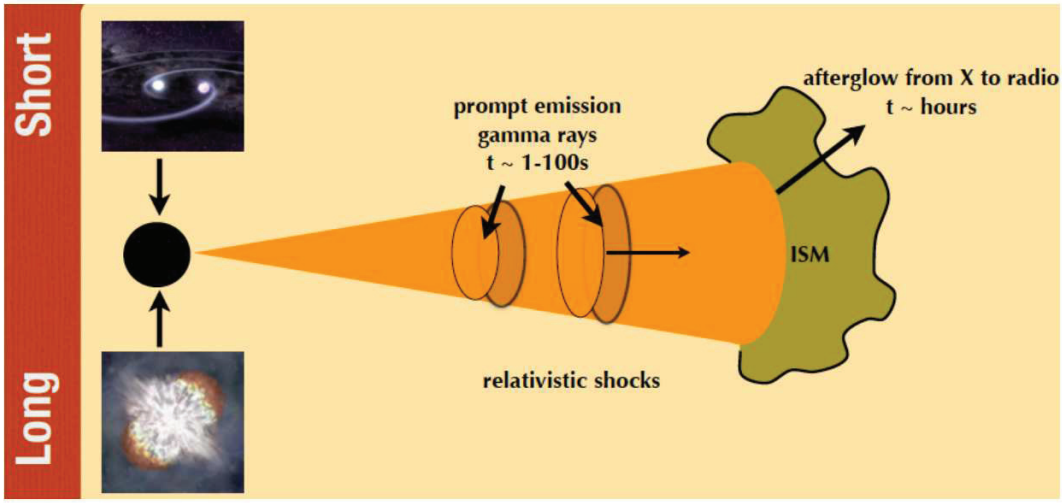

Fig. 1.3: Cartoon of the fireball model (see Piran 2004; Zhang & Mészáros 2004; Mészáros 2006). For both kinds of progenitors (long: collapsing massive stars; short: merging compact stars), a temporary accretion disk around a stellar mass black hole (or magnetar) is formed which channels a relativistic outflow with a very high Lorentz factor. The collision of individual shells inside this outflow produces an observable GRB, while a long-lasting afterglow is formed once the outflow is decelerated in the circumburster medium. In the latter case it emits synchrotron radiation from the X-ray to the radio band. Adapted from Vergani & Chassande-Mottin (2015)

(Fig. 1.3; Piran 2004; Zhang & Mészáros 2004; Mészáros 2006).

Worldwide, a substantial observational effort is devoted to follow-up observations of GRBs, their low-energy afterglows (e.g., Sánchez-Ramírez et al. 2016) as well as their host galaxies (e.g., Nicuesa Guelbenzu et al. 2014; Thöne et al. 2014). For the former, an increasing number of robotic telescopes of the 0.5-m class has been installed (e.g., the BOOTES[2] telescopes; Castro-Tirado et al. 1999a; Jelínek et al. 2016, `http://bootes.iaa.es/`). Nowadays, the world-largest optical telescopes are intensively used for photometric as well as spectroscopic studies to perform all kinds of GRB afterglow observations (e.g., de Ugarte Postigo et al. 2014) as well as GRB-host galaxy studies (e.g., Greiner et al. 2016; Perley et al. 2016a). Finally, dedicated multi-imager instruments like *GROND*[3] (Greiner et al. 2008) mounted at the Max Planck Gesellschaft (MPG) 2.2 m telescope on La Silla Observatory, Chile, and operated by our team at MPE[4] Garching and the Thüringer Landessternwarte Tautenburg (TLS), or the future OCTOCAM (Gorosabel & de Ugarte Postigo 2010; de Ugarte Postigo 2015) at the Gemini-South telescope, complete the diverse variety of instruments that are used to follow GRBs.

[2] `Burst Observer and Optical Transient Exploring System`
[3] `Gamma-Ray Burst Optical/Near-Infrared Detector`
[4] `Max Planck Institute for Extraterrestrial Physics`

In the last years, the electronic Gamma-ray Burst Coordinates Network (GCN) circular system has developed into a very powerful tool for any kind of GRB follow-up observations, rapid data delivery, and coordinated observing campaigns with more than 21 000 GCN circulars by June 2017 (Barthelmy et al. 1995; Barthelmy 2008). Besides, in order to understand better the nature of GRB progenitors and to learn more about the physical conditions required to produce them, studies of the host galaxies of GRBs become more and more important.

1.1.3 GRB progenitor models

According to the current picture, **long GRBs** originate from the collapse of massive stars into stellar-mass black holes (MacFadyen & Woosley 1999) or strongly magnetized neutron stars (e.g., Usov 1992; Mazzali et al. 2006; Greiner et al. 2015). Within the collapsar scenario, a highly magnetized, temporary accretion disk is formed around a freshly-formed black hole in the center of the collapsing star (Woosley 1993). This accretion disk is rotating at very high speed and feeds the black hole for seconds, minutes or even hours, providing the energy for the formation of an ultra-relativistic jet (plus a counterjet) along its symmetry axis (Woosley & Bloom 2006). These jets are then propagating outwards through the star. If its outer shells are very massive, the jets will die out before reaching the stellar surface. Therefore, stars with a completely removed outer H and He envelope (Wolf Rayet stars) are the prime candidates as long-GRB progenitors.

The standard model about the origin of **short GRBs** is the neutron star (NS) merger model which was first developed in the 1980s (e.g., Paczynski 1986). In its present context the model relies on the idea that a NS-NS or a NS-black hole binary merges due to orbital decay caused by the emission of gravitational waves. Although the progenitors for the central engine in case of long and short GRBs are different, the GRBs are produced following the same physical processes as described by the fireball model (Fig. 1.3; Piran 2004; Zhang & Mészáros 2004; Mészáros 2006).

The physical association of long bursts with the collapse of massive stars has been well established by observations during the last two decades, starting with GRB 980425/SN 1998bw (Galama et al. 1998; Kulkarni et al. 1998). Supernova bumps have been seen in about 50 long-GRB afterglows (Fig. 1.4; e.g., Zeh et al. 2004; Ferrero et al. 2006; Fruchter et al. 2006; Woosley & Bloom 2006; Kann et al. 2016; Cano et al. 2017), about 50% of these have a spectroscopic confirmation (e.g., Hjorth et al. 2003; Kawabata et al. 2003; Matheson et al. 2003; Stanek et al. 2003; Pian et al. 2006; Woosley & Bloom 2006; Greiner et al. 2015; Klose et al. 2017). However,

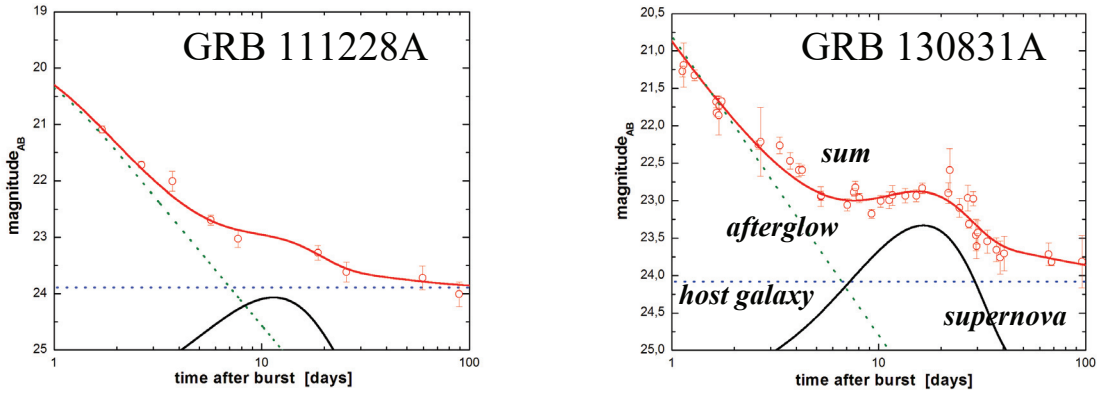

Fig. 1.4: Afterglows and supernova bumps following two GRBs that were in detail observed by our team with *GROND* (Klose et al. 2017). In red is shown the light curve of the optical transient, which is composed of afterglow light (green), supernova light (black) and flux from the underlying host galaxy (blue). Drawings by S. Schmidl, Tautenburg, private comm.

the observational situation with short bursts is less clear.

1.1.4 Short GRBs

Until 2005 no optical/NIR/X-ray/radio afterglow of a short burst had ever been detected, while many important discoveries had already been made for the long-burst sample (cosmological redshifts, supernova light, collimated explosions, circumburst wind profiles). The first well-localized short burst (GRB 050509B; Gehrels et al. 2005) was seen close in projection to a massive early-type galaxy at z=0.225 (Hjorth et al. 2005a; Bloom et al. 2006), supporting the model that compact stellar mergers are the progenitors of short-duration GRBs. However, the observational progress in the case of short GRBs has been rather modest compared to the long-burst population (for recent reviews, see Berger 2014; D'Avanzo 2015).

There are two main reasons for this situation. Firstly, there is a substantially smaller detection *and* precise localization rate of short bursts compared to long bursts: *Swift* detects and localizes at the arcsec scale about 100 GRBs per year but of these ~90% are long. Secondly, short-burst afterglows are usually much fainter than their long-burst cousins (e.g., Kann et al. 2010; Nicuesa Guelbenzu et al. 2012). This general faintness makes their discovery and detailed follow-up very challenging. It is therefore not surprising that the number of well-localized short-burst afterglows is still small (about 40 cases). Secondly, only the precise detection of an afterglow with sub-arcsec accuracy enables a secure determination of its putative host galaxy and its redshift. Moreover, the X-ray and optical light curves provide information about the physical processes

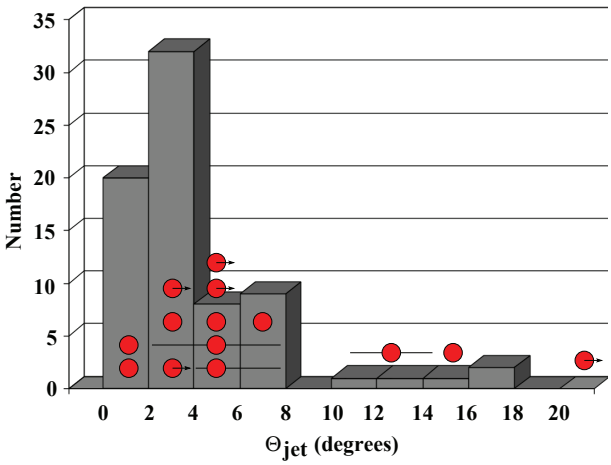

Fig. 1.5: Observed distribution of jet half-opening angles of 74 long bursts (based on the compilation in Lu et al. 2012) compared to the short-burst sample. Since the latter has much less data, here only points are plotted (in red). An arrow indicates a lower limit on $\Theta_{\rm jet}$. Adapted from Nicuesa Guelbenzu et al. (2012).

after the explosion and the properties of the environment of the GRB progenitor along with clues about the physics of the central engine.

Theoretical studies suggest that long GRBs are followed by more luminous afterglows than short bursts, mainly due to the difference in the circumburst density around the GRB progenitors (say, < 0.01 cm^{-3} for short GRBs compared to > 100 cm^{-3} for long GRBs; Panaitescu et al. 2001). The distribution functions of the jet-opening angles of long and short bursts (Fig. 1.5) should also be different from each other because an extended massive envelope of a collapsar collimates the relativistic outflow (Zhang et al. 2004), while the lack of such a medium in NS merger events might allow for wider jet-opening angles (Aloy et al. 2005; Rezzolla et al. 2011).

While (cosmologically nearby) long GRBs are usually followed by a detectable supernova (SN) component that can even outshine the optical afterglow from early-on (e.g., Ferrero et al. 2006; Klose et al. 2017), short GRBs lack such a bright electromagnetic signal. Though, in recent years we have learned that also in the case of NS-NS mergers a specific, and in particular detectable electromagnetic signal should exist.

In the 1990s Li & Paczyński (1998) predicted that a NS-NS merger should be followed by an optical transient (OT) which has a similar origin like a classical SN, it is heated by radioactive matter released during the explosion. Li & Paczyński (1998) called it 'a mini-supernova' although the literature prefers the name 'kilonova light'. In recent years substantial progress has been made in the modeling of kilonova light (e.g., Bauswein et al. 2013; Just et al. 2015; Kasen et al. 2015). First claims about its observational detection have already been published (GRB 130603B at z=0.36: Berger et al. 2013a; Tanvir et al. 2013; GRB 0606014 at z=0.125: Yang et al. 2015). The quality of these data is nevertheless inconclusive since no true kilonova light curve was observed and there is no convincing multi-color information available. More detailed observations of future short bursts are needed to confirm this interpretation. Progress in this re-

spect might be challenging, since kilonova light might only be detectable for the very nearest short GRBs and it will require 8-m class optical telescopes (e.g., Tanaka & Hotokezaka 2013).

The interest on short bursts has gained further interest in recent years as merging compact stellar objects should be the sources of gravitational radiation. Given that they are followed by optical afterglows, they offer a superb localization accuracy for a gravitational wave event. The current number of gravitational wave observatories is small with the Advanced LIGO[5] (Aasi et al. 2015) in the USA, the Advanced Virgo (Acernese et al. 2015) in Italy and KAGRA[6] (Aso et al. 2013) in Japan. They provide a rather poor localization based on triangulation methods with error boxes of 100 deg^2 large.

During the last years there was increasing hope that a short GRB could be found in the near future that is physically associated with a gravitational wave event detected by LIGO and Virgo. Such an association would be without doubt if LIGO/Virgo on the one hand and any GRB satellite on the other hand trigger at the same time. The discovery of such an event would be a milestone in theoretical and observational physics. It would not only confirm the technological concept of LIGO/Virgo, it would also be the ultimate proof that the NS-NS merger hypothesis is correct. In addition, if the short GRB would be followed by an optical afterglow, this would allow for a subarcsec localization and possibly a redshift determination. Such an event occured in August 2017 (Castelvecchi 2017).

1.2 Long-GRB host galaxies

The best studied GRB host galaxies are the hosts of long GRBs with optically bright afterglows. Long GRBs pinpoint to massive stars and as such they are powerful tracers of star-forming galaxies into the cosmologically remote universe.

1.2.1 Photometric studies

Understanding which is the main stellar population in a GRB host galaxy is an important source of information. For this purpose, the integrated $(R-K)$-color has often been used as an observational tool (e.g., Savaglio et al. 2009; Rossi et al. 2012). Formally, the K band traces the old stellar population while the R band traces the contribution from younger stars (strictly speaking this refers to the host frame). It was discovered that the hosts of long bursts with bright optical afterglows (and in the redshift range $0.5 \lesssim z \lesssim 1.5$) are usually faint, blue star-forming galaxies,

[5] Laser Interferometer Gravitational-Wave Observatory
[6] Kamioka Gravitational Wave Detector

dominated by a young stellar population. Based on their deduced faint K-band luminosities the galaxies were found to be of rather low stellar mass (e.g., Le Floc'h et al. 2002, 2003). Observations with the *Spitzer Space Telescope* showed that most long-GRB hosts are not infrared-bright galaxies (Le Floc'h et al. 2006; Vergani & Chassande-Mottin 2015).

Fruchter et al. (2006), making use of the Hubble Space Telescope (*HST*), compared the morphology of long-GRB host galaxies with those of core-collapse SN host galaxies at redshifts z <1. These authors found that GRB hosts are fainter and more irregularly shaped than those that harbor other types of core-collapse SNe. Their study also revealed that the GRB explosion sites reside in the bluer part of these galaxies, where the star formation is highest. Similarly, Svensson et al. (2010) found that the hosts associated with long GRBs have on average lower masses than those of core-collapse SNe without GRB.

Studies of the hosts of long-GRBs for which no optical afterglow could be found down to deep flux limits in spite of a rapid response with optical follow-up observations (the so-called dark bursts) revealed that these are often luminous, massive and dust-enshrouded galaxies (Hunt et al. 2011; Krühler et al. 2011; Rossi et al. 2012; Perley & Perley 2013). This revised the picture that long GRBs seem to prefer compact, blue host galaxies. They occur in all kinds of star-forming galaxies, in extremely seldom cases also in post-starburst galaxies (Rossi et al. 2014).

1.2.2 Spectroscopic studies

A new generation of spectrographs, like X-Shooter (Vernet et al. 2011) mounted at the ESO/VLT, have revolutionized emission-line studies of galaxies. X-Shooter is able to observe simultaneously from 300 to 2500 nm using three different arms: the ultra-violet/blue (300 to 560 nm), the visible (550–1002 nm), and the near-infrared (1.00–2.48 μm).

Krühler et al. (2015) collected X-Shooter spectroscopy for 96 long-GRB host galaxies at redshifts between 0.1 and 3.6. This is the most comprehensive emission-line survey of GRB hosts currently available. The hosts in this sample are faint (21< R < 26 mag), their brightness distribution peaks around R ~25 mag, with a median value of ~24.3 mag (see figure 1 in Krühler et al. 2015). Most of the targets (75%) are located at 0.5< z <2.5, with a median redshift of z ~1.6, a much larger value than any previous spectroscopic survey of GRB hosts (e.g., Savaglio et al. 2009). Out of the 96 events, in 89 cases an emission-line spectrum was observed allowing for a detailed study of the interstellar medium (ISM) in the corresponding galaxy. The fraction of galaxies with super-solar metallicities turned out to be ~20% at z < 1, which is significantly less than the corresponding fraction in field galaxies. This supports theoretical expectations (see

Sect. 1.2.2.2) that GRB progenitors disfavor high-metallicity environments.

1.2.2.1 Star formation rates

Once an afterglow has faded away, important details can be obtained by studying the physical properties of the host galaxy as a whole. The presence of emission lines like [O II], [O III], Hα, Hβ, or even He II, is an indicator for ongoing star formation. The star formation comes from gas which is ionised by hot young stars with masses $\gtrsim$10 $M_\odot$ and lifetimes in the order of 10 Myr (e.g., Crowther 2012). In order to convert a measured line flux into a star formation rate (SFR), several theoretical and observational studies have been performed (e.g., Kennicutt 1998; Savaglio et al. 2009; Murphy et al. 2011).[7]

Krühler et al. (2015) show the distribution of SFRs for 89 hosts observed with VLT/X-Shooter. The SFR of 68 hosts is based on the Hα line flux, of 10 hosts on Hβ, of eight hosts on [O II] and of three hosts on [O III]. All hosts are forming stars but the distribution of the SFR is very broad, ranging from 0.05 $M_\odot$ yr^{-1} to 200 $M_\odot$ yr^{-1}, with the peak at about 20 $M_\odot$ yr^{-1}. The most heavily star-forming galaxies are located at redshifts z >2 or are dusty galaxies.

Most interesting is the efficiency at which a galaxy is forming stars, i.e., its *specific* star formation rate (sSFR). The sSFR can be defined by dividing the global SFR of a galaxy by its total mass in stars (SFR/M_{star}). Typical values for field galaxies lie in the range from log sSFR (yr^{-1}) = −11 to −7 (see Hunt et al. 2014, their figure 4)[8] Observations show that the host galaxies of long GRBs belong to those galaxies with the highest sSFR (e.g., Castro Cerón et al. 2006; Hunt et al. 2014; Schulze et al. 2015, 2016; Klose et al. 2017). In a recent work, Schulze et al. (2016) report on a mean sSFR of long-GRB hosts of log sSFR (yr^{-1}) = −9.15 ± 0.11. The distribution is rather broad, ranging between about −10 and −8 (see Hunt et al. 2014).

1.2.2.2 GRB environments, ISM metallicities

The metal content of the interstellar medium (ISM) from which a star is formed, is an important ingredient that determines its evolutionary track. For massive stars this includes the details of its explosive end too. According to theoretical studies this holds in particular for long-GRB progenitors because of two reasons: (a) The emerging ultra-relativistic jet, inside which the GRB is formed, has to be able to penetrate the outer stellar enevelope. This might require stars with

[7] The interstellar gas can also be ionized by AGN activity and by shocks when galaxies collide. The extinction-corrected emission-line ratios can be used to distinguish between these scenarios (e.g., Fensch et al. 2016; Alatalo et al. 2016).

[8] In other words, the inverse (in log scale) gives the time to reproduce the current mass in stars if the present SFR would hold on for ever. For example, if log sSFR (yr^{-1}) = −7, then it would take 10^7 years.

a removed H and He envelope (Wolf-Rayet stars). For a single star (not member of a binary system) a certain metallicity is needed to expell the outer stellar regions (mass loss) via a line-driven stellar wind. (b) On the other hand, the formation of the jet itself requires a rapidly rotating stellar core during stellar collapse so that a temporary accretion disk can form. If the metallicity is too high, the stellar wind might be strong and carry away too much angular momentum from the star (Yoon & Langer 2005; Woosley & Heger 2006, 2012). For example, according to Woosley & Heger (2012), a 25 $M_{\odot}$ solar metallicity star even when rotating rigidly with an equatorial speed of 200 km s^{-1} on the main sequence will finally collapse to a black hole without forming a temporary accretion disk. Recently, the optical disappearance of the star N6946-BH1 that was located in a spiral galaxy at a distance of 0.6 Mpc has been confirmed with *HST* (Adams et al. 2017). It is a failed supernova [9] candidate that was monitored with the Large Binocular Telescope (LBT) as part of a supernova survey of galaxies within 10 Mpc (Gerke et al. 2015).

One of the first observational hints with respect to the implication of metallicity in the formation of long-GRB progenitors came by the study of five nearby ($z < 0.3$) long-GRB hosts by Stanek et al. (2006). These authors found that the metallicity in these galaxies was lower than the corresponding metallicity of galaxies with similar luminosity in the nearby universe. Later, Modjaz et al. (2008) discovered that the metallicity of nearby ($z < 0.14$) long-GRB hosts was smaller than the metallicity of the hosts of type Ic SNe. Similar results were obtained by Levesque et al. (2010b) based on a spectroscopy of a larger sample of 14 long-GRB hosts for which the metallicity, stellar mass, and stellar population age could be measured. This supported the picture that the formation of long-GRB progenitors is linked to the endpoint of the evolution of metal-poor, massive Wolf-Rayet stars (e.g., Woosley & Bloom 2006). Several other studies also found a low-metallicity in GRB host galaxies or even in the vicinity of the GRB explosion sites (e.g., Rau et al. 2010; Schulze et al. 2015; Vergani & Chassande-Mottin 2015; Niino et al. 2017). On the other hand, several other host galaxies revealed even super-solar metal abundances (e.g., Levesque et al. 2010a; Savaglio et al. 2012; Krühler et al. 2012; Elliott et al. 2013; Schulze et al. 2014; Schady et al. 2015). Although most long GRBs seems to prefer low metallicity environments (Krühler et al. 2015), the role of the metallicity in the formation of long GRBs is still an open question.

Most long-GRB host galaxies are located at such high redshifts that the explosion site of the optical transient within the galaxy cannot be analyzed in detail. The standard procedure then is to extrapolate the global characteristics of the host galaxy to the local environment of the optical transient. However, significant metallicity variations can occur. For example, in the Andromeda

[9] a massive star that collapsed to a black hole without a SN explosion

Galaxy different HII regions vary in their metallicity by more than 0.3 dex on scales of <1 kpc (Sanders et al. 2012). It appears reasonable to assume that a similar metallicity variation on kpc scales characterizes GRB host galaxies too. It is therefore of fundamental importance to study GRB explosion sites in cosmologically nearby hosts where current telescopes allow us to zoom-in. In this respect the most interesting examples are the long GRB 980425, 060505, 100316D, and 111005A. The picture that emerges from these four cases is mixed, however:

- GRB 980425 is the closest long GRB observed to date and was followed by a bright supernova (SN 1998bw; Galama et al. 1998) which even after nearly two decades is still the best studied GRB-SN at all (z =0.0085; Tinney et al. 1998). The progenitor was located in a dwarf spiral galaxy and placed about 800 pc away from a Wolf-Rayet star-forming region (Hammer et al. 2006; Fig. 1.6). Based on Integral-field-unit spectroscopy it was found that this region exhibits the lowest metallicity among the star-forming regions in the entire host galaxy (Christensen et al. 2008; Krühler et al. 2017).
- GRB 060505 is one of three relatively nearby long GRBs for which no SN component was found down to about 1% the luminosity of SN 1998bw (Fynbo et al. 2006). It originated from a spiral host galaxy at z =0.089 (Thöne et al. 2006). VLT spectroscopy showed that the metallicity of the ISM at the birth-place of the GRB progenitor is the lowest in this galaxy with ∼1/3 solar (Thöne et al. 2008, 2014).
- The host galaxy of GRB 100316D lies at z = 0.0591 (Vergani et al. 2010). VLT/MUSE[10] observations revealed that the GRB exploded in the most active star-forming region of the galaxy, characterized by a low metallicity and a young stellar population (Izzo et al. 2017).
- The host of GRB 111005A was the galaxy ESO 580-49 at z=0.01326 (Levan et al. 2011). Again, it belongs to one of three cosmologically nearby long GRBs for which no SN component was found down to very deep luminosity limits (in this case down to about 5% the luminosity of SN 1998bw). The metallicity found at the GRB explosion site turned out to be twice solar (Michałowski et al. 2016).

A recent comprehensive work on long-GRB host galaxies at various redshifts by Perley et al. (2016b) suggests that the observational data are best understood if the long-GRB progenitor population contains single as well as binary stars, where the latter subpopulation is much less sensitive on the original ISM metallicity from which the exploding star was formed (van den Heuvel & Portegies Zwart 2013).

[10] Multi Unit Spectroscopic Explorer

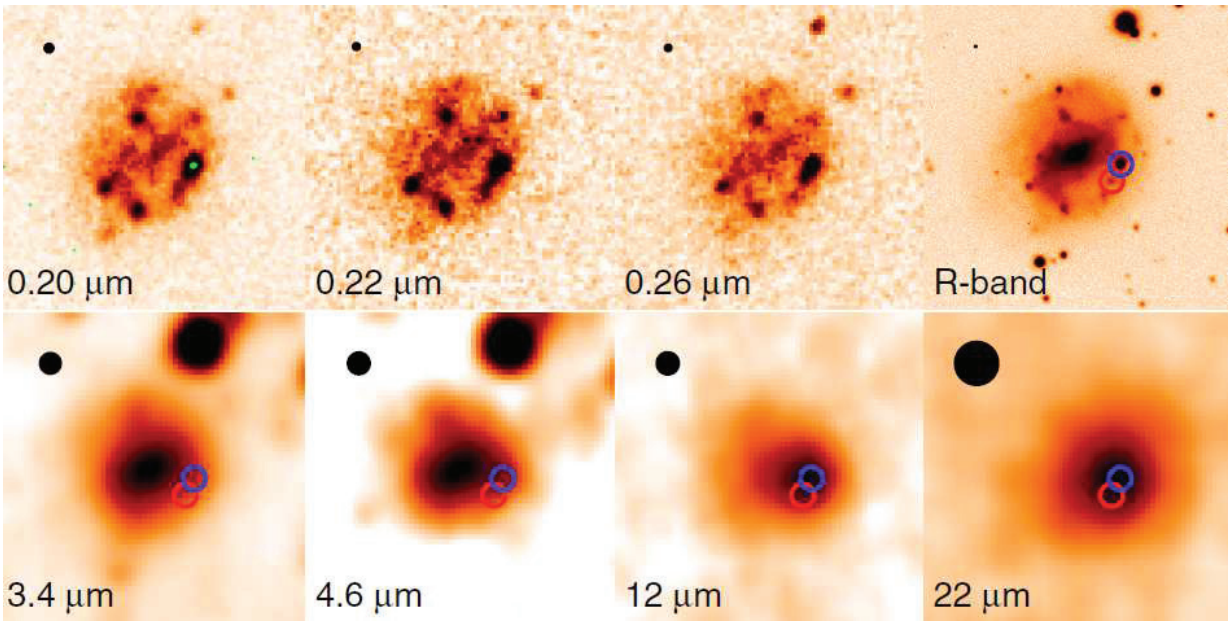

Fig. 1.6: Multi-wavelength view of the host galaxy of the nearest long burst, GRB 980425. Thanks to its low redshift, z=0.0085, the data allow for a closer look into the GRB explosion site. Each panel is $80'' \times 80''$ (14×14 kpc^2). The red and blue cirlces show, respectively, the GRB position and a nearby Wolf-Rayet star-forming region. Adapted from Michałowski et al. (2014).

1.2.3 Legacy samples

It is possible that the current picture about long-GRB host galaxies is biased due to selection criteria. Most of these galaxies that were studied in detail are the hosts of bright optical afterglows at low redshifts (z <0.25). Savaglio et al. (2009) summarize the data for 46 GRB host galaxies (long and short), including GRBs from the years 1997 to 2006 and redshifts ranging between z= 0.0085 (GRB 980425) and z=6.3 (GRB 050904). At that time, the general belief was that host galaxies of long GRBs tend to be small, blue, star-forming galaxies with a mean stellar mass similar to that of the Large Magellanic Cloud (LMC).

Later on, different studies revealed the different properties of host galaxies of dark GRBs. Dark GRBs come either from very dusty environments (very red host galaxies; Greiner et al. 2011; Rossi et al. 2012; Hunt et al. 2014) or from high redshift (Lyman drop-out; Tanvir et al. 2012; McGuire et al. 2016). The host galaxies of dark GRBs seems to be different from those with a bright optical afterglow.

One of the most successful attempts to work on a clean sample of host galaxies not selected according to the brightness of the corresponding afterglows is represented by The Optically Unbiased GRB Host (TOUGH) survey (Hjorth et al. 2012). It contains 69 hosts from *Swift* bursts with an X-ray afterglow, contrary to the optical afterglow criteria of the previously mentioned

studies. For every target, the authors obtained deep *R* and *K*-band photometry from the VLT, optical spectroscopy based on FORS1[11], FORS2, ISAAC[12] and X-Shooter at the VLT, and radio data with the VLA[13] radio interferometer. The majority of the GRB hosts has been detected (54 out of 69 targeted fields) where 32 targets have new detections of suspected hosts. The suspected host galaxies cover a wide redshift range (up to z ~6.5), and allowed for, e.g., a determination of the GRB-host-galaxy luminosity function (Schulze et al. 2015).

Perley et al. (2016a) built a homogeneous and unbiased sample of host galaxies of long GRBs (Gamma-Ray Burst Host Galaxy Legacy Survey, SHOALS). It contains 119 *Swift* long GRBs from the years 2005 to 2009. It is the largest sample of host galaxies of long GRBs to date. For every SHOALS target, deep *Spitzer*/IRAC observations plus multicolor optical/ near-IR observations, as well as spectroscopy has been acquired. The main breakthrough of the SHOALS sample compared to the TOUGH sample (Hjorth et al. 2012) is the extension in redshift domain. The SHOALS sample contains host galaxies with redshifts between 0.03 and 6.29. The TOUGH sample beyond z ~3 suffers from small number statistics (see figure 4 in Jakobsson et al. 2012). However, contrary to the TOUGH sample, the SHOALS sample has enough targets to split the sample into six redshift bins and study the snapshot of the host population of long GRBs at a particular epoch. Among other things, the study by Perley et al. (2016a) finds that dust-obscured GRBs dominate the massive host-galaxy population.

1.2.4 Radio observations

Dust-enshrouded, star-forming galaxies (for a recent review see Casey et al. 2014) can have a SFR exceeding 1000 $M_\odot$ yr^{-1} (contrary to our Milky Way with 1 to 2 $M_\odot$ yr^{-1}; Robitaille & Whitney 2010). As such they contain the most intense starburst episodes in the Universe. Most of the time, this starburst is optically obscured.

Since the launch of the *Swift* satellite (Gehrels et al. 2004), in almost all cases an X-ray afterglow has been detected after a GRB trigger. However, in only of about 50% of the cases an optical afterglows has been observed (see `http://www.mpe.mpg.de/~jcg/grbgen.html` for a statistics). While this is partly due to observing constraints, a substantial fraction of bursts appeared to be "dark". The term dark GRB is used for those events that have a very faint optical afterglow (or no optical afterglow is detected at all) compared to the observed flux of the X-ray afterglow (Jakobsson et al. 2004). There can be several reasons to explain the optical faintness

[11] FOcal Reducer and low dispersion Spectrograph
[12] Infrared Spectrometer And Array Camera
[13] Very Large Array

of these events:

- the optical afterglow had an intrinsically low luminosity (i.e., the spectral energy distribution was such that the afterglow was very faint in the optical bands)
- the optical radiation of the afterglow was absorbed by intervening material in the GRB host galaxy
- a high redshift event ($z \gtrsim 6$); this would depress radiation in the optical bands due to the cosmological Lyman drop out.

Recent studies of dark GRBs have shown that dust extinction plays the major role in these events (Greiner et al. 2011). Besides, some host galaxies of dark GRBs have been found to be very red objects, which is potential evidence for very dusty environments (Krühler et al. 2011; Rossi et al. 2012). Radio observations of dark-GRB host galaxies seem to be the right strategy to understand what is the SFR in these galaxies.

Star-formation rates (in the following SFRs) in GRB host galaxies are usually derived from measured emission line fluxes, e.g., [O II](3727 Å) and [O III](5006.8 Å) in the case of redshifts $z \lesssim 1$. These measurements suffer however from the unknown extinction by cosmic dust in these galaxies and, therefore, represent only a lower limit on the present SFR. On the other hand, radio observations are unaffected by extinction by cosmic dust and provide an unobscured view on the star-forming activity in a galaxy via synchrotron radiation from electrons originating from supernova remnants. These radio-emitting electrons trace star-formation over a relatively broad time span of about 100 million years. Consequently, in recent years radio observations of the host galaxies of *long GRBs* have been undertaken with the goal of deriving the unobscured SFR based on the measured radio continuum flux (Berger et al. 2003; Stanway et al. 2010; Hatsukade et al. 2012; Michałowski et al. 2012; Perley & Perley 2013; Greiner et al. 2016). Since long GRBs pinpoint to star-forming galaxies, they have the potential to be reliable tracers of the SFR in the Universe. Therefore, it is worth to obtain the SFR for each GRB host galaxy. Several studies have tackled this task.

Michałowski et al. (2012) deduced that the SFR and dust properties for galaxies in the TOUGH sample which have z <1 are similar to the general star-forming field-galaxy population. Stanway et al. (2014) performed *ATCA* radio continuum observations at 5.5 and 9.0 GHz of a sample of 17 long-GRB host galaxies at redshifts up to $z = 1.9$ (their table 1). Four targets are clearly detected (33%) with an SFR between 60 and 200 $M_\odot$ yr^{-1}. Two of these targets are the hosts of dark GRBs.

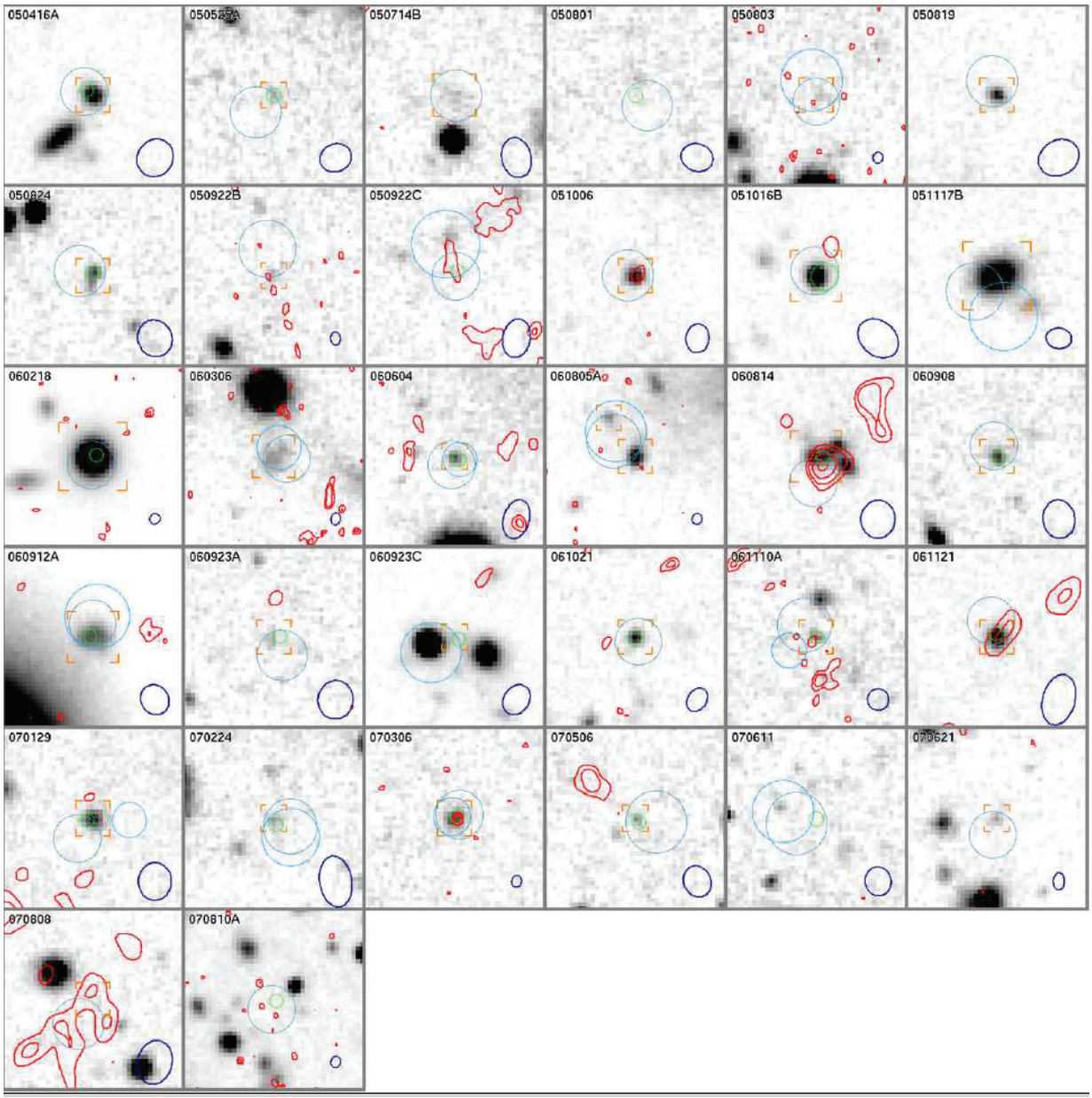

Fig. 1.7: Composit of the 32 TOUGH targets observed with *VLA* at 3 GHz. Optical *R*-band images have been overlaid radio contours in red with 2.3, 3, 4, 5, and 6 times the *VLA* rms. Blue circles show the XRT position and green circles the position of the optical transient. Adapted from Perley et al. (2015).

Perley & Perley (2013) performed *VLA* radio continuum observations of 15 dust-enshrouded host galaxies in order to constrain the fraction of dark GRBs that were produced in luminous submillimeter hosts. Their sample (GRBs from the years 2005 to 2009) contains only hosts from *Swift* bursts the afterglows of which were heavily obscured ($A_{\rm V}^{\rm host}$ >1.0 mag). The observations were performed at 4.7 and 5.7 GHz. Most of the targets (11) were not detected. Of the remaining four objects, one has a marginal detection and in two other cases the contribution of the several years old radio afterglow can not be excluded. The remaining target has a secure detection but

its SFR is roughly consistent with the optical SFR. These authors therefore conclude that most galaxies hosting obscured GRBs are not forming stars at extreme rates and the corresponding SFR is not high enough to be detected in the radio regime.

The same authors (Perley et al. 2015) performed a more extensive study using the TOUGH sample (Hjorth et al. 2012). Deep optical photometry was available for every target. The final sample they were observing with the VLA contained 32 GRB hosts (Fig. 1.7). Of these, 27 have a secure redshift and lie at $z < 2.5$. Out of the 32 observed targets, only four galaxies were detected in the radio bands with a SFR between 50 and 300 $M_\odot$ yr^{-1} .

Greiner et al. (2016) performed radio-continuum observations of 11 long-GRB hosts with *ATCA* at 2.1 GHz. Their sample contains very massive galaxies and galaxies with clear evidende of a high UV-optical star formation rate. No radio emission related to star-forming activity could be found for any target. The radio emission detected for one event (GRB 020819B) is very likely afterglow flux.

Summing up, most host galaxies of long GRBs are not detected at radio wavelengths, with typical radio-derived SFR limits ranging from $\lesssim$10 $M_\odot$ yr^{-1} for low-redshift hosts to $\lesssim$1000 $M_\odot$ yr^{-1} for high-redshift hosts. Only in $\sim$ 10 cases are SFRs found to be $\sim$100 $M_\odot$ yr^{-1}. The non-detections often leave room for a substantial optically hidden SFR since the redshifts are ususally not that small, even though much deeper constraints on the radio flux might not be achieved in the near future.

1.3 Short-GRB host galaxies

1.3.1 Host galaxies as tracers of the nature of the short-GRB progenitors

Short GRBs are usually detected from events at notably smaller redshifts than most long bursts. Therefore, their host galaxies are comparably easier accessible for more detailed studies.

Within the context of the compact stellar merger model, the progenitors underlying short bursts are primarily associated with an old stellar population ($\sim$ billions of years). Consequently, short GRBs should occur in all morphological types of galaxies, from quiescent elliptical galaxies to star-forming irregular and spiral galaxies. Indeed, the first short GRB which was well-localized by *Swift* in the X-ray band, GRB 050509B (Gehrels et al. 2005), was most likely associated with a giant elliptical galaxy located in a cluster of galaxies at $z = 0.225$ (Gehrels et al. 2005; Pedersen et al. 2005; Bloom et al. 2006), while the second short burst that could be localized to subarcsec precision, GRB 050709, occurred in an irregular dwarf galaxy (Hjorth

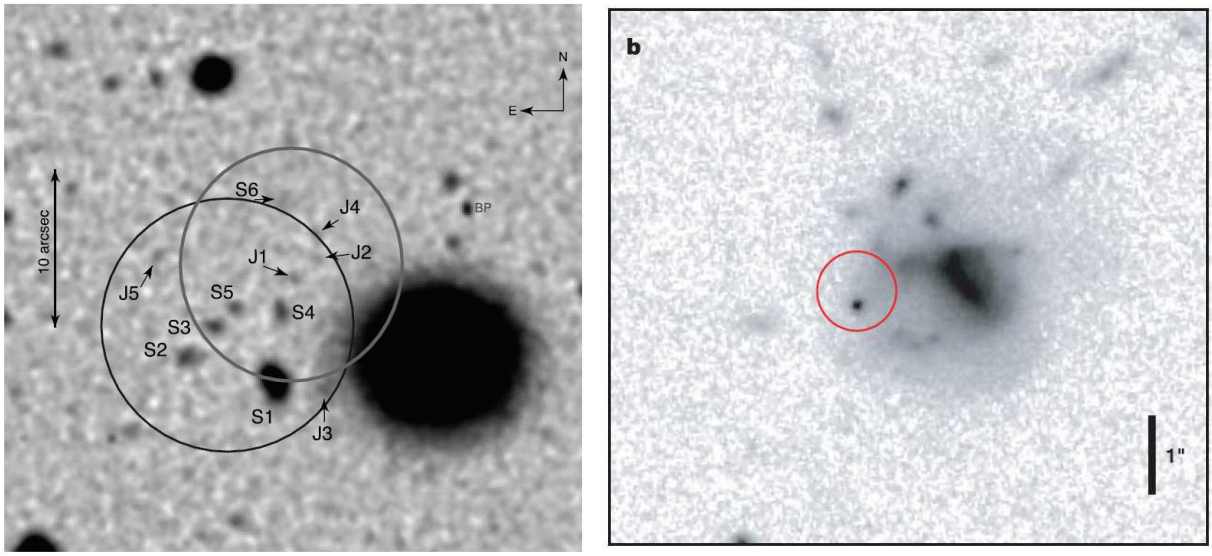

Fig. 1.8: *Left:* Keck image of the field covered by the XRT error circle of the short GRB 050509B (adapted from Bloom et al. 2006). It shows the original and the revised (largely bigger) XRT error circle. Both circles touch the outer region of a giant elliptical galaxy at z=0.225 (Gehrels et al. 2005). Indicated are also several background galaxies. *Right:* HST host galaxy image of the afterglow of GRB 050709. The red circle is the Chandra X-ray localization. The host is an irregular galaxy at z=0.1606 (Fox et al. 2005).

et al. 2005a; Fig. 1.8). Similarly, the short GRB 060502B might have had its origin in a bright elliptical at $z = 0.287$ (Bloom et al. 2006), while the short GRB 051221A was associated with an isolated star-forming dwarf (Soderberg et al. 2006), and the host of the short GRB 060121 might be a dusty edge-on irregular or spiral (Levan et al. 2006). This "mixed-bag" of host types is consistent with the idea that merging compact binaries sample all types of galaxies.

Nevertheless, while the physical link between long-duration, soft gamma-ray bursts and the core collapse of massive stars has been conclusively confirmed by the spectroscopic detection of supernova light following some bursts (e.g., Hjorth et al. 2003; Ferrero et al. 2006; Pian et al. 2006; Greiner et al. 2015; Kann et al. 2016; Cano et al. 2017; Klose et al. 2017), the nature of the sources responsible for the short bursts remains to be revealed in full. This partly unsatisfactory situation calls for several observational approaches to check out if the stellar merger hypothesis is correct. A particular key parameter here can be the characteristic age of the short-GRB progenitor population.

Individual and qualitative age estimates of a short-GRB progenitor can in principle be obtained once a host galaxy is identified. Even though a substantial fraction of short-GRBs afterglows seems to be hostless (Tunnicliffe et al. 2014), for more than 50% of all well-localized events host galaxies or host-galaxy candidates have been found. While in elliptical galaxies

at $z \lesssim 1$ the GRB progenitors are most likely members of an old stellar population (formally they could still be hosted in undetected smaller satellite galaxies), in star-forming galaxies they could also be young. Interestingly, about 3/4 of all short-GRB hosts have been found to be star-forming galaxies (e.g., Leibler & Berger 2010; Fong & Berger 2013; Fong et al. 2013), with star-formation rates deduced from ultra violet (UV)/optical data ranging from 0.01 to 100 $M_\odot$ yr^{-1} and stellar masses ranging from $\sim 10^9$ to 10^{11} $M_\odot$. Even more interesting, in several cases the broad-band photometric properties of these hosts imply dominating stellar populations with young ages down to ~0.1 Gyr (Leibler & Berger 2010).

Theoretically, a relatively significant number of NS-NS systems is indeed expected to merge within a delay time of $\lesssim 100$ Myr (Voss & Tauris 2003; Belczynski et al. 2006) with correspondingly small travel distances from their birth sites to the places where they finally coalesce. The general existence of such young binary systems has been recently confirmed even for the Milky Way Galaxy. The NS-NS system PSR J0737−3039 which will merge in only ~85 Myr (Burgay et al. 2003), is located in the Galactic disk and has a small measured transverse velocity of <10 $km\,s^{-1}$ (Kramer et al. 2006). Hence, this is a progenitor system of a short GRB in a potential star-forming region in our Galaxy.

If merging compact objects represent the progenitors of short GRBs, some fraction of short bursts should be located close to star-forming regions in their host galaxies. However, the observational situation is not straightforward. While the data do not exclude the existence of a subpopulation of *young* short-GRB progenitors, observationally their existence has not yet been proven and as such is still a matter of debate (for a review see Berger 2014). It would be a substantial step forward in this direction if a short burst could be found that originated close to or inside a star-forming region. Radio observations can help to find this potential missing link.

1.3.2 Identifying the host galaxies of short GRBs

While more than 100 host galaxies of long bursts have been studied so far, only about three dozen hosts of short bursts have been identified (e.g., Berger 2014). Contrary to most long-GRB afterglows, identifying the host galaxy of a short GRB can be tricky as in most cases optical afterglows are already starting faint so that no spectrum can be taken. While in the case of long bursts the short lifetime of the corresponding progenitors implies that the event is always occurring inside a galaxy, within the context of the compact stellar merger model this is not necessarily the case for short GRBs.

Short GRBs with subarcsec localization show a median projected offset of 4.5 kpc with re-

spect to the center of their host. This is 3.5 times larger than for long GRBs. About 25% of all short GRBs exhibit offsets even larger than 10 kpc. Between 30 to 45% of the bursts are located in regions of their hosts galaxies that have no detectable stellar light and 55% in regions with no UV light (Fong & Berger 2013). These data suggest that most progenitors of short GRBs migrate from their birth sites to their corresponding explosion sites much more than long-GRB progenitors.

Supporting this observational data, Tunnicliffe et al. (2014) pointed out that ~25% of all short GRBs do not have a reliable host galaxy candidate, i.e., these are apparently host-less GRBs. Several reasons can explain these observations:

- The underlying host is simply too faint for the best current observing facilities like 8-m class telescopes or even the *HST*. While this might also be the case for long GRBs (e.g., the host of GRB 030228 is not detected down to R=26.2; Klose et al. 2004), for short GRBs the additional difficulty is that they could also occur in globular clusters (consisting of an old stellar population) orbiting their galaxies at galactocentric distances of several dozen kpc (e.g., Salvaterra et al. 2010; Church et al. 2012).
- Most redshifts for short GRBs are based on a spectroscopy of the suspected host galaxies. Only in two cases, GRB 090426 (z = 2.609; Levesque et al. 2010a) and GRB 130306B (z = 0.356; Cucchiara et al. 2013; de Ugarte Postigo et al. 2014) the redshift was obtained via spectroscopic observations of the optical afterglow.
- Theoretical models suggest space velocities for NS-NS systems that can reach 100 to 200 km s^{-1} (Eldridge et al. 2011), or even higher (Wong et al. 2010). Therefore, a compact stellar merger that occurs billions of years after the formation of the binary system could take place in intergalactic space several Mpc away from its original host galaxy.

The identification of a host galaxy for a short GRB becomes even more difficult when only an X-ray afterglow is detected. Then, the localization accuracy degrades from precise coordinates with errors of ±0.5 arcsec or less, to an error circle of several arcsec (typically ~3 arcsec radius; see table 1 in Nicuesa Guelbenzu et al. 2012). Then often several host-galaxy candidates are found inside or nearby the X-ray error circle. Thereby, the issue of a potential Mpc-long journey of the short-GRB progenitor in intergalactic space is not ignored. The host-galaxy candidates are usually well defined based on statistical arguments.

The approach to define a host-galaxy candidate via statistical arguments was first applied for long bursts by Bloom et al. (2002), though it is a well-known approach in other fields of extragalactic astronomy (Zvyagina 1968). According to this concept, the chance probability p

to find on the sky a galaxy with a magnitude brighter than m inside a circular area of radius r is (Bloom et al. 2002)

$$p = 1 - \exp(-\eta), \quad \text{with} \quad \eta = \pi r^2 \sigma(\leq m)\,, \tag{1.1}$$

where σ is the mean surface density of galaxies (per deg^2) with magnitudes brighter than m. The best host-galaxy candidates are those with very small p values. Here I consider galaxies with $p < 0.1$ as good candidates.

For short GRBs this procedure is only a first guess, as it ignores the problem of the potentially huge offsets between a host galaxy and the explosion of the short-GRB progenitor due to its long lifetime on the one hand and its non-negligible space velocity on the other hand (gained by two SN explosions). Although the aforementioned probabilities have to taken with care, I will use them for a lack of alternatives. Additional arguments can come from a search for potential peculiarities of the host-galaxy candidates, like a very dusty host for long bursts or a morphologically disturbed host for short bursts (for the case of long GRBs, see Perley et al. 2009; Rossi et al. 2012). This approach is formally similar to the one adopted ~40 years ago, when GRB afterglows were not known and at best arcmin-sized GRB error boxes obtained via satellite triangulation were available (e.g., Vrba et al. 1995; Klose et al. 1996).

Finally, it is worth to mention that sometimes the best statistics do not help. For example, the short GRB 100702A was followed-up by our team with *GROND* starting only 2.5 min after the burst. This is the most rapid follow-up of a short GRB ever, and this in seven bands simultaneously from the optical to the near-infrared. The burst even had a relatively small X-ray error circle with a radius of only $r = 2\farcs4$ (Siegel et al. 2010). Unluckily, the field was located close to the Galactic plane ($b = -4$ deg) and is therefore heavily crowded with stars. Even worse, a group of Galactic foreground stars lies inside this tiny error circle (Fig. 1.9). I performed point spread function (PSF) photometry in each $\tilde{\text{G}}$ROND band, subtracted the stars after PSF fitting, but no evidence for an afterglow was found and no obvious host-galaxy candidate could be identified (Nicuesa Guelbenzu et al. 2012).

1.3.3 Previous radio studies of short-GRB host galaxies

Radio upper limits on the flux of short-GRB afterglows have been obtained for a number of events so far (Chandra & Frail 2012; Fong et al. 2015). Naturally all these upper limits also constrain the permanent radio flux from the corresponding host galaxy. Nevertheless, in contrast to increasing attempts to explore the hosts of *long bursts* in the radio-continuum bands, at the start of this work no systematic radio investigations of the hosts of *short bursts* had been performed. A recent study

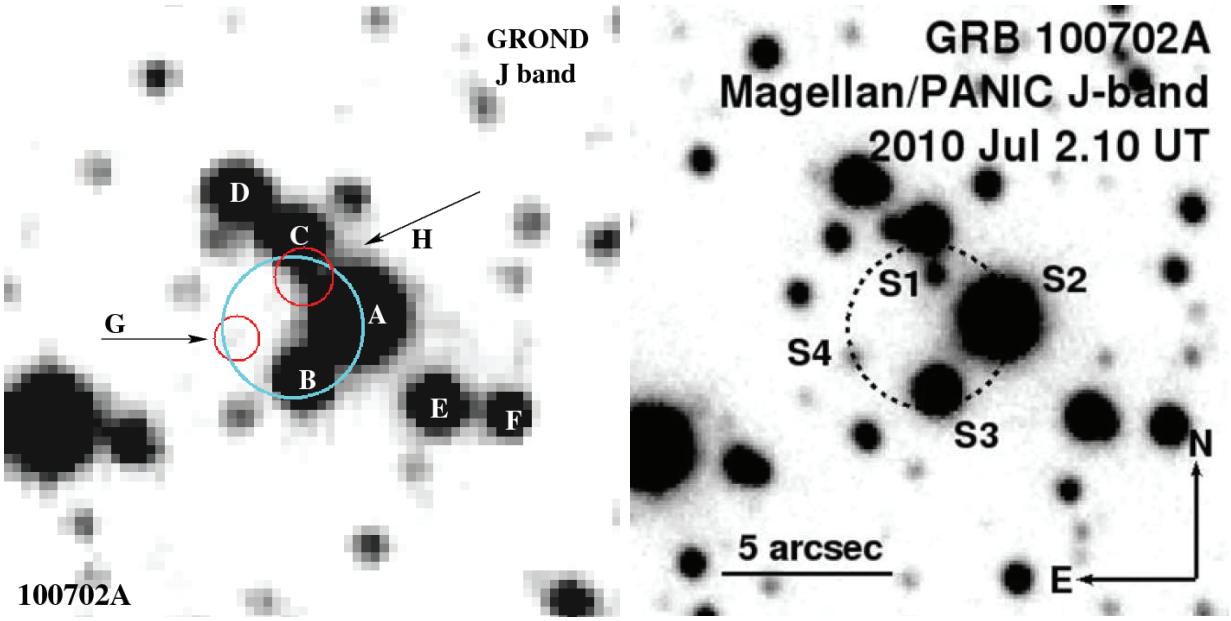

Fig. 1.9: Finding chart of the field of GRB 100702A which was followed-up with *GROND* (Nicuesa Guelbenzu et al. 2012). *Left: GROND*, *J*-band image. *Right:* For comparison 6.5 m Magellan/Panic, *J* band (adapted from Fong et al. 2013). Shown also is the r=2.″4 XRT error circle (Siegel et al. 2010). No obvious host-galaxy candidate has been found for this short GRB.

by Fong et al. (2016) has to be mentioned as their data on nine short-GRB hosts do also constrain the permanent radio flux due to a potential star-formation activity. Using *VLA* 6.0 GHz radio-continuum observations, these authors searched for evidence of radio emission from long-lived magnetars, the potential end-products of NS-NS merger events. No emission was found down to a flux level between about 17 and 32 μJy (3σ).

Before I have started this work, in basically all cases the derived SFR in short-GRB hosts was based on optical emission-line fluxes. However, as the hosts of short GRBs are also affected by internal extinction by cosmic dust, this also holds for their optically derived SFRs. Although the host-galaxy extinction along the sight lines of short GRBs can also be measured via the SED of their optical/NIR afterglows, such studies require multi-color data. Given the usual faintness of short-GRB afterglows compared to their long-GRB cousins such data are often not available, however. Moreover, analogous to the case of long GRBs, the non-detection of signatures for dust in an optical/NIR afterglow is not necessarily evidence for a dust-free GRB environment. The burster can either be located in front or aside of a star-forming region. Also, the burst itself could have burned away the dust along the line of sight. It is therefore worth to explore also the hosts of short GRBs in the radio-continuum bands.

1.4 Immediative objective of this work

The goal of the radio-continuum observations reported here was to measure the unobscured star-formation rate in short-GRB host galaxies and to address the question whether the radio data provide evidence for the theoretically predicted subpopulation of young short-GRB progenitors. An important question in this respect is if radio observations can reveal optically hidden star-formation in short-GRB host galaxies (in those which are not elliptical galaxies). Thereby, it is desirable to measure the unobscured radio-SFR close to the GRB explosion sites, within a radius of a few kpc. The cosmologically nearest known short-GRB hosts lie at redshifts $z = 0.1-0.5$. At these redshifts 1 arcsec corresponds to about 2-6 kpc projected distance. A radio interferometer with long baselines was therefore the best choice to perform such observations.

In the following, after a description of the sample construction and the observational details in Chapter 2, in Chapter 3 and 4 I present the results of *ATCA* radio observations of 12 short-GRB host galaxies. *ATCA* was chosen since it is located at the southern hemisphere and therefore allowed me to use additional optical/NIR data of these hosts taken with the ESO/VLT or with GROND at the 2.2-m telescope on La Silla.

At first I will focus in three targets which I could detect with *ATCA* (GRB 050709, 071227 and 100628A). Thereafter, I report on those remaining nine cases for which I could not detect any of the suspected host galaxies. Chapter 5 provides a summary and discussion of the complete *ATCA* data set. Besides, I put into context the results of my radio observations with the radio upper limits of other short-GRB hosts published in the literature. These latter data are mostly based on upper limits which were obtained for the flux of the radio afterglows of the corresponding short GRBs. Finally the data is compared to the corresponding data for long-GRB host galaxies.

Chapter 2

Target selection, observations, and data reduction

2.1 ATCA target selection

2.1.1 Building the sample

From the point of view of angular resolution, sensitivity, and offered radio bands, the most suited radio interferometer for a study of short-GRB hosts are the *Karl Jansky* Very Large Array (*VLA*) in the northern hemisphere and the Australia Telescope Compact Array (*ATCA*) in the southern hemisphere. In this work I only focus on observations with *ATCA*, which in its widest configuration has a baseline of 6 km.

ATCA is equipped with the Compact Array Broadband Backend (CABB) correlator (Wilson et al. 2011; see also Sect. 7.2) which offers six different radio bands. For this study I have chosen the 4 cm band, corresponding to observations centered at 5.5 and 9.0 GHz with 2 GHz bandwidth each (in the following called 5.5 and 9.0 GHz band).

In its 5.5 GHz radio-continuum band, *ATCA* goes down to $\sim$ 5 μJy beam^{-1} (1 $\sigma_{\rm rms}$) in a 10-hour exposure. Thereby, weather conditions play a minimal role. The 5.5 GHz band is a good compromise between sensitivity and expected radio flux on the one hand and relatively less Radio Frequency Interference (RFI) on the other hand. CABB integrates in both bands simultaneously with 2048 channels, beginning at 4.476 and 7.976 GHz, respectively, with an increment of 1 MHz. In principle, observations in the 2.1 GHz band (16 cm) could provide a better signal-to-noise ratio (S/N) since for a star-forming region the radio flux scales as $F_\nu \propto \nu^{-\beta}$, β $\sim$0.7 (synchrotron radiation). However, this band is more sensitive to RFI. In addition, source crowding at 2.1 GHz is higher and it makes the identification of faint radio sources more

challenging. Moreover, compared to observations in the 2.1 GHz band, around 5.5 GHz the radio sky is much less affected by bright radio sources.

Most of the *ATCA* targets were observed during a first observing run in Narrabri (Australia) in mid 2013. These targets were selected according to the following criteria:

- The suspected host galaxy is at a redshift $z < 0.5$. This should help to increase the detection probability.
- The host-galaxy morphology on the available optical images suggests the existence of a disk component or an irregular structure, i.e., elliptical galaxies were not selected.
- There is a strong host-galaxy candidate. This includes three possibilities: (a) If an optical afterglow was found, any galaxy underlying the afterglow is considered as the host (GRB 050709, 050724, 061006, 071227, 080905A). (b) If there was an optical afterglow but no underlying galaxy was found, I included cases where a galaxy nearby (within 10 to 20 arcsec) is the suspected host-galaxy candidate (GRB 061201, 070809). (c) If no optical afterglow was found but the arcsec-sized *Swift*/XRT error circle includes a host-galaxy candidate, or a host-galaxy candidate lies close to this error circle, I also have included these targets (GRB 080123, 100628A).
- Declination < -15 deg, suitable for *ATCA* observations.

Altogether this provided nine targets.

2.1.2 Adding more targets

In the year 2015 I introduced a new selection criterium by looking for the dustiest short-GRB hosts since in these cases the presence of large amounts of dust could be a hint for optically obscured star-formation. In doing so, I made use of the *WISE*[1] satellite database (Wright et al. 2010).

WISE observed the complete sky in the far-infrared domain in four different bands at 3.35 (W1), 4.60 (W2), 11.56 (W3) and 22.08 μm (W4). The *WISE* catalog[2] lists all sources with a measured signal-to-noise ratio greater than 5 in at least one band. The major caveat of this catalog is that it is not homogeneous, it has not the same sensitivity level in all directions.

According to the *WISE* color-color diagram (Wright et al. 2010), which combines the W1-W2 with the W2-W3 color (Fig. 2.1), it is possible to infer if a detected target is a star, a galaxy, a Luminous Infrared Galaxy (LIRG), or an Ultra-luminous Infrared Galaxy (ULIRG). Having

[1] Wide-field Infrared Survey Explorer
[2] http://wise.ssl.berkeley.edu/

this in mind, I built a sample of short-GRB host galaxies (till the end of 2016) with detections by *WISE* in at least one band.

Table 2.1 shows 13 short-GRB host galaxies that have been detected by *WISE*, which is ∼1/3 of the present world-sample of short-GRB hosts. No galaxy has been detected at the longest wavelengths (W4) while five are detected in the W1, W2 *and* W3 bands (GRB 060502B at z=0.287, GRB 071227 at z=0.381, GRB 100206A at z=0.407, GRB 150101B at z=0.134 and GRB 161104A with unknown z). Interestingly, these are not the cosmologically nearest host galaxies. Among these objects, only the field of GRB 071227 lies at a declination suitable for *ATCA*, though this host was already part of my sample (see above). According to their position in the *WISE* color-color diagram (Fig. 2.1), only the hosts of GRB 071227 and 100206A are falling into the starburst category. The host of GRB 060502B might be a spiral galaxy while the suspected hosts of GRB 150101B and 161104A lie in the region occupied by elliptical galaxies. The latter two hosts are not in agreement with my selection criteria.

Another group of six hosts have been detected by *WISE* in W1 *and* W2 but not in W3 and W4. Among these six objects, GRB 070729 and 150424A were added to the target list while a third one, GRB 050724, was already in my sample. Two other fields are not accessible for *ATCA* while one host, which fulfills all selection criteria (GRB 070724), was proposed as an *ATCA* target but observations were never scheduled.

Finally, two further host galaxies have only a detection in filter W1. This does not qualify them as promising candidates for observations in the radio band. Hence, the inclusion of potentially dusty hosts added only two more targets to my short-GRB host-galaxy sample.

Last but not least, I also added the host of GRB 130515A to my sample although its redshift is not known. In publicly available VLT/FORS2 images the suspected host is a nearly face-on, morphologically disturbed spiral galaxy with an optical diameter of about 4 arcsec. If it lies at a redshift of z=0.5, then this corresponds to about 25 kpc, a size comparable to the size of the Milky Way Galaxy. Given its brightness and optical angular diameter, a higher redshift appears not to be very likely.

2.1.3 The final sample

Putting all information together, my final *ATCA* sample contains 12 targets (Table 2.2), representing approximately 1/3 of the present world sample of well-identified short-GRB host galaxies (Berger 2014).

Figure 2.2 summarizes the 12 targets observed with *ATCA* and indicates which are host

Table 2.1: Host galaxies of short GRBs in the *WISE* satellite archive (all-sky).

GRB (1)	Decl. (2)	W1 (3)	W2 (4)	W3 (5)	W4 (6)	W1-W2 (7)	W2-W3 (8)	z (9)
050724 G1	−27	15.35±0.05	15.41±0.13	>12.37	>8.42	−0.06 ± 0.14	<3.04	0.258
060502B	+52	15.29±0.03	14.94±0.04	12.88±0.35	>9.65	0.35 ± 0.05	2.06 ± 0.35	0.287
070429B	−32	17.38±0.15	>16.68	>12.44	>9.01	<0.70	–	0.902
070724	−18	17.09±0.14	16.79±0.37	>12.63	>9.08	0.30 ± 0.40	<4.16	0.394
070729 G1	−39	16.54±0.05	16.69±0.18	>13.22	>9.34	−0.15 ± 0.19	<3.47	–
..... G3	−39	16.23±0.04	16.22±0.12	>12.72	>9.63	0.007 ± 0.05	<3.08	–
071227	−55	15.58±0.03	15.15±0.05	11.88±0.16	>9.70	0.43 ± 0.06	3.27 ± 0.17	0.381
100206A	+13	15.73±0.06	15.13±0.11	10.76±0.09	>8.57	0.60 ± 0.13	4.37 ± 0.14	0.407
100816A	+26	17.15±0.17	>16.95	>12.41	–	<0.20	–	0.804
111222A	+65	13.24±0.02	13.15±0.02	>12.63	>9.08	0.09 ± 0.03	<0.52	–
130603B	+17	17.05±0.11	16.95±0.37	>12.53	>8.91	0.10 ± 0.39	<4.42	0.356
150101B	−10	13.43±0.03	13.18±0.03	12.39±0.48	>8.78	0.25 ± 0.04	0.79 ± 0.48	0.134
150424A G1	−26	16.44±0.07	16.10±0.17	>12.12	>8.69	0.34 ± 0.18	<3.98	0.3
161104A	+51	13.13±0.02	13.06±0.03	12.27±0.21	>9.49	0.07 ± 0.04	0.79 ± 0.21	0.79?

Notes: WISE filters are centered at 3.35 (W1), 4.60 (W2), 11.56 (W3) *and* 22.08 (W4) μm. All magnitudes are in the Vega photometric system. Listed here are all short-GRB host galaxies and host-galaxy candidates with detections in at least one of the four *WISE* bands (Wright et al. 2010). Upper limits are given according to the *WISE* catalog. Column #2 gives the Declination (J2000), #9 provides the redshift of the suspected short-GRB host galaxy. In two cases (GRB 070729, 111222A) no precise redshift of any host-galaxy candidate is known.

galaxies (HGs) and which are host-galaxy candidates (HGCs). Several hosts from GRBs from the years 2005–2010 have very deep optical imaging data (partly obtained during this work with VLT/FORS2 and *GROND*) which reveal the morphological nature, the angular and spatial size as well as the brightness of these galaxies.

The enhanced *Swift*/XRT error circle data are taken from `http://www.swift.ac.uk/xrt_positions/` (Evans et al. 2009). Since the data on this website are sometimes updated without any notice, in the following all reported XRT coordinates and error circle radii refer to early January 2017. All *Swift*/XRT error radii represent the 90% confidence level.

In all cases (including all HGCs), the angular distance between the OT or the border of the XRT error circle and the outer regions of the suspected host is between $<$ 1 and $\sim$ 15 (GRB 061201). These distances correspond to projected spatial distances between $\sim$1 and 30 kpc (largest distances: GRB 061201, 070729, 080123, 130515A) Assuming space velocities for NS-NS binaries of up to 100 to 200 km s^{-1} (Sect. 1.3.2), this would correspond to travel distances of 10 to 20 kpc after 100 Myr. Distances as large as 30 kpc would then lie close to the border line where a potential physical connection to such an old star-forming activity could be considered.

Only five out of the 12 bursts discussed here have a secure identification of their host (GRB 050709, 050724, 061006, 071227, 080905A). In these five cases an optical afterglow was found

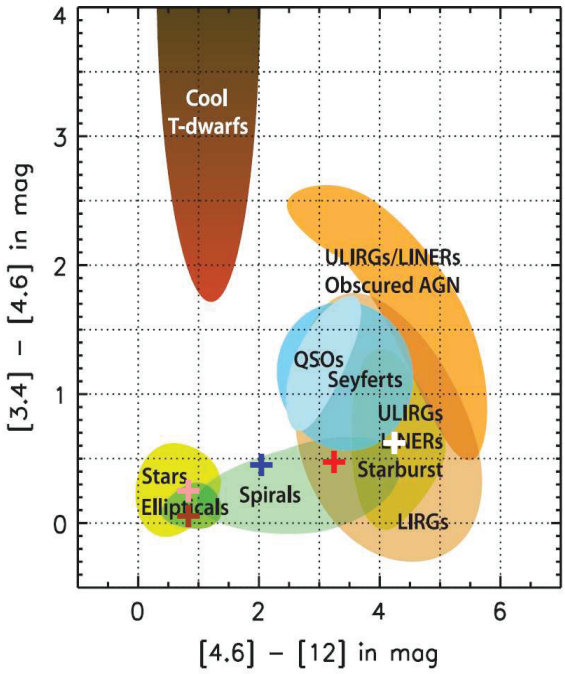

Fig. 2.1: *WISE* color-color diagram (adapted from Wright et al. 2010) and the position of the five short-GRB hosts detected by the *WISE* satellite (all-sky). The host of GRB 071227 (in red) and 100206A (in white) are falling in or close to the starburst category but only the first target is visible for *ATCA*. The host of GRB 060502 (in blue) is a spiral galaxy. The suspected hosts of GRB 150101B (in pink) and 161104A (in brown) lie in the region of elliptical galaxies. Magnitudes are given in the Vega magnitude system.

Table 2.2: *ATCA* target list.

GRB (1)	z (2)	Ref. (3)	RA, Decl. (J2000) (4)	T_{90} (5)	Ref. (6)	OT? (7)	$E(B-V)$ (8)
050709	0.1606	[1]	23:01:26.96, −38:58:39.5	70 ± 10 ms	[2]	Y	0.01
050724	0.258	[3]	16:24:44.36, −27:32:27.5	3.0 ± 1.0 s	[4]	Y	0.61
061006	0.4377	[5]	07:24:07.66, −79:11:55.1	0.42 s	[6]	Y	0.32
061201	0.111	[7]	22:08:32.09, −74:34:47.1	0.9 ± 0.1 s	[8]	Y	0.08
070729	0.5..1.0 ph	[9]	03:45:15.32, −39:19:26.4	1.5 s	[10]	N	0.02
070809	0.2187	[11]	13:35:04.55, −22:08:30.8	1.3 ± 0.1 s	[12]	Y	0.09
071227	0.381	[13]	03:52:31.26, −55:59:03.5	1.8 ± 0.4 s	[14]	Y	0.01
080123	0.496	[15]	22:35:46.10, −64:54:03.2	0.5 ± 0.1 s	[16]	N	0.03
080905A	0.1218	[17]	19:10:41.73, −18:52:47.3	1.1 ± 0.1 s	[18]	Y	0.14
100628A	0.102	[19]	15:03:52.41, −31:39:30.2	36 ± 9 ms	[20]	N	0.17
130515A	0.5..1.0 ph	[21]	18:53:45.82, −54:16:46.9	0.6 ± 0.1 s	[22]	N	0.07
150424A	0.2981	[23]	10:09:13.38, −26:37:51.5	0.5 s	[24]	Y	0.06

Notes: Columns #2,3 give the redshift, and the corresponding reference. A "ph" stands for a photometric redshift estimate. Column #4 gives the coordinates used for the *ATCA* pointing. Column #5 provides the burst duration T_{90} in the *Swift*/BAT energy band, column #7 states if an optical afterglow was found for this burst (Y) or not (N). Column #8 provides the Galactic reddening (in magnitudes) along the line of sight (Schlegel et al. 1998). *References:* [1] Price et al. (2005), [2] Boer et al. (2005), [3] Prochaska et al. (2005), [4] Barthelmy et al. (2005b), [5] Berger et al. (2007a), [6] Urata et al. (2006), [7] Berger (2006), [8] Stratta et al. (2007), [9] this work, [10] Guidorzi et al. (2007a), [11] Perley et al. (2008), [12] Barthelmy et al. (2007), [13] D'Avanzo et al. (2007), [14] Sakamoto et al. (2007a); Sato et al. (2007), [15] Leibler & Berger (2010), [16] Ukwatta et al. (2008b,b), [17] Rowlinson et al. (2010), [18] Cummings et al. (2008), [19] Cenko et al. (2010), [20] Immler et al. (2010), [21] this work, [22] Malesani et al. (2013), [23] Castro-Tirado et al. (2015); Tanvir et al. (2015), [24] Beardmore et al. (2015).

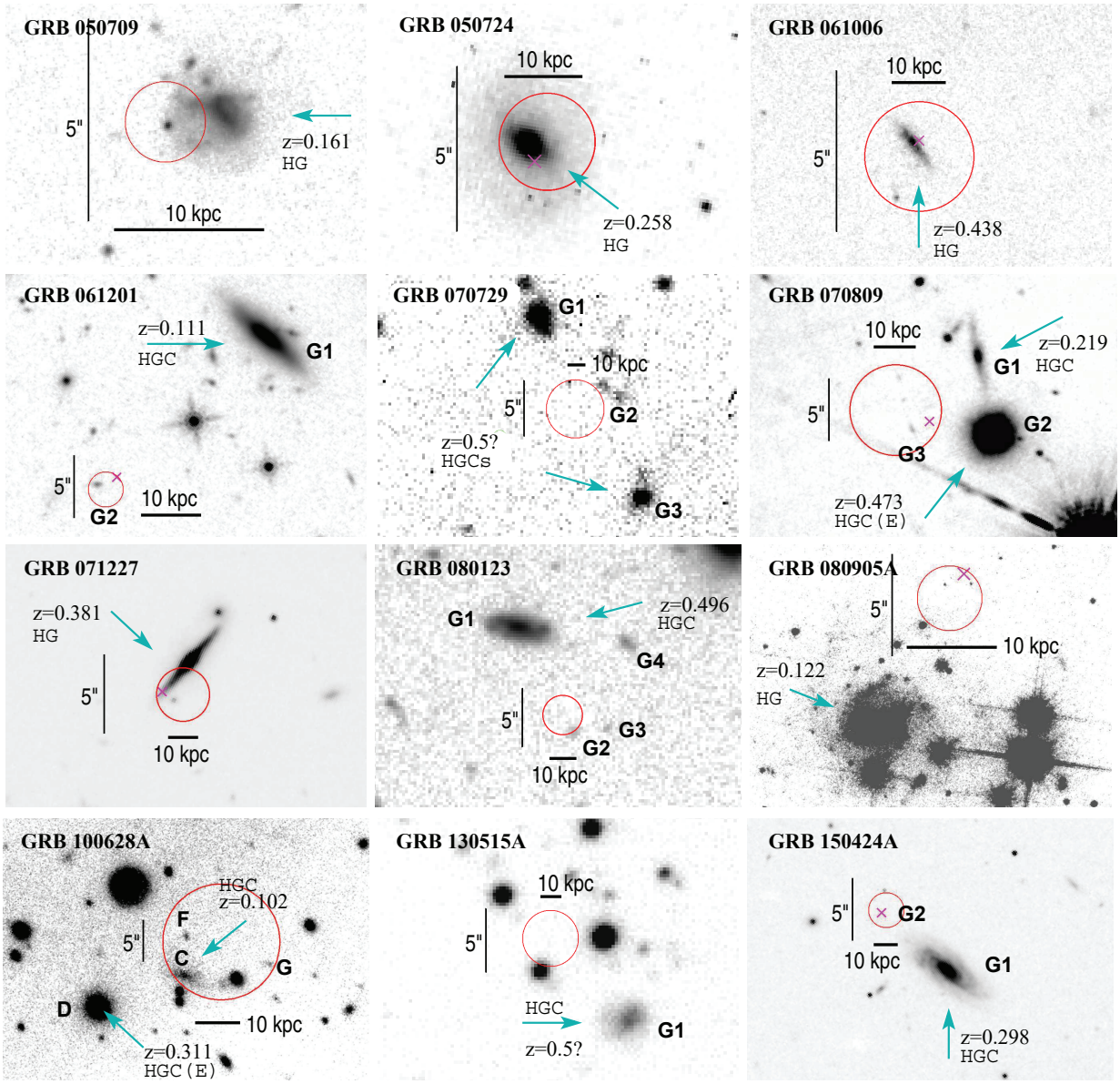

Fig. 2.2: The 12 host galaxies (HGs) and host-galaxy candidates (HGCs) which were the target of my *ATCA* survey. In red is shown the corresponding *Swift*/XRT error circle (90% c.l.). If there was an optical transient (OT) then its position is indicated by a cross (in pink color). Only in the case of GRB 050709 the OT is visible as a bright spot in the XRT error circle. In all other cases the underlying optical image was taken when the OT had already faded away. The arrows and corresponding redshifts point to the HG or a HGC, even if a second and much fainter candidate was found (GRB 061201, 070729, 150424A). For GRB 070809 and 100628A a second bright HGC exists which is an elliptical galaxy, indicated by an additional 'E'. All other HGs and HGCs, except the host of GRB 050724, are either irregulars or late-type galaxies with a clearly visible disk component. The size of the vertical scale bar is 5 arcsec in each case. The size of the horizontal scale bar is 10 kpc at the redshift of the corresponding HG or HGC (in the case of an additional elliptical HGC the redshift of the non-elliptical galaxy was used). East is left, North is up.

(this means a subarcsec positional accuracy) and optical images reveal a galaxy underlying the position of the optical transient. Moreover, there is no other HGC in the field.

In the remaining seven cases the observational situation is different because of various reasons. In three cases an optical afterglow could be localized with high precision and a very faint galaxy could be identified very close to the optical transient (GRB 061201, 070809, 150424A), but there is also at least one relatively bright galaxy nearby. Applying Eq. (1.1) shows that also these galaxies have a relatively high probability for beeing the host. Finally, in four cases no observed optical afterglow could be found, only an X-ray afterglow could be detected. Then there is no subarcsec precise localization, only an X-ray error circle with a radius of some arcsec is known (GRB 070729, 080123, 100628A, 130515A). If the field contains several galaxies then the procedure discussed in Sect. 1.3.2 is used to identify HGCs (Eq. 1.1).

The calculated chance coincidence probabilities (Eq. 1.1) are presented in Table 2.3. In most cases, with the exception of GRB 070729, the brightest galaxy has a small probability of $p < 0.1$. In other words, the probability that this is the host, $(1 - p)$, is larger than 0.9. In several cases the brightest galaxy is even the most likely host candidate.

The field of GRB 070729 is an exception here. The position of its *Swift*/XRT error circle (calculated by the *Swift* team) underwent several iterations so far (Sect. 4.4), suggesting that its position and radius is not well known (within a range of some arcsec). Moreover, optical multi-color photometry based on *GROND* data shows that at least two HGCs are very red and one is even forming stars at a high rate (Sect. 4.4). Therefore, it was worth to explore these host galaxies in the radio band.

As noted beforehand, GRB 150424A might be a special case as well (Sect. 4.9). The chance coincidence probability (p) for the faint HGC *G2* is very small. This value (p) is also very small for the much brighter galaxy *G1* (z=0.298). Even though Tanvir et al. (2015) estimate for *G2* a redshift of $z > 0.7$, one might still have some doubt on this value based on rather rough photometry. A simple hypothesis to solve this conundrum would be to assume that *G2* is a satellite galaxy of *G1*. Although this hypothesis cannot be proved conclusively, the radio observations can at least check if *G1* appears in the radio band, i.e., if it shows evidence for optically hidden star-forming activity near the GRB explosion site.

To summarize, it is well justified to observe short-GRB fields which have more than one HGC. The radio observations can help to reveal if once of these HGCs is special in some sense (e.g., a high star-formation rate). Optically faint and therefore possibly cosmologically remote HGCs might not be detectable for *ATCA* but optically bright and hence possibly nearby HGCs could show up in the radio band.

Table 2.3: Chance coincidence probabilities for those seven GRBs where only host-galaxy candidates are known.

GRB (1)	Gal. (2)	RA (J2000) (3)	Decl. (4)	$E(B-V)$ (5)	mag (6)	Filter (7)	Ref. (8)	r (9)	p (10)
061201	G1	22:08:29.10	−74:34:35.8	0.08	18.17	r	[2]	16.3	0.03
061201	G2	22:08:32.50	−74:34:47.7		∼25.5	r	[2]	1.8	0.10
070729	G1	03:45:16.32	−39:19:12.3	0.02	22.74±0.07	r	[1]	10	0.36±0.02
070729	G2	03:45:15.70	−39:19:18.9		23.47±0.15	r	[1]	2.6	0.05±0.01
070729	G3	03:45:15.50	−39:19:28.5		23.62±0.16	r	[1]	10	0.58±0.04
070809	G1	13:35:04.22	−22:08:27.4	0.09	21.7±0.03	r	[3]	6.5	0.07±0.01
070809	G2	13:35:04.14	−22:08:33.5		19.89±0.02	r	[4]	5.0	0.01
070809	G3	13:35:04.64	−22:08:31.8		25.0±0.3	r	[1]	1.5	0.05±0.01
080123	G1	22:35:46.92	−64:53:55.1	0.03	21.01± 0.01	r	[1]	8.2	0.08±0.01
080123	G2	22:35:46.18	−64:54:04.1		25.52± 0.17	r	[1]	1.7	0.10±0.01
080123	G3	22:35:45.73	−64:54:03.8		25.73± 0.20	r	[1]	4.0	0.50±0.05
080123	G4	22:35:45.48	−64:53:56.4		23.49± 0.09	r	[1]	8.2	0.41±0.02
100628A	C	15:03:52.81	−31:39:33.6	0.17	∼21.5	i'	[5]	6.0	0.07
100628A	G	15:03:52.02	−31:39:32.3		∼23.8	i'	[5]	5.0	0.64
100628A	F	15:03:52.80	−31:39:28.8		∼24.1	i'	[5]	4.5	0.77
100628A	D	15:03:53.59	−31:39:37.8		∼20.2	i'	[5]	17	0.05
130515A	G1	18:53:44.88	−54:16:50.9	0.07	∼21.2	r	[1]	6.0	0.04
150424A	G1	10:09:13.00	−26:37:55.9	0.06	20.15±0.05	r	[1]	6.3	0.022±0.001
150424A	G2	10:09:13.37	−26:37:51.3		∼26.8	r	[6]	0.2	0.004

Notes: Most columns are self-explanatory. Column #2: for the naming see Fig. 2.2. Column #5 gives the Galactic reddening along the line of sight (in mag; Schlegel et al. 1998). Apparent magnitudes in column #6 are AB magnitudes. Column #9 is the angular distance to the position of the OT or to the center of the XRT error circle (in arcsec). Column #10 gives the chance coincidence probability p to find a galaxy of the given magnitude in an area with radius r on the sky (Eq. 1.1). Probabilities have been calculated based on galaxy number counts in the R band by Hogg et al. (1997) and in the Sloan i band by Henriques et al. (2012). *References*: [1] this work, [2] Fong & Berger (2013), [3] Perley et al. (2008), [4] Leibler & Berger (2010), [5] Nicuesa Guelbenzu et al. (2015), [6] Tanvir et al. (2015).

2.2 Observations and data reduction

Table 2.4 summarizes the *ATCA* radio-continuum observations performed during this work (programme ID C2840, PI: A. Nicuesa Guelbenzu). All observations were carried out in the 5.5 and 9.0 GHz bands (corresponding to 6 and 3 cm) using the upgraded CABB detector (Wilson et al. 2011) and all six 22-m antennae with the 6 km baseline in order to achieve the best possible angular resolution. When possible I stayed on target between 10 and 12 hours in order to get the best coverage of the *uv* plane as well as the deepest sensitivity.

The general observing procedure was as follows:

1. Calibrate the bandpass and the flux at the beginning of the observing run. For *ATCA* the recomended calibrator for flux as well as bandpass is PSR 1934–638. It is a bright and for *ATCA* well observable source with a nearly constant radio flux and a well known spectral

Table 2.4: Log of the *ATCA* observations.

GRB (1)	Date obs. (2)	$t_{\rm obs}$ (3)	Flux calib. (4)	Phase calib. (5)
050709	24-07-2013	10.4 hr	1934–638	2244–372
050724	24-10-2015	10.4 hr	0823–500	1622–253
061006	20-07-2013	7.0 hr	1934–638	0637–752
061201	21-07-2013	11.5 hr	0823–500	2142–758
	26-07-2013	3.2 hr	1934–638	2142–758
	23-07-2013	0.7 hr	1934–638	2142–758
070729	24-09-2015	11.0 hr	0823–500	1934–638
070809	19-06-2013	9.5 hr	1934–638	1308–220
071227	26-07-2013	11.3 hr	1934–638	0308–611
080123	25-07-2013	8.7 hr	1934–638	2353–686
080905A	20-07-2013	1.5 hr	1934–638	1908–201
	25-10-2015	9.0 hr	1934–638	1908–201
100628A	23-07-2013	10.8 hr	1934–638	1451–375
130515A	26-10-2015	7.1 hr	1934–638	1824–582
150424A	19-06-2015	1.8 hr	1934–638	1034–293
	24-10-2015	3.2 hr	0823–500	1034–293

Notes: Column #2 provides the date of the start of the observations, column #3 gives the time on target (host galaxy). Column #4: The primary calibrators are 0823–500 at coordinates RA, Decl. (J2000) = 08:25:26.869, −50:10:38.49 and PKS 1934–638 at RA, Decl. (J2000) = 19:39:25.026, −63:42:45.63. Preferentially, PKS 1934–638 was observed for bandpass and flux calibration. Column #5: For the coordinates of the phase calibrators see `https://www.narrabri.atnf.csiro.au/calibrators/c007/atcat.html`.

energy distribution in the *ATCA* bands. The bandpass calibration is similar to the flatfield procedure for optical observations. Because the flux of the calibrator is known it can be used to determine the absolute flux density scale.

2. Calibrate the phase of the interferometer by observing a relatively bright source next to the target within reasonable time intervales. Since the science target was observed in many cases for almost ∼10 hours, its altitude was constantly varying. Consequently, the phase shift among the individual antennas of the interferometer is not stable. For observations in the 5.5 and 9.0 GHz band it is sufficient to perform the phase calibration once per hour. It is performed by observing a well documented bright radio source which should be located not more than a few degrees away from the science target. During my observations I observed the phase calibrator each hour for 7 min followed by the science target for 53 minutes.

3. Finish an observing run by visiting the flux calibrator again to be on the safe side in case the first data suffer problems (e.g., RFI). It happened that at the end of the observations PSR 1934–638 was not visible anymore. Then 0823–500 was observed (and vicy versa: If

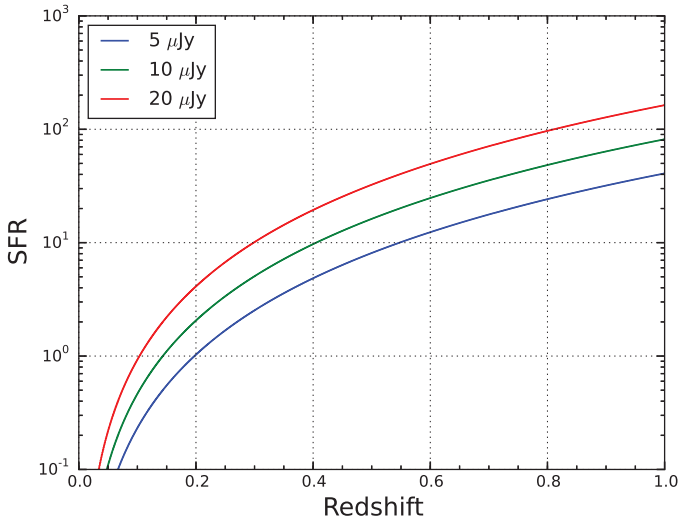

Fig. 2.3: Theoretical star-formation rate (SFR; $M_\odot$ yr^{-1}) as a function of redshift for different sensitivity limits in the 5.5 GHz band. The calculations are based on Eq. (2.1), which connects radio flux with radio-SFR, and assumed a spectral energy distribution of a star-forming region according to $F_\nu \sim \nu^{-\beta}$, with β=0.7. Here and in the following I adopted a ΛCDM cosmology with a Hubble constant H_0 = 68 km s^{-1} Mpc^{-1} and density parameters Ω_M = 0.31 and Ω_Λ = 0.69 (Planck Collaboration et al. 2016).

I started with 0823–500 then I tried to finish with PSR 1934–638).

According to the *ATCA* sensitivity calculator[3], for ∼10 hr on target, and using the full CABB bandwidth, the expected 1 $\sigma_{\rm rms}$ at 5.5 GHz goes from ∼ 6 μJy[4] beam^{-1} (with robust[5]=0) to ∼ 4 μJy beam^{-1} (with robust=2). Similar values are found for 9.0 GHz.

For 5.5 GHz this corresponds to an unobscured 3σ SFR limit of ∼ 0.7 – 25 $M_\odot$ yr^{-1} (per beam) for redshifts between z=0.1 and 0.5 (Fig. 2.3). In other words, for low-redshifts *ATCA* can find very low star-formation rates and up to median redshifts it can identify potential starburst galaxies within a, say, 10-hr exposure. In principle, even at z=1 *ATCA* observations could reveal star-forming activities down to ∼100 $M_\odot$ yr^{-1}. As such the *ATCA* observations can answer the question what fraction of short-GRB host galaxies is forming stars at a high rate. If this fraction would be large then a physical link between recent star-formation activity and the formation of short-GRB progenitors would be indicated.

Data reduction was performed in a standard manner[6] using the Multichannel Image Reconstruction, Image Analysis and Display (Miriad) software package[7] (Sault et al. 1995). Miriad consists of a collection of individual tasks that have the form of unix-executables which can be invoked either by unix command lines or by shell scripts.

All data were cleaned from RFI using the `pgflag` routine. The effective bandwidth was then reduced by ∼ 10%. Deconvolution of the obtained data was performed using the `mfclean` procedure. In doing so, the calibrated and RFI-cleaned visibilities were finally Fourier-transformed

[3] `http://www.narrabri.atnf.csiro.au/myatca/interactive_senscalc.html`
[4] `1 Jy = 10^-26 Ws s^-1 m^-2 Hz^-1`
[5] The robust parameter is in detail explained in Sect. 7.3.3.
[6] `using http://www.atnf.csiro.au/computing/software/miriad/tutorials.html`
[7] `http://www.atnf.csiro.au/computing/software/miriad/`

using the Briggs[8] robust weighting option (Briggs 1995), varying this parameter between `0.5`, `1.0`, and `2.0` and selecting among these the one that gave the best signal-to-noise ratio.

The synthesized beam size varied from target to target. At 5.5 GHz and for a robust parameter of 0.4 it was smaller than 3 arcsec in both directions for three targeted fields (GRB 061201, 071227, 080123), while in three cases it was between 7 and 12 arcsec in one direction (GRB 070809, 080905A, 150424A; Table 7.2). Appendix 7.3 provides a more detailed overview about the data reduction procedure and its individual Miriad commands.

2.3 Radio-derived star formation rates

As I have outlined in Sect. 1.2.4, radio-continuum observations of the hosts of long GRBs have been performed by several groups in the last 15 years using *ATCA* (Australia), the *VLA* (USA), the Westerbork Synthesis Radio Telescope (WSRT; The Netherlands) and the Giant Metrewave Radio Telescope (GMRT; India). Observations were performed between 1.4 and 9.0 GHz and star-formation rates have been derived using partly different equations.

Recently, Greiner et al. (2016) performed *ATCA* radio-continuum observations of 11 *long*-GRB host galaxies in the 2.1 GHz band, collected all previously published results (Berger et al. 2003; Michałowski et al. 2008; Stanway et al. 2010; Hatsukade et al. 2012; Michałowski et al. 2012; Perley & Perley 2013) and reanalyzed these within the same theoretical framework. In doing so, Greiner et al. (2016) provided a comprehensive summary of all known SFRs for long-GRB host galaxies in the radio band.

In order to compare the SFRs of my ensemble of *short*-GRB host galaxies with these data of *long*-GRB host galaxies, I followed the approach of these authors and calculated the radio-based SFRs (and upper limits) using the same equation:

$$\left(\frac{\mathrm{SFR_{Radio}}}{\mathrm{M_\odot/yr}}\right) = 0.059 \left(\frac{F_\nu}{\mu\mathrm{Jy}}\right) (1+z)^{-(\beta+1)} \left(\frac{d_L}{\mathrm{Gpc}}\right)^2 \left(\frac{\nu}{\mathrm{GHz}}\right)^{-\beta}, \tag{2.1}$$

where F_ν and ν are the observed radio flux and frequency, respectively, z is the redshift, d_L the luminosity distance, and β the spectral slope.

I have also checked other relationships published in the literature like equation 6 in Bell (2003) and equation 15 in Haarsma et al. (2000). The Bell equation directly relates the SFR to the radio flux of a galaxy at 1.4 GHz. Since I have 5.5/9.0 GHz data (luminosities) at hand, I calculated (estimated) the radio flux of a galaxy at 1.4 GHz by assuming synchrotron radiation

[8] see Sect. 7.3.3

($F_\nu \sim \nu^{-\beta}$) with β=0.7. The Haarsma equation contains the sum of radio emission from SN remnants as well as thermal radio emissions from H II regions. The approach of Bell (2003) and Haarsma et al. (2000) leads to similar results as Eq. (2.1), within a factor of about 2.

In the following, the so-called radio-derived SFRs will be compared with optically-derived SFRs. In the majority of cases the corresponding values are taken from the literature and are based on emission-line spectroscopy. In four cases the optical SFR was derived either from spectroscopic observations performed during this work or by a re-analyis of archived data (GRB 050709, 071227, 100628A, 150424A). It was based on the following equations (e.g., Kennicutt 1998; Savaglio et al. 2009):

$$\mathrm{SFR(H}\alpha) = 4.39 \times 10^{-42}\, L(\mathrm{H}\alpha)_{\mathrm{corr}}\ \mathrm{M}_\odot\ \mathrm{yr}^{-1}\,, \tag{2.2}$$

$$\mathrm{SFR(H}\beta) = 12.6 \times 10^{-42}\, L(\mathrm{H}\beta)_{\mathrm{corr}}\ \mathrm{M}_\odot\ \mathrm{yr}^{-1}\,, \tag{2.3}$$

$$\mathrm{SFR([O\,II])} = 5.54 \times 10^{-42}\, L([\mathrm{O\,II}])_{\mathrm{corr}}\ \mathrm{M}_\odot\ \mathrm{yr}^{-1}\,. \tag{2.4}$$

Here L (in units of erg s^{-1}) is the corresponding luminosity in the (redshifted and extinction-corrected) line which is related to the observed and extinction-corrected line flux F by $L = 4\pi\, d_L^2 \times F$. In principle all these equations should give the same result. The wavelengths in the bluer part of the spectrum are more affected by extinction by dust, while those in the redder part can be shifted out of the optical window, depending on the redshift of the source.

In four cases (GRB 070729, 071227, 130515A, 150424A), the optical SFR was also estimated based on either a `Le Phare` or a GRASIL analysis of the broad-band spectral energy distribution (SED) of the galaxy.

Chapter 3

Results I: Targets with radio detection

In the first part of this chapter I report about *ATCA* observations of the host galaxy of GRB 050709. This was the first short burst with a detected optical afterglow (Hjorth et al. 2005b). Besides, it is still one of the cosmologically nearest short GRBs (z=0.1606; Fox et al. 2005; Price et al. 2005; Covino et al. 2006). Hubble Space Telescope (*HST*) imaging revealed that its host shows a disturbed morphology.

In the second part I focus on the host galaxy of GRB 071227. Also in this case is the burst position well known since an optical afterglow was detected (D'Avanzo et al. 2009). Broad-band photometry of the host suggested a notable internal extinction (Leibler & Berger 2010). Since the host is located at a relatively low redshift ($z = 0.381 \pm 0.001$; D'Avanzo et al. 2009), it was a promising target to search for radio emission caused by star-forming activity.

The third part finally deals with the results of a comprehensive multi-wavelength observing campaign to reveal and study the putative host galaxy of the short GRB 100628A. This burst has no detected optical afterglow but an arcsec-sized X-ray afterglow error circle. I made use of *GROND* multi-color photometry, long-slit spectroscopy with VLT/FORS2, VLT/X-Shooter as well as *ATCA* radio-continuum observations in order to study this GRB field.

3.1 The morphologically disturbed host of GRB 050709

The detection and subsequent localization of the short GRB 050709 was one of the scientific highlights of the *High Energy Transient explorer* (*HETE−2*; Ricker 1997) mission. GRB 050709 was the first short burst for which an optical afterglow was found (Hjorth et al. 2005b) and the second short burst with a detected X-ray afterglow (Cameron et al. 2005; Fox et al. 2005; Villasenor et al. 2005). With a redshift of z=0.1606 (Fox et al. 2005; Price et al. 2005; Covino et al. 2006) it is still one of the cosmologically nearest short GRBs detected so far (e.g., Berger

2014). Its host galaxy is therefore an ideal target to explore the environment of a GRB progenitor on kpc scales.

3.1.1 The burst and its afterglow

GRB 050709 triggered the *HETE−2* satellite at 22:36:37 UT on 9 July 2005. It consisted of a single hard spike with a duration of $T_{90} = 70 \pm 10$ ms in the 30–400 keV band. Its peak energy was 83 keV (Boer et al. 2005; Villasenor et al. 2005). About ∼30 s after this spike the burst was followed by a soft ($\lesssim$10 keV) extended emission lasting for ∼150 s. It was this soft, second component that allowed *HETE−2* to localize a possible X-ray afterglow with its *Soft X-ray Camera* at coordinates RA, Decl. (J2000) = 23:01:30, −38:58:33, with a positional uncertainty of 1.34 arcmin (Butler et al. 2005).

Consecutive observations with the *Chandra X-ray Observatory* around 2.5 days after the burst led to the precise localization of its X-ray afterglow at coordinates RA, Decl. (J2000) = 23:01:26.96, −38:58:39.5 (±0.″5; Fox et al. 2005). Finally, optical follow-up observations performed 33 h after the GRB trigger with the Danish 1.5 m telescope located on La Silla resulted in the identification of a faint ($R \sim 23$ mag), fading source at RA, Decl. (J2000) = 23:01:26.957, −38:58:39.76 (±0.″25; Hjorth et al. 2005b), coincident with the *Chandra* afterglow position. The optical transient was located in the outskirts of an irregular host, about 1.″4 away from its optically brightest region. For a measured redshift of z=0.1606 (Fox et al. 2005; Price et al. 2005; Covino et al. 2006) this corresponds to a projected distance of 4.0 kpc. No supernova component was found up to 18 days after the burst down to deep optical flux limits, supporting the short-burst nature of this event (Hjorth et al. 2005b).

3.1.2 The host galaxy

Photometry: The host is a blue dwarf galaxy with an absolute magnitude $M_B = -16.9 \pm 0.1$. Its SFR based on its broad-band SED is about ∼0.1 $M_\odot$ yr^{-1} (Hjorth et al. 2005b). It is also detected in the NIR bands (Leibler & Berger 2010) but not in any band of the *WISE* satellite explorer. According to Leibler & Berger (2010), the observed broad-band SED of this galaxy points to a dominating stellar population with an age of about 2 Gyr and a stellar mass of $\log M_\star/M_\odot = 8.8$. In the galaxy sample discussed by these authors, $\log M_\star/M_\odot$ varies between 8.8 and 11.6 (their table 2), so the host of GRB 050709 is one of the less massive short-GRB host galaxies.

Multi-wavelength broad-band imaging of the host galaxy was performed with VLT/FORS1 and FORS2 (programme ID 075.D-0787, PI: G. Tagliaferri). Based on these images, the mor-

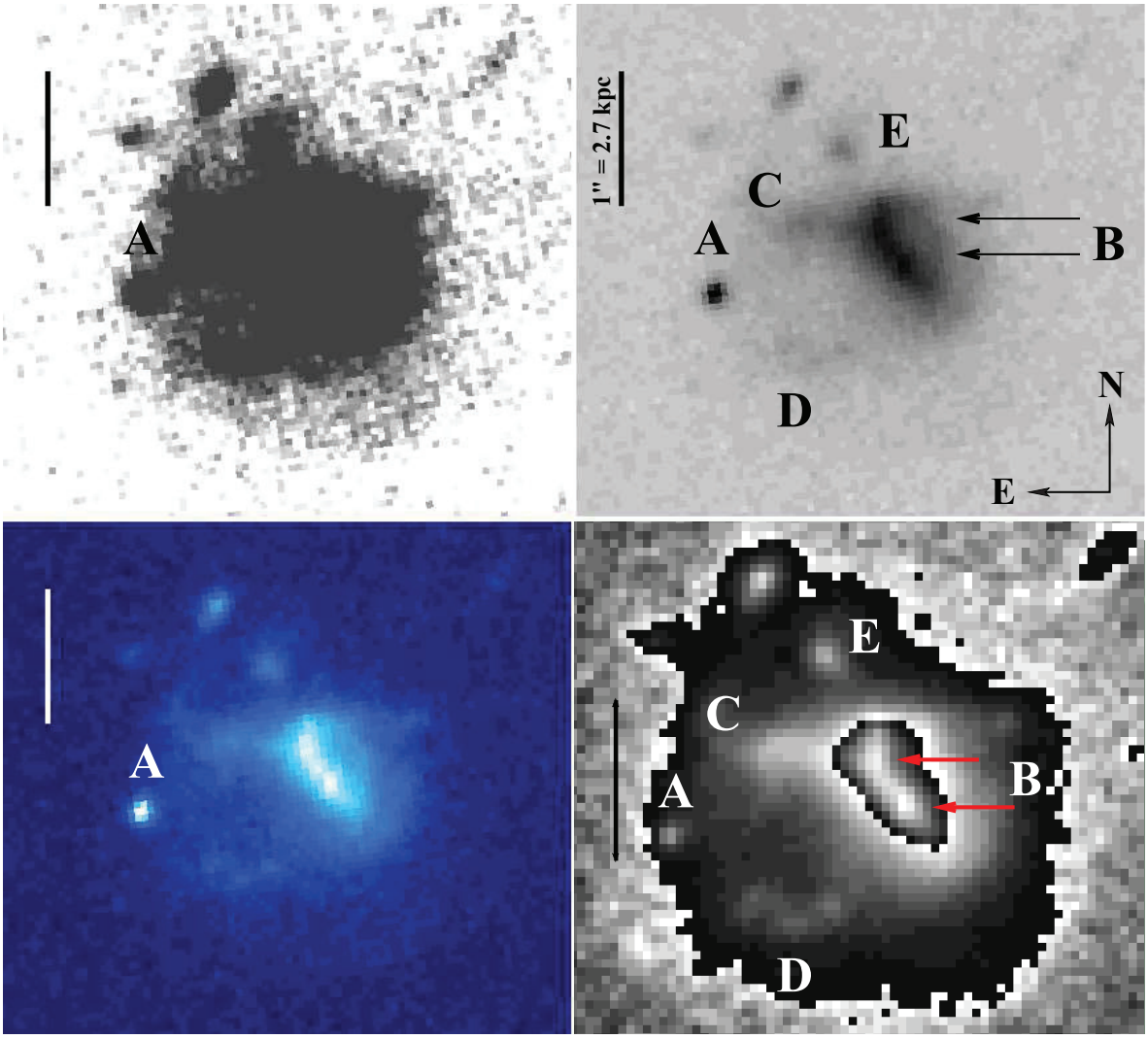

Fig. 3.1: HST/ACS F814W image (programme ID 10624, PI: D. Fox) of the host of GRB 050709 as well as its afterglow. The four subimages have different contrast parameters to emphasize the faintest as well as the brightest parts of the galaxy. Labels indicate the afterglow (A), the brightest part of the host, probably an interacting pair of galaxies (B), two tidal tails (C, D) and one of potentially several star-forming regions (E) placed along the tidal arms. The optical transient was located near a faint bridge between the northern and the southern tidal tails.

phology of the host galaxy cannot be studied in great detail however. Several HST image-observing campaigns were performed with the *Advanced Camera for Surveys* (ACS) right after the GRB trigger and up to one year later (programme ID 10624, PI: D. Fox). The afterglow was found to be located in a region with very low surface brightness and no evidence for star-forming regions.

I have combined all available archived *HST* images taken with the *F814W* filter and astrometrized them by using the USNO-B1.0 catalogue (Skiff 2002). In the combined optical image (~9 hours of observation) the host appears as an irregular object with signatures of galaxy-

galaxy interaction (Fig. 3.1). Its brightest optical part (B) has a size of approximately $1\farcs1 \times 0\farcs7$, corresponding to about 3.1×2.0 kpc^2. There are signs of at least two faint structures to which in the following I refer as (suspected) tidal tails. One is located at the N-E part and expands up to about $1''$, then curves (C) and seems to end up in an optically brighter, possibly star-forming region (E). A second tidal tail is located in the S-E part of the galaxy, fainter than the northern one and extends up to about $1\farcs5$ (D). The optical transient was located in a faint bridge between the northern and the southern tidal tail (Fig. 3.1).

Spectroscopy: VLT/FORS2 observed the host using the *300V* (~1.5 hr) and *600I* (~4 hr) grisms on 31 July 2005 (programme ID 075.A-0718; PI: L. Pellizza). Together, both spectra cover the wavelength range from 3800 to 9000 Å. The observations were performed at an airmass of ~1 and a seeing of 1 arcsec. The long slit was placed along the E-W axis of the galaxy and the slit width was 1 arcsec (see left panel in Fig. 3.2).

In order to check if at the position of the optial transient line emission from a star-forming region can be detected, I have re-reduced these spectra. Wavelength calibration was performed relative to He+Ar+Ne calibration lamps. *LTT6248* was the spectrophotometric standard star used to flux-calibrate the spectra. The spectra show emission lines from Hα, Hβ, the [O III] doublet as well as the [S II] doublet (see bottom panel in Fig. 3.2) at a common redshift of z=0.1606±0.0002, in agreement with the findings reported by Covino et al. (2006). If this line emission is due to star-formation activity, then the deduced SFR is not larger than 0.1 M$_\odot$ yr^{-1} (Table 3.1). Correcting for slit losses, it might be twice as high, in agreement with the conclusions reported in Fox et al. (2005), Covino et al. (2006), and Prochaska et al. (2006). No emission-line flux is detectable from the position where the GRB progenitor was placed ('A' in Fig. 3.1), implying that in this region the optical SFR is smaller than 0.1 M$_\odot$ yr^{-1}.

Table 3.1: Emission lines in the spectrum of the host galaxy of GRB 050709.

Line	Wavelength Å	z	Flux 10^{-17} erg s^{-1} cm^{-2}	SFR M$_\odot$ yr^{-1}
[O II] (3727.0)	4326.89	0.1609	19.0±0.9	0.07±0.003
Hβ (4861.3)	5641.40	0.1605	8.6±0.5	0.06±0.002
[O III] (4958.9)	5755.67	0.1606	9.5±0.6	–
[O III] (5006.8)	5810.31	0.1604	20.6±1.4	–
Hα (6562.8)	7615.87	0.1605	19.7±1.2	0.06±0.003
[S II](6717.0)	7795.80	0.1606	8.0±0.4	–
[S II](6731.3)	7814.87	0.1609	4.7±0.2	–

The second column gives the observed wavelength, the third the corresponding redshift, the forth the observed flux, and the last column the deduced SFR using Eqs. (2.2)-(2.4).

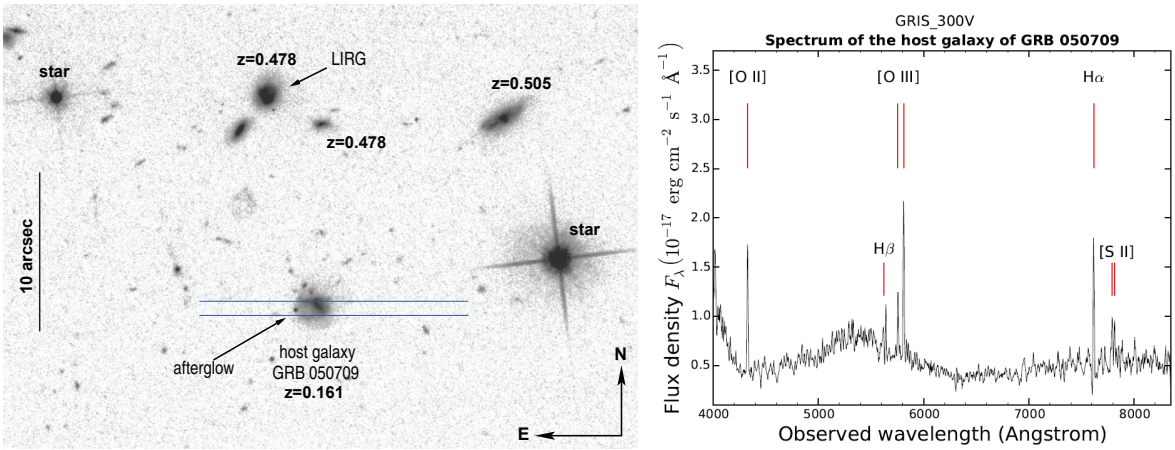

Fig. 3.2: *Left:* HST image of the field of GRB 050709. The blue lines show the slit width and position during the spectroscopic observations of the host of GRB 050709 (programme ID 075.A-0718, PI: L. Pellizza). The galaxy ∼13 arcsec north of the GRB host is a luminous infrared galaxy (LIRG; designated GALEXASC J230127.17-385825.6). In the *ATCA* data it shows up as a relatively bright 5.5 GHz source. The redshift I have measured (z=0.478) characterizes it as a background object. *Right:* 1D spectrum of the host galaxy of GRB 050709 (programme ID 075.D-0787, PI: G. Tagliaferri). Several emission lines are detected at a common redshift of z = 0.1606±0.002.

3.1.3 Was the GRB progenitor a collapsing massive star?

As discussed beforehand, spectroscopic observations reveal the presence of emission lines from which a star formation rate (SFR) of ∼0.2 $M_\odot$ yr^{-1} can be derived (Fox et al. 2005; Covino et al. 2006; Prochaska et al. 2006), provided that this emission is primarily caused by star-forming activity. Since such an SFR is substantially higher than what had been found for the host of the first well-localized short GRB 050509B (a giant E1 elliptical at a redshift of z = 0.225; Gehrels et al. 2005; Bloom et al. 2006), this led Covino et al. (2006) to speculate that the progenitor of GRB 050709 might have been located in a star-forming region.

Evidence for star-formation activity around the position of the optical transient is supported by the fact that the optical afterglow SED revealed a relatively high host-galaxy visual extinction along the line of sight, $A_V^{host} \sim 0.7$ mag (Prochaska et al. 2006; Ferrero et al. 2007; Kann et al. 2011). Such a value is more typical for the sight lines towards long GRBs which are linked to star-forming activity (Kann et al. 2010) than towards those of short bursts (e.g., Kann et al. 2011). In other words, the afterglow data point to the existence of substantial amounts of obscuring material in the vicinity of the GRB position.

A potential link of the progenitor of the short GRB 050709 to a star forming region could suggest that the burst is misclassified and in fact had its origin in a collapsing massive star. A good example of such case is the short GRB 090426 (at z=2.609). In the observer frame it had

a duration of T_{90} = 1.25±0.25 s (rest frame 0.33 s). However, several arguments have been put forward that GRB 090426 was due to a collapsar event rather than a NS-NS merger. The rather high afterglow luminosity and circumburst gas density as well as the GRB spectral and energy properties suggest that this burst was most likely due to a collapsar event (see Antonelli et al. 2009; Levesque et al. 2010a; Xin et al. 2010; Nicuesa Guelbenzu et al. 2011; Thöne et al. 2011).

In the case of GRB 050709 several arguments speak against such an interpretation as a collapsar. Firstly, in the high-energy band, its isotropic energy release ($E_{\gamma,\mathrm{iso}}$(25–2000 keV)$\sim 7 \times 10^{49}$ erg; Fox et al. 2005) is 2–3 orders of magnitude smaller than what is usually found for the long-GRB population. Furthermore, the GRB does not follow the Amati $E_{\mathrm{iso}} - E_{\mathrm{peak}}$ relation (Amati et al. 2008), which brings into relation the observed isotropic equivalent energy of the burst with its peak energy in the gamma-ray band. Not following this relation is a typical sign for short bursts. Secondly, the luminosity of its optical afterglow lies in the region occupied by other short-burst afterglows, which separate from the more luminous long-burst population (Ferrero et al. 2007; Kann et al. 2011). Thirdly, despite the relatively small redshift, no supernova component following the burst was detected down to very deep flux limits (Fox et al. 2005; Hjorth et al. 2005b; Kann et al. 2011), disfavoring its origin in a collapsing massive star.

3.1.4 *ATCA* radio observations of the host galaxy

Having in mind that the simplest interpretation of the observational data is that the GRB progenitor was placed in a dusty region, I performed *ATCA* radio-continuum observations of its host in the 5.5/9.0 GHz band. Observations were done on 24 July 2013. Bandpass and flux calibration was performed using *PKS B1934–638*, phase calibration by observing the source *2244–372* (F_ν(5.5 GHz) = 0.79 Jy, F_ν(9.0 GHz) =0.74 Jy; angular distance 3.48 deg). Altogether 10 such 1-hr cycles were executed.

The astrometry of the resulting 5.5 GHz radio image was double-checked by comparing the position of two known radio sources in the field with their published coordinates. These are the quasar *B2258–391* (measured peak flux 103 ± 10 μJy) and *NVSS J230132–385927* (measured peak flux 1160 ± 77 μJy). The *ATCA* positions of both sources were found to agree with their catalogued values to better than 0.″3 in right ascension and 0.″1 in declination.

Interestingly, at 5.5 GHz a radio source is detected in the eastern part of the GRB host galaxy with a flux density of F_ν = 24±7 μJy, assuming a point source (robust parameter = `2.0`; Fig. 3.3). This source is not detected in the 9.0 GHz band ($F_\nu < 15$ μJy; 3 σ), constraining the spectral slope ($F_\nu \sim \nu^{-\beta}$) between both bands to a rather broad range of β = 0.2 to 1.5 (within the 1σ

error of the flux at 5.5 GHz). At 5.5 GHz the radio source is centered at RA, Decl. (J2000) = 23:01:26.98, −38:58:39.6, with a positional uncertainty in RA of 0.″4 and in Decl. of 1.″0 (as it follows from the `imfit` task under Miriad). This position is 0.″3 in RA and −0.″1 in Decl. offset from the position of the optical (Hjorth et al. 2005b) and X-ray (Fox et al. 2005) afterglow. It lies ∼1.″5 east of the optically brightest region of this galaxy (projected distance 4.2 kpc), which is not detected (F_ν(5.5 GHz)< 15 μJy).

On the optical HST image (Fig. 3.1) the entire eastern region of the host appears very faint and is evident only when the contrast of the image is substantially enhanced. Optically brighter clumps exist (maybe additional star-forming regions), but mainly in the northern part (e.g., 'E'). The asymmetric shape of the radio flux contours suggests that some flux is coming from this region, and perhaps even from the south-western area, but the peak of the radio emission is clearly centred in the eastern part.

In order to look for possible diffuse low surface-brightness emission (e.g., Martinez Aviles et al. 2016), I applied a gaussian taper in the data reduction (Miriad `invert`, command option: fwhm). This increased the extended emission level to a peak flux of 40±5 μJy, suggesting that this is not a point source, since otherwise the peak flux would not increase.[1]

3.1.5 What is the nature of the radio source?

The radio source is not point-like and therefore it cannot be related to the GRB radio afterglow which, in any case, was not expected to be detectable anymore eight years after the burst. It also cannot be due to a potential late-time radio flare from non-relativistic ejecta related to a NS-NS merger (e.g., Margalit & Piran 2015). Given the redshift, for *ATCA* these sources would appear as point sources.

If the extended *ATCA* source is indicative for a (wide-spread) star-forming area, then using Eq. (2.1) the observed 5.5 GHz flux corresponds to an unobscured SFR in the eastern part of the host galaxy of $\sim 3\ M_\odot\ yr^{-1}$. Compared to the derived optical star-formation rate in this area of $< 0.1\ M_\odot\ yr^{-1}$, the radio observations would then suggest a substantial hidden star-forming activity. Within this context, the fact that the radio source is (within the errors) centered at the position of the GRB afterglow is formally very encouraging, as it might imply a physical link between the star-forming region and the GRB. Some caution is required with this interpretation, however.

The optical HST image suggests that the host of GRB 050709 is an interacting galaxy-galaxy

[1] I thank Dr. Mark Wieringa, Australia Telescope National Facility, CSIRO, Sydney, Australia, for pointing this out.

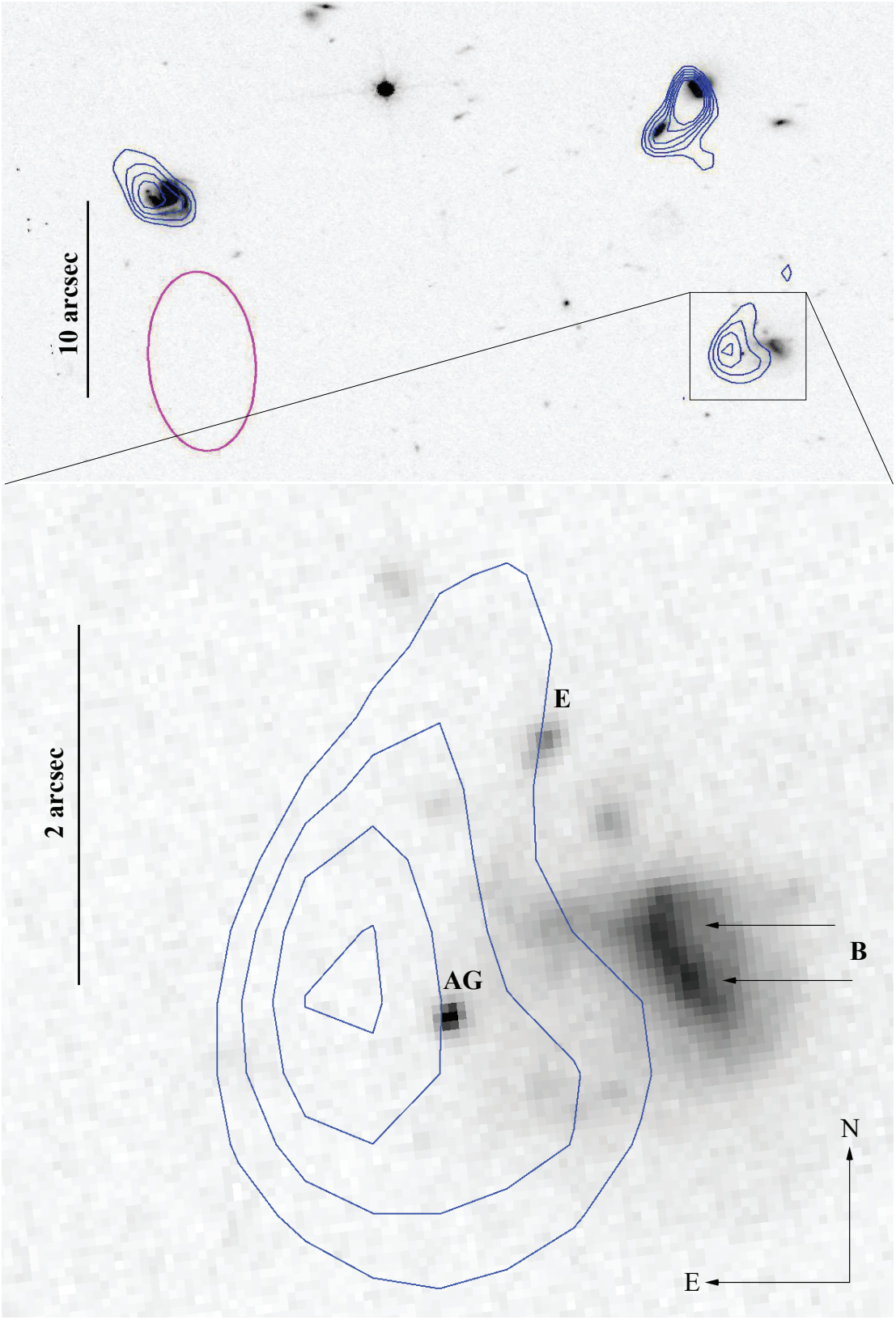

Fig. 3.3: *Top: ATCA* 5.5 GHz radio contours overlayed the HST image. Shown are only the galaxies nearest to the host of GRB 050709. Contour levels (in blue) correspond to F_ν= 3 to 5.5 times the image 1 $\sigma_{\rm rms}$ of 5.0 μJy beam^{-1} (in steps of 0.5 $\sigma_{\rm rms}$). The size of the synthesized beam (drawn in magenta) was $4\farcs55 \times 2\farcs26$, the beam position angle 3.8 deg (robust parameter 2.0). *Bottom:* Zoom-in, showing the GRB host galaxy. The afterglow (AG) is indicated.

system. A certain percentage, if not all, of the radio emission could then be due to shocked gas. As such the radio-continuum emission would trace the dynamical history of the interacting pair of galaxies (e.g., Condon et al. 1993). If this picture is correct, a physical link between the radio-continuum emission, star formation, and the GRB progenitor is not immediately apparent but the radio data reflect that the host of GRB 050709 is an interacting galaxy-galaxy system.

The observed emission-line flux ratios can be used to figure out if star formation is the main origin of the lines. Diagnostic diagrams have been developed for this purpose, whereby often the concept introduced by Baldwin et al. (1981) is used (e.g., Alatalo et al. 2016; Prieto et al. 2016). Applying this formalism to the FORS2 data given in Table 3.1[2], the observed log ([O III]/Hβ) flux ratio (=1.5) suggests that this is emission form shocked gas (for the diagnostic diagram see Rich et al. 2015). Indeed, in a recent study Donevski & Prodanović (2015) find that interacting galaxies show an excess of radio-continuum flux when compared to the far infrared domain. This flux is due to shocked gas. Nevertheless, one has to keep in mind that these FORS2 data do only refer to the optically brightest part of the host galaxy. It remains open whether this conclusion can also be drawn for the eastern part of the galaxy.

Numerical simulations show that during a galaxy-galaxy collision interstellar gas, dust as well as stars are expelled form the merging partners and form tidal structures, tails and bridges, a process that finally lasts some 10^7 to 10^8 years (e.g., Manthey et al. 2008; Renaud et al. 2015). In this respect, even if star formation is finally triggered in the resulting tidal tails, these structures could also contain members of the originally old stellar populations of the two colliding galaxies. Hence, the progenitor of GRB 050709 could have been the original member of the old stellar population of one of the two interacting galaxies. In other words, given the optical and radio data in-hand, evidence for a young GRB progenitor cannot be claimed. Even though the *ATCA* data are very promising, more detailed spectroscopic observations of the host galaxy are necessary in order to reveal the detailed physical properties of the interstellar medium at the GRB explosion site.

3.1.6 Summary of Section 3.1

The *ATCA* radio observations detect a faint, extended source in the eastern part of this galaxy where the optical transient was placed. If this radio source is due to star-forming activity then the radio SFR is ~5 $M_\odot$ yr^{-1}, which is substantially above the optically derived SFR and thus would reveal the presence of a large amount of obscured star formation. However, the radio source

[2] The Galactic reddening along the line of sight is negligible ($E(B-V)$ = 0.01 mag; Schlegel et al. 1998).

might have its origin in shocked gas produced in a galaxy-galaxy interaction as suggested by the observed log ([O III]/Hβ) emission line flux ratio and the disturbed morphology of the host. Further observations are needed here to distinguish between the star-forming interpretation and the shocked gas scenario.

3.2 The starburst host galaxy of GRB 071227

3.2.1 Archival observations of the GRB and its host galaxy

The burst and early afterglow data: GRB 071227 triggered *Swift*/BAT at 20:13:47 UT on 27 December 2007. The burst showed a main spike with a duration of T_{90}(15-350 keV) = 1.8 ± 0.4 s (Sakamoto et al. 2007a; Sato et al. 2007), followed by a softer extended emission for about 100 seconds (Sakamoto et al. 2007b). The prompt phase of the burst was also detected by *Konus-Wind* (with a duration of ~1.7 s, Golenetskii et al. 2007a) and *Suzaku-WAM* (T_{90} ~1.5 s, Onda et al. 2008), confirming in both cases the short-burst nature of this event.

Swift/XRT started to observe the event around 80 seconds after the GRB trigger and localized a bright X-ray afterglow at coordinates RA, Decl. (J2000) = 03:52:31.58, −55:58:59.9, with a small X-ray error circle of 3.″7 (radius, 90% c.l.). The final XRT error circle is located at RA, Decl. (J2000) = 03:52:31.20, −55:59:02.9 with an error of 1.″7.[3]

Swift/UVOT follow-up observations started 86 seconds after the GRB trigger and were performed with the white-band filter, leading to the discovery of a potential optical transient inside the XRT error circle at coordinates RA, Decl. (J2000) = 03:52:31.102, −55:59:00.65 (with a positional uncertainty of 0.6 arcsec; Cucchiara & Sakamoto 2007). Optical follow-up observations performed with the 6.5 m Magellan telescope revealed that this source is in fact not the afterglow but a galaxy with a magnitude in the *R* band of ~22 mag (Berger et al. 2007b). Further observations showed that this is an edge-on, late-type galaxy that clearly resolves into a bulge and a disk component (Leibler & Berger 2010). Based on optical spectroscopy with VLT/FORS2, its redshift was determined to $z = 0.381 \pm 0.001$. A modest SFR of ~0.6 $M_\odot$ yr^{-1} was deduced based on the observed [O II] emission line flux (D'Avanzo et al. 2009). The optical afterglow was identified via image subtraction using the FORS2 R_C-band images. The optical transient was located in the outskirts of the galactic disk, about 3 arcsec away from the center of its host, at a projected distance of about 15 kpc away from the galactic nucleus (D'Avanzo et al. 2009).

Unfortunately, the afterglow was not detected by GROND, even though first-epoch observa-

[3] http://www.swift.ac.uk/xrt_positions/00299787

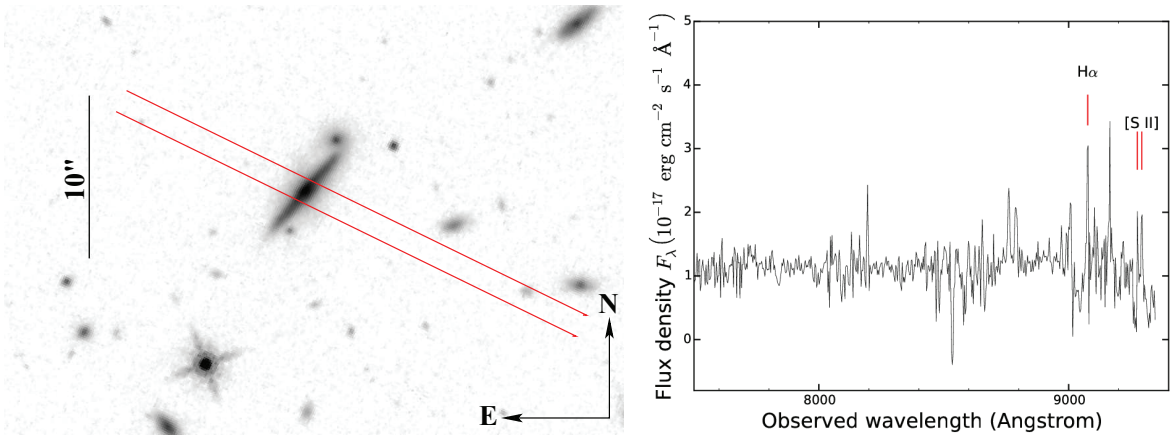

Fig. 3.4: *Left:* HST image of the GRB host galaxy (PI: A. Levan). The red lines show the position of the 1 arcsec slit during the FORS2 spectroscopy run (programme ID 080.A-0825; PI: A. Tagliaferri). It covered only around 40% of the galaxy. *Right:* Flux-calibrated spectrum of the host galaxy obtained with GRIS 300V+10 grism in combination with the GG435+81 order separation filter. The main emission lines, Hα and the [S II] doublet lie at a common redshift of z=0.381 ±0.001.

tions of the field were already performed 4 hours after the GRB trigger. At that time the weather conditions were not good. Even after combining the $g'r'i'z'$ band-images into a white-band image, I could not identify the afterglow.

FORS2 and *HST* observations: In order to study in more detail the morphology of the host galaxy of GRB 071227, I have combined all publicly available VLT/FORS2 images (programme ID 080.A-0825; PI: A. Tagliaferri). Based on the combined FORS2 image (5 hours), the size of the galactic disk of the host galaxy of GRB 071227 can be precisely measured. It has an angular extension of about $8\farcs2 \times 3\farcs2$, corresponding to 44×17 kpc^2. HST/F438W and F160W observations of the host galaxy performed on 12 June 2010 (PI: A. Levan), three years after the burst, do not reveal more details about the morphology of this galaxy than the deep FORS2 observations.

Spectroscopic observations of the host galaxy: VLT/FORS2 observed the afterglow plus host galaxy on 28 December 2007, the exposure time was around two hours (programme ID 080.A-0825; PI: A. Tagliaferri). All observations were performed at an airmass < 1.4 and at a seeing $< 0\farcs8$, using a slit width of 1.0 arcsec and the GRIS 300V+10 grism in combination with the GG435+81 order separation filter. During the observations, the slit-width was placed along the bulge of the galaxy, basically perpendicular to the galactic disk (Fig. 3.4). Wavelength calibration was performed by observing a helium-argon lamp while the flux calibration was made using the spectrophotometric standard star LTT 3864.

I have re-reduced and re-analyzed the spectroscopic data which are available in the ESO archive. The right panel of Fig. 3.4 shows the flux-calibrated spectrum for the host galaxy of

GRB 071227 which is noisy due to the very low S/N. Nonetheless, the spectrum allows for the identification of the emission lines of Hα and the [S II] doublet at a common redshift of z=0.381, in agreement with D'Avanzo et al. (2009). I could not identify any absorption lines (Table 3.2).

The SFR based on the Hα emission-line flux is small, $\sim$0.3 $M_\odot$ yr^{-1}. D'Avanzo et al. (2009) derived the SFR based on [O II], but I could not find such a line in the spectrum. Nevertheless, the SFR that I could determine based on Hα is roughly in agreement with the value reported by these authors ($\sim$0.6 $M_\odot$).

Table 3.2: Summary of the spectrum of the host galaxy of GRB 071227.

Line	Wavelength Å	Flux 10^{-17} erg/s cm^2	z	SFR $M_\odot$/yr
Hα (6562.8)	9075.7	13±1.2	0.382	0.3±0.03
[S II](6717.0)	9274.8	1.4±0.4	0.381	–
[S II](6731.3)	9292.7	6.3±1.2	0.381	–

Notes: The second column gives the observed wavelength (Å), the third column the observed flux based on the IRAF task *splot*, the forth column the corresponding redshift, and the last column the deduced SFR (see Eq. 2.2). The data is not corrected for internal host-galaxy extinction. The Galactic reddening along the line of sight is negligible, $E(B-V)$= 0.01 mag (Schlegel et al. 1998).

3.2.2 Radio-continuum detection of the GRB host galaxy

Radio-continuum observations of the host of GRB 071227 were executed on 26/27 July 2013. Bandpass and flux calibration was performed by observing PKS B1934–638. Phase calibration was done by observing the source 0308–611. Altogether 11 such 1-hr cycles were executed.

The host galaxy of GRB 071227 is clearly detected with *ATCA* in the 5.5 GHz radio band with an integrated flux density of $F_\nu = 43 \pm 11$ μJy. The peak of the radio flux is 23 ± 3 μJy (using the Miriad command `imfit`). The data imply that this is not a point source. The source is centered at coordinates RA, Decl. (J2000)= 03:52:30.952, −55:59:00.502. Within the measurement error (0.″235 in RA, 0.″204 in Decl.) this is in agreement with the galactic bulge (Nicuesa Guelbenzu et al. 2014). Though, the radio flux cannot be due to AGN activity: (1) The galaxy's colors in the *WISE* diagram (Fig. 2.1) place it significantly far from the region occupied by AGNs. (2) The source is slightly extended along the galactic plane.

Neither radio emission is detected from the position of the optical afterglow nor from any other position along the galactic disk (Fig. 3.5). The galaxy (and the GRB explosion site) is not detected in the 9 GHz band, $F_\nu < 26$ μJy (3 $\sigma_{\rm rms}$). For the discovered radio source the

spectral slope between both bands is then 1.0 ± 0.5, formally in agreement with synchrotron radiation. According to the aforementioned spectroscopic observations, the spectral slit was centered perpendicular to the bulge of the galaxy (left panel in Fig. 3.4). The Hα flux I have measured comes from the region where the peak of the radio emission lies.

In Nicuesa Guelbenzu et al. (2014) we made use of additional archival data to build the SED of the host galaxy from the ultra-violet to the radio domain and analyzed it using the Grasil code (Silva et al. 1998). Grasil builds a library of stellar population synthesis models, including the effects of dust (emission, extinction) in a galaxy. We followed the numerical approach as detailed in Michałowski et al. (2008) (SED fitting based on χ^2 minimation of Grasil models) and used 35 000 templates in the library of Iglesias-Páramo et al. (2007) plus some templates of Silva et al. (1998) and Michałowski et al. (2008). The analysis of the SED of the galaxy[4] results in a SFR of about 25 $M_\odot$ yr^{-1}, substantially higher compared to what can be derived based on the Hα emission line flux (Table 3.2). The deduced mean global host extinction is about 2.0 mag, a value close to what was found by Leibler & Berger (2010) based on optical/NIR broad-band photometry. The infrared data alone lead to an estimated SFR of 40 $M_\odot$ yr^{-1}, while the 5.5 GHz radio flux translates into an unobscured SFR of ~35 $M_\odot$ yr^{-1}. These numbers characterize the host of GRB 071227 as a galaxy that is undergoing an episode of intense star-formation activity.

3.2.3 Could GRB 071227 be a member of the long-GRB population?

Could GRB 071227 be a member of the long-GRB population, i.e., could its progenitor have been a collapsar similar to the already mentioned case GRB 090426 (Sect. 3.1.4)? At least its measured duration (T_{90} = 1.8 ± 0.4 s) could place this event into the long-GRB ensemble. Also the position of the optical afterglow projected on the galactic disk of its host galaxy ($\lesssim$ 0.2 arcsec above the galactic plane, corresponding to $\lesssim$ 1 kpc) could suggest that the progenitor of GRB 071227 was a collapsing massive star inside a star-forming region. However, no sign of a GRB supernova was discovered down to R_C = 24.9 mag (D'Avanzo et al. 2009), which is about 3 mag fainter than the expected peak magnitude of a SN 1998bw-like event at this redshift. Moreover, the rather low luminosity of the optical afterglow of GRB 071227 (D'Avanzo et al. 2009) lies in the region occupied by short GRBs (Kann et al. 2011). Nevertheless, internal extinction by dust could have dimmed the afterglow and the expected SN light as well.

Stronger arguments against a collapsar origin of GRB 071227 come from the properties of its prompt emission. Firstly, the arrival time difference between high and low-energy photons (the

[4] I thank Dr. Michal Michałowski, Edinburgh, for performing these calculations.

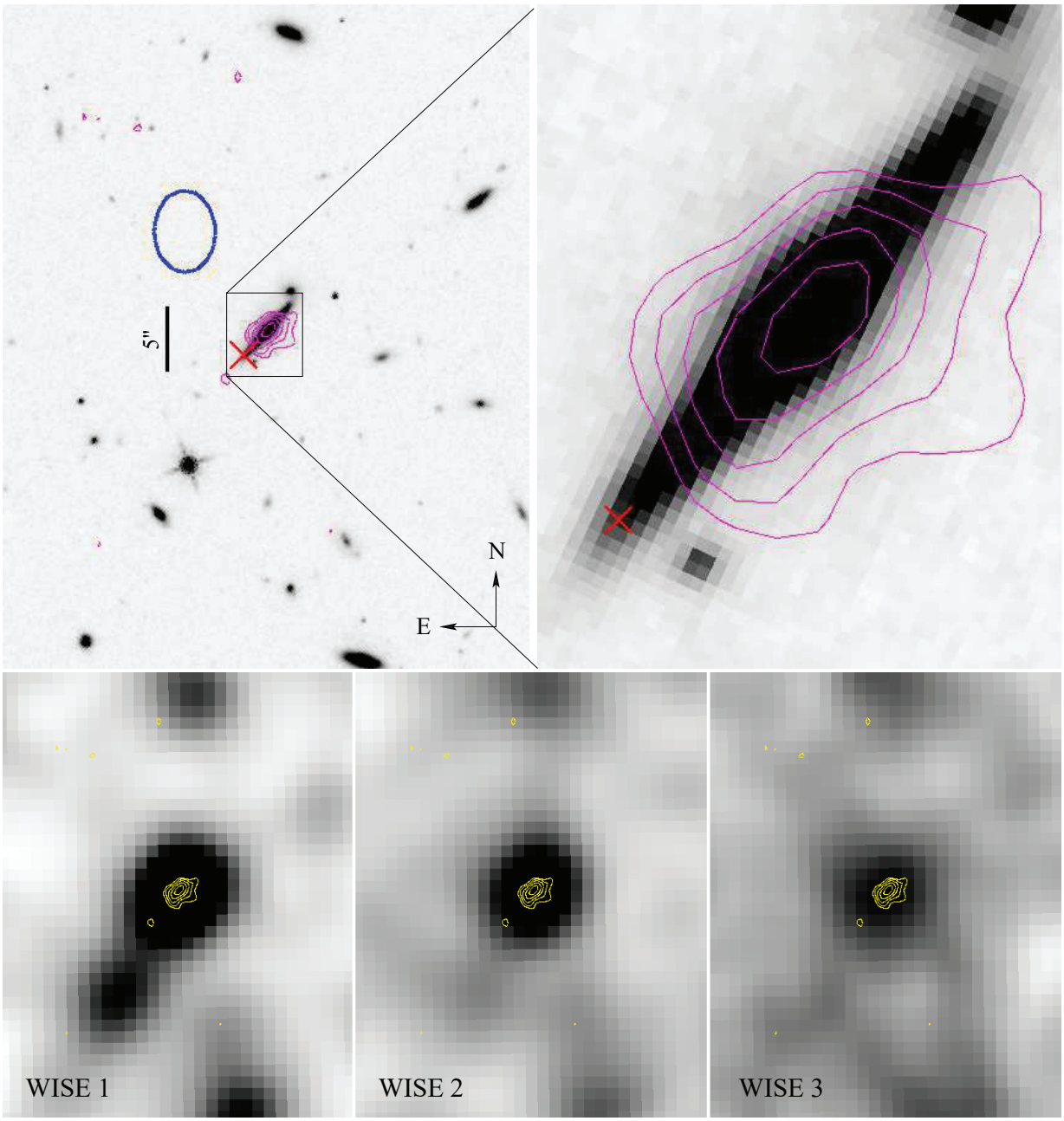

Fig. 3.5: *Top:* HST and radio image of the host galaxy of GRB 071227 (redshift z=0.381; D'Avanzo et al. 2009). Overlayed the HST image are the *ATCA* 5.5 GHz radio contours. All radio data refer to a robust parameter of `2.0`. The cross marks the position of the optical afterglow (not visible anymore), which was located in the outskirts of the galactic disk. In blue are shown the radio contour levels starting at 3 $\sigma_{\rm rms}$ in steps of 0.5 $\sigma_{\rm rms}$ (1 $\sigma_{\rm rms}$ = 4.6 μJy beam^{-1}). The synthesized beam size is drawn in blue (3.″2 × 2.″4). *Bottom:* WISE satellite images of the host in the three WISE bands 3.35 μm (W1), 4.60 μm (W2), and 11.56 μm (W3). The scale is the same as in the upper left image. Overplotted are the 5.5 GHz radio contours.

so called spectral lag) of the first, intense spike is consistent with zero (Sakamoto et al. 2007b). This feature has been found to be characteristic of the short-GRB population (Norris & Bonnell 2006; Zhang et al. 2006). Secondly, in the Amati $E_{\rm iso} - E_{\rm peak}$ diagram (Amati et al. 2002, 2008;

see Sect. 3.1.4), GRB 071227 falls into the region occupied by the short-burst ensemble. Bianco et al. (2012) and Caito et al. (2010) have in detail discussed the properties of GRB 071227 and after a careful analysis concluded that the properties of the prompt emission exclude that the burst is a member of the long-GRB population.

3.2.4 Was GRB 071227 due to a young NS-NS progenitor system?

The *ATCA* radio observations show that GRB 071227 originated in a galaxy that is undergoing an episode of intense star formation. There are two other short bursts, GRB 100206A (z=0.407) and 120804A (z ~1.3), that were hosted in galaxies with a high SFR of ~ 30 $M_\odot$ yr^{-1} (Perley et al. 2012) and ~ 300 $M_\odot$ yr^{-1} (Berger et al. 2013b), respectively. In the light of the high SFR found for the host galaxy of the short GRB 100206A, Perley et al. (2012) discussed the question whether the GRB progenitor was a member of an old or a young stellar population, but no definite conclusions could be drawn.

In their comprehensive study of short-burst host galaxies, Leibler & Berger (2010) conclude that on average the age of the dominating stellar population in late-type galaxies which hosted a short burst is between about 0.03 to 0.5 Gyr. While the median they found, ~0.25 Gyr, is substantially higher than the median found for the hosts of long GRBs (~65 Myr), it is still substantially different to what they found for the characteristic age of the dominating stellar population in early-type galaxies which hosted a short burst (~3 Gyr). This finding could suggest that the evolutionary channels of short-burst progenitors in late and early-type galaxies are different from each other.

In the case of GRB 071227, a possible link between the high SFR and the origin of the GRB progenitor cannot be established. If the GRB progenitor, i.e., the NS-NS binary, was born in the galactic bulge where star-formation is observed, it would have needed a (projected) kick velocity of about 150 km s^{-1} in order to travel 15 kpc within 100 million years. Such a kick velocity would be relatively modest when compared with the kick velocities of some Galactic neutron stars (e.g., Tomsick et al. 2012). It would also fit into the theoretical models mentioned in Sect. 1.3.2 which predict space velocities for NS-NS systems of up to 200 km s^{-1} (Eldridge et al. 2011). Nevertheless, the data-in-hand cannot confirm such a scenario.

An alternative scenario was discussed by D'Avanzo et al. (2009), in which the progenitor could have been born in a star-forming region within the galactic disk and exploded (merged) within even shorter time scales of 10^6 to 10^7 years. This scenario avoids the need for a high kick velocity and for a kick velocity vector that lies nearly parallel to the orientation of the galactic

plane.

3.2.5 Summary of Section 3.2

ATCA detected the host galaxy of the short GRB 071227 at 5.5 GHz with a flux density of $\sim 45\mu$Jy. Since an AGN activity can be ruled out and no evidence for shocked gas due to galaxy-galaxy interaction is seen, this flux implies a SFR of about 30 $M_\odot$ yr^{-1}. The *ATCA* radio-continuum observations thus revealed that the host of GRB 071227 belongs to the most actively star-forming short-GRB host galaxies known to date.

The question whether the progenitor of GRB 071227 was a young NS-NS binary remains unanswered, as with the *ATCA* data no evidence for star-forming activity was found in the vicinity of the GRB explosion site.

3.3 Identifying the host galaxy of GRB 100628A

GRB 100628A triggered *Swift*/BAT (Immler et al. 2010) as well as the *INTEGRAL* satellite (Beckmann et al. 2010). In the BAT energy window (15-350 keV) it had a duration of T_{90} = 0.036±0.009 s, classifying it as a bona fide short burst. The *Swift*/XRT data revealed the presence of a faint, fading source at coordinates RA, Decl. (J2000)= 15:03:52.41, −31:39:30.2 (90% c.l. error radius 7 arcsec; Starling et al. 2010). No UV/optical/NIR afterglow was detected, either by *Swift*/UVOT or by other ground-based observatories (Berger 2010b; Berger et al. 2010b,a; Burenin et al. 2010; Immler 2010; Levan et al. 2010; Suzuki et al. 2010; Nicuesa Guelbenzu et al. 2012). Two galaxies were found inside the XRT-error circle (Berger 2010b). For the brightest and most extended galaxy, Cenko et al. (2010) measured a redshift of z=0.102 using the Gemini telescope and noticed that it shows evidence for a galaxy-galaxy interaction. The location of this galaxy inside the XRT error circle and its relatively small cosmological distance define it as *the* suspected GRB host galaxy.

3.3.1 Archival observations of the GRB and its host galaxy

***GROND* multi-wavelength observations:** *GROND* started to observe the field of GRB 100628A at 01:30 UT on the 29 June 2010, about 17 hours after the GRB trigger and was on target for ∼1.5 hours. No optical or NIR afterglow could be identified (Updike et al. 2010). Figure 3.6 (left panel) shows the *GROND* white-band image of the field. This image revealed that there are two objects inside the XRT error circle (in red). The PSF of object *A* suggested that this

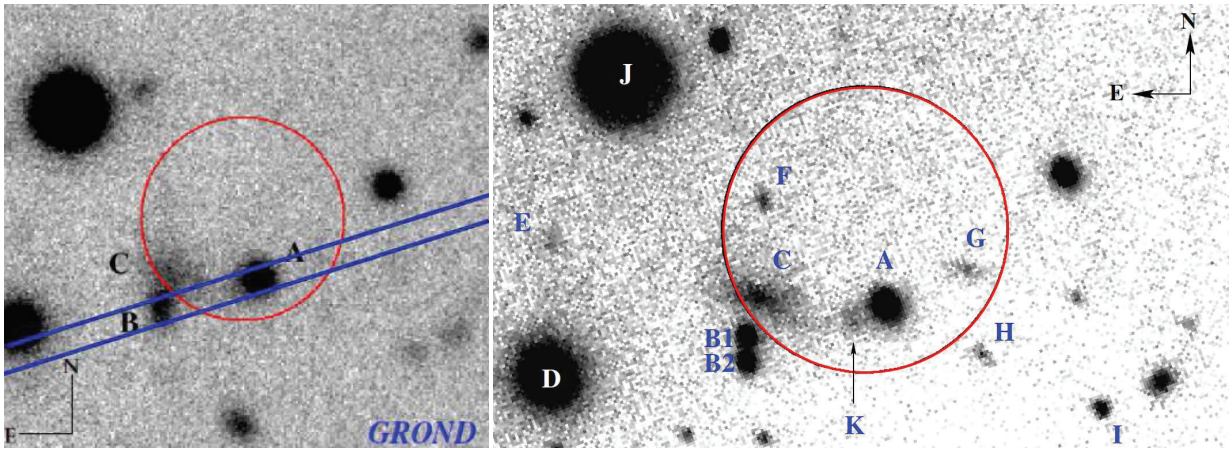

Fig. 3.6: *Left: GROND* $g'r'i'z'$ combined white-band image of the field of GRB 100628A. In red is shown the X-ray error circle (r=7 arcsec, 90% c.l.), in blue the slit position of the first FORS2 spectroscopy run. *Right:* Gemini i'-band image. It shows a light bridge between *A* and *C*, probably a tidal tail of *C*. Objects *A, B1, B2*, and *J* are stars, the others are galaxies. Redshifts from the FORS2 observations: *C (0.102), D (0.311), E (0.099), F (0.406), I (0.179), K (0.102)*. No redshifts could be obtained for *G* and *H*. Note that due to a slight tracking error, the stars appear slightly elongated.

is a star but some faint, fuzzy structure around it made this classification not secure. Object *B/C* looks like a single extended object, possibly a disturbed galaxy-galaxy system similar to *NGC 4194* (the Medusa merger), with its northern (diffuse) part (*C*) inside the XRT error circle and its brightness center (*B*) touching it. The *GROND* images were the only data available when writing a FORS2 proposal for follow-up spectroscopy (see Sect. 3.3.2).

Gemini-S observations: The field was also observed with the Gemini-S telescope on 29 Jun 2010 using the *Gemini Multi-Object Spectrograph* (GMOS; programme IDs GN-2010A-Q-7 and GS-2010A-Q-5; PIs: N. Tanvir and D. Fox, respectively). GMOS has several observing modes and can act as an spectrometer as well as an imager. It is able to perform broad-band imaging using the SDSS filters, has a field of view of $5\farcm5 \times 5\farcm5$ and a resolution of 0.072 arcsec/pixel[5]. In the case of GRB 100628A, the field was observed in the *i*-band for about 30 minutes (Levan et al. 2010). When re-reducing these publicly available archived data, I performed the photometric calibration of the *i*-band image based on the *GROND* i'-band data.

The Gemini *i*-band image as well as the FORS2 acquisition images obtained for the spectroscopy (see below) revealed that object *B/C* actually consists of three objects, two point-like objects (*B1, B2*) and the disturbed galaxy *C* which was already mentioned by Cenko et al. (2010) (Fig. 3.6). Moreover, the fuzzy structure seen in the GROND images around object *A* now revealed as a diffuse, extended feature, in the following called object *K*.

[5] `http://www.gemini.edu/sciops/instruments/gmos/imaging`

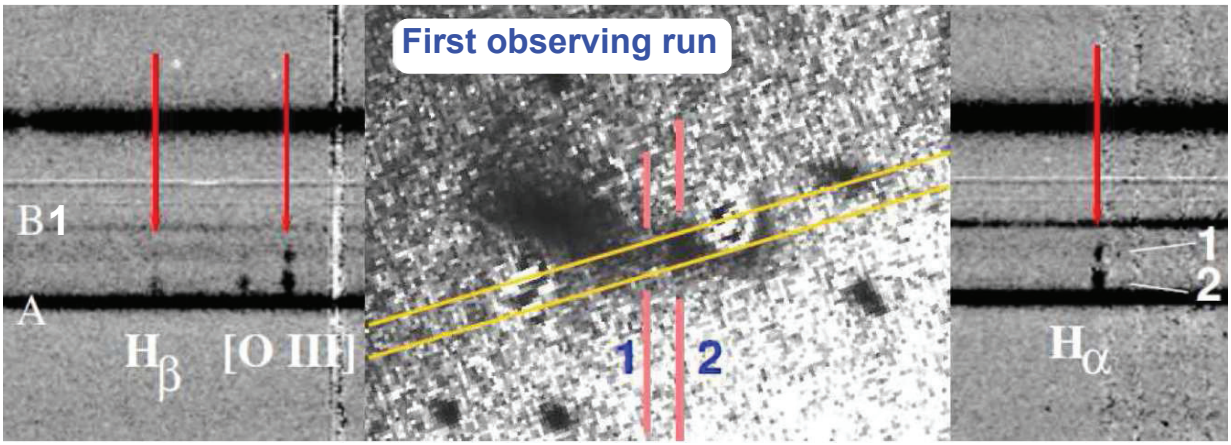

Fig. 3.7: *Left/Right:* FORS2 2D long-slit spectrum obtained during the first FORS2 observing run of the field of GRB 100628A (programme ID 087.D-0503; PI: A. Nicuesa Guelbenzu), mainly intended to cover the two brightest objects inside and close to the XRT error circle (*A, B*; Fig. 3.6), which however turned out to be stars. Red arrows point to bright emission lines of two blobs along the slit (marked 1 and 2). These lines turned out to have their origin in the outer western region of galaxy *C* and in what could be a tidal tail between C and A. *Middle:* Gemini *i*-band image of the suspected host of GRB 100628A. In yellow it is shown the slit position.

3.3.2 VLT spectroscopy of the GRB field

First FORS2 spectroscopy run: Having only the *GROND* images at hand, the first spectroscopy run requested a long-slit spectroscopy of the brightest object inside/nearby to the XRT error circle, namely objects *A* as well as *B* (Fig. 3.6). These observations (2 hr) were executed in April and May 2011 (programme ID 087.D-0503; PI: A. Nicuesa Guelbenzu; Table 7.5). Figure 3.7 shows a composite that summarizes the results of the first spectroscopy run. In the flux-calibrated 2D spectrum the trace of objects *A* and *B1* are clearly detected. Both objects turned out to be stars. Interestingly, the data revealed the presence of two regions with bright emission lines (in the following named blobs *1* and *2*). The middle panel in Fig. 3.7 shows the Gemini *i*-band image. At the position of objects *A* and *B1*, PSF subtraction revealed a potential tidal tail extending from object *C* up to the position of *A*.

Second FORS2 spectroscopy run: Figure 3.8 shows the slit orientation during the second FORS2 spectroscopy run (programme ID 290.D-5194; PI: A. Nicuesa Guelbenzu). The immediate objective of this run was to study the galactic disk of object *C* as well as its extended tidal tail.

In both FORS2 runs the observations were performed at an airmass < 1.1. In the first run I used a slit width of 1.0 arcsec while in the second run the slit width was degraded to 1.3

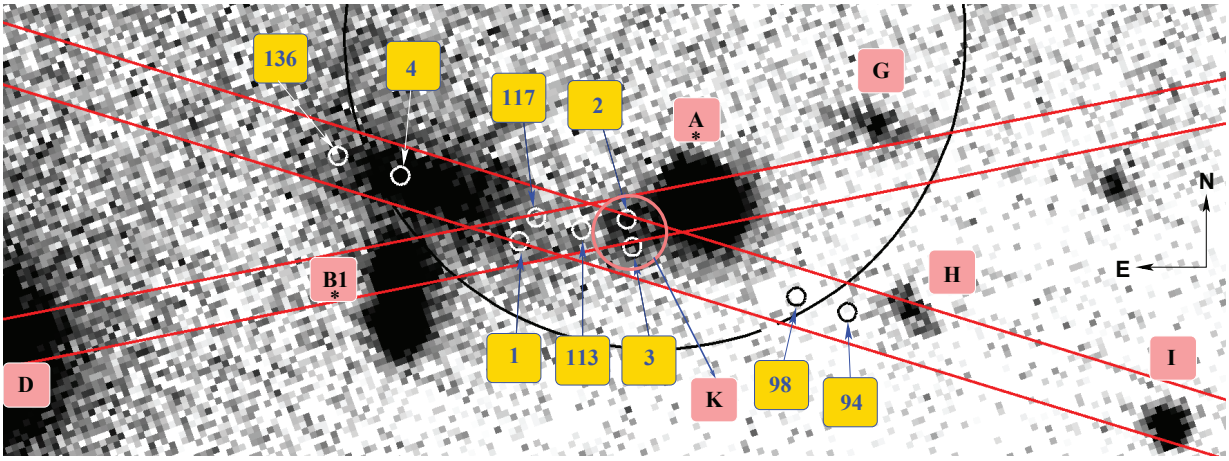

Fig. 3.8: Sketch of the two different slit positions during the FORS2 observations of the field of GRB 100628A, overlayed the Gemini *i*-band image (Nicuesa Guelbenzu et al. 2015). Positions with strong emission lines in the 2D spectra (in the following called blobs) are marked with small circles and numbered (numbers larger than *4* refer to the pixel coordinate along the corresponding slit). Blobs *1*, *113*, and *2* are seen in the 2D spectrum with the slit oriented from south-east to north-west, i.e., when the slit covered objects *B1* and *A*. All other blobs were detected in the 2D spectrum with the slit oriented in the other direction. Possibly, blobs *1* and *117* belong to the same emission-line region in galaxy *C*. The same holds for blobs *2* and *3*, which possibly belong to object *K*. Regions marked in yellow are at a common redshift $z = 0.102 \pm 0.001$, the redshift of galaxy *C*. Except for object *K*, all objects marked in pink are either foreground stars (*A*, *B1*) or galaxies (*D*, *G*, *H*, *I*). Object *K* could be the interacting partner of *C*. It is mainly hidden by the Galactic foreground star *A*.

arcsec due to poorer seeing conditions. In both runs the 300V+10 grism was used (dispersion 112 Å mm^{-1}, 1.68 Å pixel^{-1}, resolution $R = 440$ at 590 nm[6]). Wavelength calibration was performed relative to HgCdHe+Ar calibration lamps. The observed spectrophotometric standard stars were LTT 7379 (in April 2011), LTT 7987 (in May 2011), and LTT 6248 (in April 2013; Table 7.5).

The derived spectrum shows several additional line-emitting regions (blobs) along the spectral slit, partly even extending towards object *H*. All lines lie at a common redshift of z=0.102. Unfortunately, for object *H* no trace could be identified in the 2D spectrum. Its redshift remains unknown. Nonetheless, its morphology clearly identifies it as a galaxy.

3.3.3 Objects inside the *Swift*/XRT error circle

The Gemini *i*-band image shows five objects inside the XRT error circle (labeled *A*, *C*, *F*, *G*, and *K* in Fig. 3.6). The FORS2 spectra revealed that object *A* is a Galactic foreground star, while a VLT/X-Shooter spectrum (taken via programme ID 090.A-0825, PI: D. Malesani) showed that

[6] FORS2 User Manual dated 26/02/2013, page 12

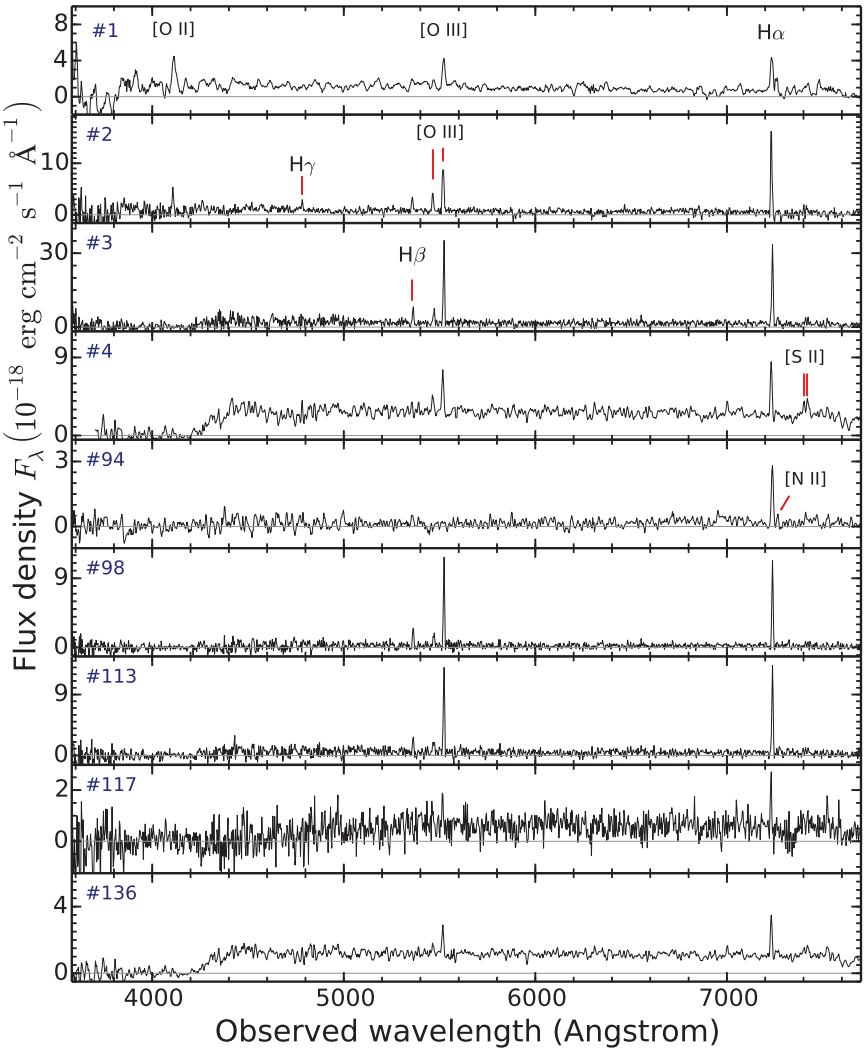

Fig. 3.9: Spectra of the nine blobs which I could identify in the FORS2 2D spectrum based on their various emission lines. All these blobs lie at a common redshift of $z = 0.102$. Blobs 94 and 98 have no optical counterpart on the Gemini *i*-band image but appear in the trace of the FORS2 spectrum. In blobs 2 and 3 the Hα and the [O III] (5007) line are very strong. For blob 3 I measure an equivalent width for these lines of 220 ± 20 Å and 170 ± 20 Å, respectively.

object *F* is a background galaxy at a redshift of $z = 0.406$. Galaxy *G* is faint but clearly extended. During the spectroscopy run it did not completely lie inside the spectral slit (Fig. 3.8), no trace of this object could be detected in the spectrum. Its redshift remains unknown.

Object *C* is the most remarkable galaxy inside the XRT error circle. It is distinguished by its comparatively large angular size, its relatively bright apparent magnitude (AB magnitude $i' \sim 21.5$), and its disturbed morphology. Using Eq. (1.1) (Sect. 1.3), the chance coincidence probability that a galaxy with $i(\mathrm{AB}) \leq 21.5$ mag lies within a region as small as the XRT error

Table 3.3: GRB 100628A: Measured emission-line flux for nine emission-line regions found in the VLT/-FORS2 spectra.

#	coordinates RA, Decl.	Hα λ6562.8	Hβ λ4861.3	[O III] λ5006.8	[O III] λ4958.9	[O II] λ3727.0	Hγ λ4340.5	[Ne III] λ3967.5	[N II] λ6583.4
1	52.65, 34.7	7.4±0.6	1.9±0.3	6.4±0.6	1.7±0.2	10.6±0.9	0.6±0.1	–	2.4±0.2
2	52.46, 34.3	15±1.1	2.8±0.4	10.4±0.9	4.2±0.4	6.6±0.5	1.8±0.2	1.2±0.3	–
3	52.45, 34.9	34±2.1	6.2±0.6	28.2±1.8	5.8±0.5	–	1.9±0.2	–	3.8±0.3
4	52.86, 33.3	7.2±0.5	1.4±0.2	6.6±0.6	3.2±0.3	–	–	–	2.5±0.2
94	52.07, 36.4	3.7±0.3	–	–	–	–	–	–	0.2±0.1
98	52.16, 36.0	9.45±0.9	2.66±0.3	9.50±0.8	1.65±0.1	–	–	0.13±0.02	0.22±0.1
113	52.54, 34.5	10±1.1	2.5±0.3	11±1.1	4.0±0.4	–	–	–	–
117	52.62, 34.2	2.23±0.2	0.43±0.1	1.9±0.3	0.46±0.1	–	–	–	–
136	52.97, 32.9	7.23±0.6	–	1.77±0.2	0.4±0.1	–	1.67±0.2	–	–

Notes: Line fluxes are given in units of 10^{-17} erg s^{-1} cm^{-2}. All lines lie at a common redshift of $z = 0.102 \pm 0.001$. Right ascension and Declination (J2000) values refer to 15:03:XX, −31:39:YY, only XX and YY is given in the table.

circle is $p = 0.07$. As already shown in Table 2.3, the corresponding probabilities for the fainter galaxies *G* and *F* are notably larger (0.64 and 0.77, respectively).

Galaxy *C* has a major axis of about 5 arcsec, corresponding to ∼10 kpc. At the western side of galaxy *C* originates a light bridge which extends into western direction towards the Galactic foreground star *A*. It has a length of about 3.″6 (7 kpc). PSF subtraction of object *A* did not help to gain more details about the morphology of object *K*. However, its optical spectrum confirms that is located at the same redshift as galaxy *C* (Table 3.3). A possible interpretation is that object *K* is either the brightest knot in a tidal tail that originates from *C* or it is a galaxy. There are also optical indications for a second and fainter tidal tail extending from the eastern side of galaxy *C* towards the position of galaxy *F*. Contrary to object *K*, galaxy *F* is a background object however.

Galaxies *C* (z=0.102) and *E* (z=0.099) have a relatively small difference in redshift (Fig. 3.6), but the corresponding difference in luminosity distance is ∼ 15 Mpc. This rules out that both galaxies are interacting with each other.

3.3.4 Star formation rate based on optical spectroscopy

In order to obtain the the star-formation rates, in Nicuesa Guelbenzu et al. (2015) we performed extinction correction of the observed line flux via the observed flux ratio $F(H\alpha)/F(H\beta)$ (after correction for the Galactic extinction; $E(B-V)_{\rm Gal}$= 0.17 mag; Schlegel et al. 1998). The host-extinction values in the emission-line blobs derived with this approach lie between 0.2 and 1.7 mag. The highest values are measured for those regions that belong to object *K* (blobs 2 and 3). The extinction-corrected Hα luminosities of these blobs lie between 0.3 and 5.3×10^{40} erg s^{-1}.

The SFRs obtained using Eqs. (2.2) and (2.4) are small, at most 0.2 $M_\odot$ yr^{-1} (Table 3.4). The specific SFR could nevertheless be high but the lack of precise multi-color data prevents a mass estimate for these emission-line regions. The fact that the visual extinctions are in the order of 1 mag (blobs 2, 3, 4, and 117) indicates that these could be giant, dusty star-forming regions. Following the procedure mentioned in Sect. 3.1.5, the Galactic extinction-corrected emission-line flux ratios (as they follow from Table 3.3) suggest that the emission is due to star-formation activity and not due to shocked gas.

Table 3.4: GRB 100628A: Internal extinction and extinction-corrected SFRs for the nine emission-line blobs listed in Table 3.3.

#	$\frac{F(H\alpha)}{F(H\beta)}$	$E(B-V)_{\rm host}$	SFR(Hα)	SFR([O II])
(1)	(2)	(3)	(4)	(5)
1	3.32	0.13	0.02±0.001	0.06±0.01
2	4.56	0.40	0.10±0.01	0.14±0.01
3	4.67	0.42	0.23±0.02	–
4	4.38	0.36	0.04±0.001	–
98	3.03	0.05	0.02±0.001	–
113	3.41	0.15	0.03±0.001	–
117	4.42	0.37	0.01±0.001	–

Notes: Column #1 follows Table 3.3, column #2 is the observed line flux ratio, column #3 the deduced internal reddening (mag), both after correcting for Galactic extinction along the line of sight ($E(B-V)_{\rm Gal}$= 0.17 mag; Schlegel et al. 1998). Errors in the resulting extinctions were calculated according to 0.80 × $E(B-V)$ [mag] (Domínguez et al. 2013). Columns #4 and #5 give the extinction-corrected SFR ($M_\odot$ yr^{-1}) based on Eqs. (2.2) and (2.4).

Additional information could come from the *WISE* satellite data (Wright et al. 2010). However, no object was detected by *WISE* inside the XRT error circle with the following upper limits: W1(3.4μm) > 20.0, W2(4.6μm) > 20.2, W3(12μm) > 17.8, and W4(22μm) >15.4 (AB magnitudes).[7]

3.3.5 *ATCA* radio observations

ATCA 5.5 and 9.0 GHz radio-continuum observations of the field of GRB 100628A were performed on 23 July 2013. Bandpass and flux calibration was done by observing the source *PKS B1934–638* at the end of the observing run. Phase calibration was performed by observing the source *1451–375* each hour for 7 minutes. Altogether ten such 1-hr cycles were executed.

[7]For the Vega-AB conversion see `http://wise2.ipac.caltech.edu/ docs/release/prelim/expsup/sec4_3g.html`.

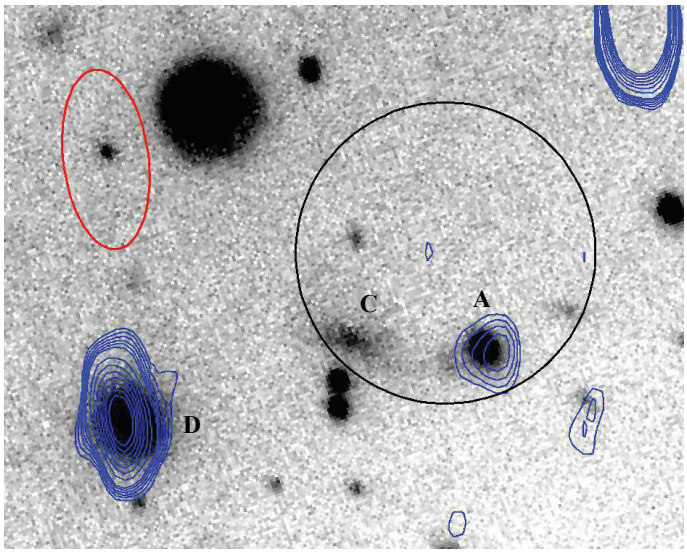

Fig. 3.10: The field of GRB 100628A as seen by *ATCA* in the 5.5 GHz radio-continuum band overlayed the Gemini *i*-band image (see also Fig. 3.6). Radio contour levels (in blue) run from F_ν= 3 to 5.5 times $\sigma_{\rm rms}$ and then from 40 to 100 μJy beam^{-1} in steps of 10 μJy beam^{-1} (robust parameter `1.0`; 1 $\sigma_{\rm rms}$ = 5.3 μJy beam^{-1}). The size of the synthesized beam is 4.″2 × 2.″0 (in red; upper left corner). Inside the XRT error circle (in black color) object C remains undetected, but emission close to object A is observed. In addition, the data reveal object *D* as a bright radio source.

Inside the XRT error circle *ATCA* finds a radio source west of object *A* at coordinates RA, Decl. (J2000) = 15:03:52.26, −31:39:34.9. Its integrated flux density at 5.5 GHz is F_ν = 46 ± 16 μJy (Fig. 3.10). The deconvolution of this radio image suggests that it is a point source. It lies about 2 arcsec north-east of blob *98*, which showed up by its emission line spectrum (Figs. 3.8, 3.9). It is not detected at 9.0 GHz, F_ν < 18 μJy (3σ), constraining the spectral slope ($F_\nu \sim \nu^{-\beta}$) to be $\gtrsim$ 1.0 (based on the 1σ lower limit for the flux at 5.5 GHz).

Galaxy *C* is not detected in the radio band, either at 5.5 GHz (F_ν < 16 μJy, 3σ) or at 9.0 GHz (F_ν < 18 μJy, 3σ; Fig. 3.10). This translates into an upper limit for the SFR of object *C* of 0.7 $M_\odot$ yr^{-1}. Compared to the SFR derived from the optical emission-line data, which suggest a total extinction-corrected SFR in this galaxy of $\lesssim$ 0.1 $M_\odot$ yr^{-1} (Table 3.4; excluding blobs *2* and *3* which belong to object *K*), this excludes a substantial optically hidden star-forming activity.

3.3.6 The radio source inside the XRT error circle

At 5.5 GHz the offset between the optical position of the star *A* and the radio source inside the XRT error circle is about 1.″4. The positional radio uncertainty is 0.″9 (Nicuesa Guelbenzu et al. 2014), hence the offset is not statistically significant (< 3σ). This provides three different explanations about the nature of this radio source.

1. The radio source is object *A*, which was already identified as a K star based on its observed spectrum (Fig. 7.2). Main sequence stars of spectral type K are known to be possible radio emitters (e.g., Güdel 1992; Güdel 2002). The optical magnitude of this star implies a distance of a few kpc. For such a distance the deduced radio luminosity would notably exceed the

observed radio luminosities of Galactic K stars (Güdel 1992). Therefore, this scenario seems to be unlikely.

2. The radio source is the 3 year-old radio afterglow of GRB 100628A. It would then be as bright as, e.g., the 2 year-old radio afterglow of GRB 100418A (Moin et al. 2013), a long burst that however was at $z = 0.624$ (Antonelli et al. 2010; Cucchiara & Fox 2010). If this radio source lies at $z = 0.102$, then its radio spectral luminosity at 5.5 GHz is about 1×10^{28} erg s^{-1} Hz^{-1}. Compared with the present world-sample of radio observations of *long*-GRB afterglows this is a rather modest luminosity for a 3 years-old event (see Chandra & Frail 2012, their figure 6). For short bursts, however, it would be extraordinary luminous. So far, no radio afterglow of a short GRB has been detected later than ten days after the corresponding burst.
3. The radio emission is due to star formation and possibly related to object *K*, which could be the interacting partner of *C* (Fig. 3.8). If due to star formation then the SED should follow a power law, $F_\nu \sim \nu^{-\beta}$, with a canonical value of $\beta = 0.7$ (with an observed range between 0.5 and 1; e.g., Condon 1992; Ibar et al. 2010). The radio data do not rule out such a spectral slope. If I interpret the flux at 5.5 GHz in this way, this translates into an unobscured SFR of $2 \pm 0.8\ M_\odot$ yr^{-1}. Unluckily, no spectroscopic data are available here since the center of this radio source lies outside the slit width during both VLT/FORS2 spectroscopy runs (Fig. 3.8).

Among these three possibilities, the last one appears to be the most likely explanation for the nature of this radio source.

3.3.7 A second host-galaxy candidate

According to the present understanding, the progenitors of short bursts can be several Gyr old when they merge (see, e.g., Berger 2014 for a review).[8] A sufficient space velocity provided, the place where a NS-NS binary was born can then lie far away from the place where it finally merges. A space velocity of a few hundred km s^{-1} over a timespan of some Gyrs would cause the merger to take place in the realm of the outer halo of a galaxy or even deep in intergalactic space. As I have already pointed out (Sect. 1.3.2), several cases of apparently host-less short GRBs are indeed known (e.g., Tunnicliffe et al. 2014). This possibility points to galaxy *D* (Fig. 3.6).

Galaxy *D* lies 17″ away from the centre of the (90% c.l.) XRT error circle. It has observed AB magnitudes of $g'r'i'z'JHK_s = 22.46 \pm 0.07, 20.72 \pm 0.02, 20.17 \pm 0.02, 19.84 \pm 0.02, 18.69 \pm 0.02,$

[8] Within this context an age of zero is defined by the second SN explosion, which finally results in the formation of the NS-NS binary. In both explosions the binary can gain space velocity, obtain a "kick", if the explosion was not symmetric.

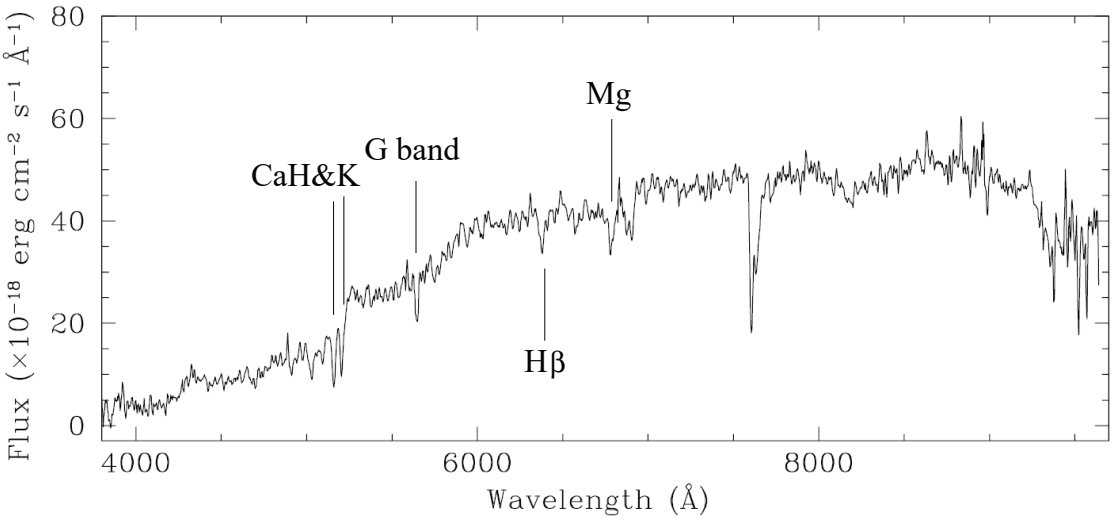

Fig. 3.11: The VLT/FORS2 spectrum of object *D*. It reveals that this is an elliptical galaxy at a redshift of $z = 0.311$. The strong absorption at 7600 Å is due to the telluric A-band.

18.35 ± 0.03, and 18.06 ± 0.05 mag. In the *ATCA* radio-continuum observations it stands out as a bright radio source with an integrated flux density of F_ν(5.5 GHz) = 151 ± 23 μJy and F_ν(9.0 GHz) = 83 ± 28 μJy (Fig. 3.10). In the entire *Swift*/BAT error circle (radius 2.1 arcmin, 90% c.l.; Immler et al. 2010) it is the second-brightest radio source. In combination with the VLT/FORS2 spectroscopy, this identifies *D* as a radio-bright elliptical galaxy at a redshift of $z = 0.311$ (Fig. 3.11).

The galaxy is also detected in the *WISE* satellite W1 & W2 bands with W1 (3.4μm) = 18.65 ± 0.08 and W2 (4.6μm) = 18.87 ± 0.18, but not detected at longer wavelengths, W3 (12μm) >17.8 and W4 (22μm) >15.4 (AB magnitudes).

The K_s-band luminosity of galaxy *D* is very high, $\log(L/L_\odot) = 11.24$, but not unusual for this class of elliptical galaxies (Sadler et al. 2014). A GRASIL (Silva et al. 1998) fit of the broad-band SED from the optical to the *WISE* bands provides a stellar mass of $M_\star = 7.7 \times 10^{10}$ $M_\odot$ (Salpeter IMF), no evidence for star-formation activity (current SFR = 0 $M_\odot$ yr^{-1}), and a metallicity of $\log Z/Z_\odot = 0.02$ (Nicuesa Guelbenzu et al. 2015).

Interestingly, the global properties of this galaxy are nearly identical to that of the likely host of the first well-localized short GRB 050509B, a giant elliptical galaxy at a redshift of $z = 0.225$ (Gehrels et al. 2005; Bloom et al. 2006). Also for this burst no optical afterglow was detected and the angular offset between the elliptical galaxy and the centre of the $r = 3\farcs6$ XRT error circle is in the order of 10″. According to Kochanek et al. (2001), and as already outlined by Gehrels et al. (2005), such luminous early-type galaxies are quite rare; the co-moving number density

of early-type galaxies as luminous as object D with $M_{K_s} \sim -24.75$ mag (Vega) is $\sim 3 \times 10^{-4}$ (Mpc/h)$^{-3}$ mag^{-1}, where h is the Hubble constant in units of 100 km s^{-1} Mpc^{-1}. As discussed by Gehrels et al. (2005) and Bloom et al. (2006), given their large reservoir of old stars these galaxies are ideal birthplaces for compact stellar binaries, i.e., short-GRB progenitors. Adopting the methodology of Bloom et al. (2002), the probability p (Eq. 1.1) of finding such a galaxy with I(Vega) ≤ 19.5 [9] inside a circle on the sky with a radius of 17″ is 5%. In other words, galaxy D is another host-galaxy candidate for GRB 100628A.

The angular distance of this galaxy to the outer edge of the XRT error circle is about 10 arcsec. At a redshift of $z = 0.311$ this corresponds to a projected distance of 45 kpc. While this would be an unusually large distance for a long-GRB progenitor (e.g., Bloom et al. 2002), for a short-GRB progenitor this is not the case.

Unfortunately, no strong arguments can be offered that clearly prefer this host-galaxy candidate at $z = 0.311$ over the interacting spiral galaxy at z=0.102. In Nicuesa Guelbenzu et al. (2015) we discuss this issue in more detail. We consider the short-GRB redshift distribution, the energetics of the burst for the two different redshifts, the luminosity of its afterglow in the optical and in then X-ray band, and several empirical relations between afterglow parameters. Even though the higher redshift seems to be preferred over the smaller one, no argument really rules out one of the two host-galaxy candidates.

3.3.8 Summary of Section 3.3

Compared to GRB 071227 (z=0.381), the suspected host galaxy of GRB 100628A (a disturbed spiral) lies nearly 4 times nearer in redshift space (z=0.102). Correspondingly more promising was the study of this galaxy that lies at such small redshift. Indeed, *ATCA* finds a radio source inside the XRT error circle. This source lies in the galactic plane of the suspected host, possibly at the position where an interacting partner of this galaxy resides. In the optical bands this object is hidden by a bright Galactic foreground star. If this emission is due to star-forming activity, then the observed flux at 5.5 GHz corresponds to an unobscured SFR of $2 \pm 0.8\ M_\odot\ \mathrm{yr}^{-1}$.

Unexpectedly, my *ATCA* observations revealed a second host-galaxy candidate, a radio-bright giant elliptical at a redshift of $z = 0.311$. Since no optical afterglow was discovered in the case of GRB 100628A, and hence no spectroscopic redshift via the afterglow is known, the available data do not allow me to decide if the interacting galaxy or the elliptical was the GRB host galaxy.

[9] after applying a AB-Vega conversion of ~0.4 mag and after correcting for the Galactic extinction along the line of sight, 0.3 mag in the *GROND* i' band

Chapter 4

Results II: Targets without radio detection

This chapter provides detailed information about all those targeted nine short-GRB host galaxies for which the ATCA radio-continuum observations did not result in a positive detection. In any case, the upper limits I can provide here in the 5.5 and 9.0 GHz bands are deep and might not improve in the coming years due to the faintness of the targets. Substantial progress in this respect might come from the next generation radio interferometer, the Australian SKA pathfinder ASKAP[1], which has recently become operational but is currently performing observations only for Large Survey Science Projects.

In the following, targets are ordered according to their GRB numbers, i.e., the date of occurence of the corresponding burst. In all cases, I start with a brief description of the properties of the burst, the status of the (world-wide) optical follow-up observing campaigns and what is known about the GRB host galaxy before I summarize the *ATCA* observations.

In all cases the 5.5 GHz data provide slightly tighter constraints on the SFR than the 9.0 GHz data. The reason is that for a similar sensitivity the expected radio flux of a star-forming galaxy is larger at 5.5 than at 9.0 GHz, if we assume the radio flux scales with a power law (synchrotron radiation, $F_\nu \sim \nu^{-\beta}, \beta \sim 0.7$).

For two short bursts discussed here the redshift of the suspected host galaxy is not known (GRB 070729, 130515A) and the available GROND as well as WISE data do not constrain the photometric redshift very much. In these cases I assumed a redshift of 0.5.

All non-detections reported here also constrain the flux of the corresponding radio afterglows, usually years but in one case also only months (GRB 150424A) after the burst. They also constrain a potential radio flux from a magnetar formed during a NS-NS merger (see, e.g., Fong et al. 2016). A discussion of this theoretical model is not the goal of this work.

All *ATCA* radio data were reduced using a robust parameter of 0.5, 1.0 and 2.0. All figures

[1] `http://www.atnf.csiro.au/projects/askap/index.html`

show 5.5 GHz radio contour lines, if within the shown fields radio sources were detected. Details on the radio observations and deconvolved images (1 σ_{rmrms}, beam sizes) are given in Tables 2.4, 5.1, and 7.2.

4.1 GRB 050724: a bulge-dominated host with a faint disk component

Observations reported in the literature: *Swift*/BAT triggered on GRB 050724 at 12:39:19 UT on 24 July 2005. XRT started observations 74 s after the trigger and found a fading, uncatalogued X-ray source at coordinates RA, Decl. (J2000) = 16:24:44.9, −27:32:34.0 (error circle 6.″0 radius; Covino et al. 2005). The final error circle is located at RA, Decl. (J2000) = 16:24:44.33, −27:32:26.9 (±1.″5). The burst had a duration of T_{90}(15–150 keV) = 3.0 ± 1.0 s. It consisted of a short (~0.25 s), hard spike (typically for short bursts) followed by a soft extended emission lasting for 152.0 ± 9.2 s (Barthelmy et al. 2005b). The fluence in the BAT window (15–150 keV) was 6.3 ± 1.0 × 10^{-7} erg cm^{-2}. GRB 050724 is the first short burst for which a NIR as well as a radio afterglow was found. The flux of the radio afterglow in the 8.46 GHz band ~14 hours after the burst was 173±30 μJy, increasing up to 465±30 μJy at 40 hours (Berger et al. 2005).

Host galaxy: The afterglow and its host are in detail discussed in the literature (Berger et al. 2005; Gorosabel et al. 2006; Prochaska et al. 2006; Malesani et al. 2007). The position of the afterglow coincided with the outskirts of a relatively bright galaxy (R ~20 mag) at a redshift of z = 0.258. The host galaxy extinction was derived based on SED fitting techniques to be $A_v^{\rm host}$ ~0.4 mag (Gorosabel et al. 2006). Based on optical spectroscopy, the galaxy has a very low star formation rate. Reported upper limits are 0.02 M$_\odot$ yr^{-1} (Berger et al. 2005), 0.05 M$_\odot$ yr^{-1} (Prochaska et al. 2006), and 0.17 M$_\odot$ yr^{-1} (Malesani et al. (2007)). The SFR, that was derived based on multi-color photometry, gave a range between 0.5 - 5 M$_\odot$ yr^{-1} (Gorosabel et al. 2006).

Though most authors classify the host galaxy as an elliptical, it was noted by Malesani et al. (2007) that it shows a faint outer spiral structure, suggesting that this could be a disk galaxy with a light-dominating central bulge. This conclusion was strengthened by *HST* images (Fig. 4.1), Fong et al. (2011) noted the presence of a weak spiral structure in the disk component.

Radio observations: *ATCA* observations were executed on 24 October 2015 and lasted for 10.4 hours (Table 2.4). Phase calibration was performed by observing the quasar *PKS 1622-253* (redshift z = 0.786), which has a radio flux of F_ν(5.5 GHz) = 1.79 Jy and F_ν(9.0 GHz) = 1.63 Jy. The 1 $\sigma_{\rm rms}$ on the deconvolved images is 4.9 ± 0.1 μJy beam^{-1} at 5.5 GHz and 5.0 ± 0.2 μJy

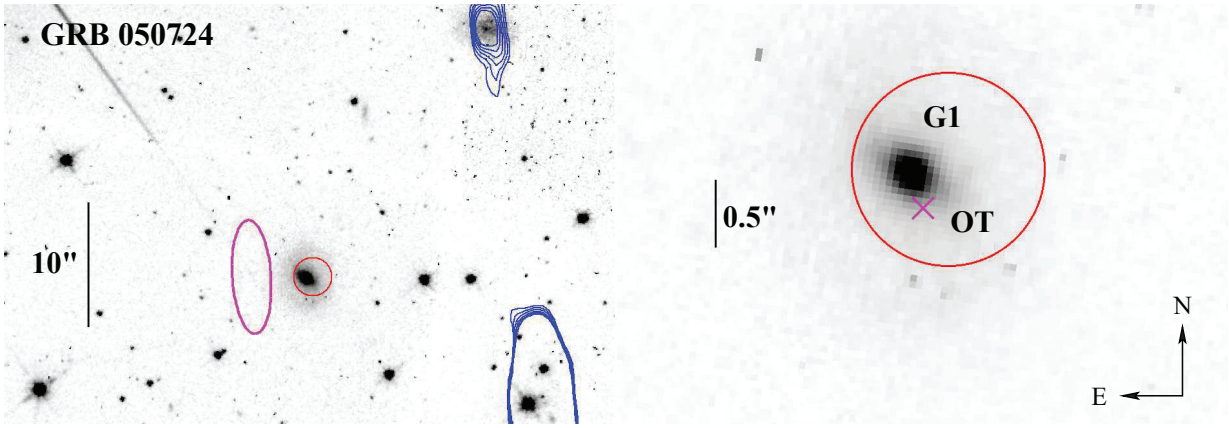

Fig. 4.1: *Left: HST*/F814W image (programme ID 11176; PI: A. Fruchter) of the field of GRB 050724. In red is shown the r=1.″5 *Swift*/XRT error circle, in magenta the synthesized radio beam (4.″4 × 1.″5, beam position angle 93.6 deg). In blue are drawn the radio contours at 5.5 GHz in steps of 1/2 $\sigma_{\rm rms}$, starting at 3 $\sigma_{\rm rms}$ (1 $\sigma_{\rm rms}$ = 5.0 μJy beam^{-1}; Table 5.1). There is no radio detection at the position of the optical transient (OT) or its host galaxy. The bright radio source ∼20 arcsec south-west of the optical transient is the *Spitzer* source (SSTSL2) J162443.32–273207.4, which has a radio flux of F_ν(5.5 GHz) = 1.79 Jy. Another bright radio source is a spiral galaxy ∼20 arcsec north-west of the position of the OT. No redshift information is available for these two radio sources. *Right:* Zoom-in of the field showing the position of the optical transient (with a cross drawn in magenta) located 0.″6 (∼2.5 kpc) away from the center of its host galaxy.

beam^{-1} at 9.0 GHz (Table 5.1). *ATCA* does not detect the host galaxy of GRB 050724 down to a 3σ upper limit of 15 μJy at 5.5 GHz as well as at 9.0 GHz. This constraints the radio SFR to <4.9 M$_\odot$ yr^{-1}. When compaerd with the optically derived SFR this does still leave room for the presence of obscured star formation.

4.2 GRB 061006: an edge-on spiral host galaxy

Observations reported in the literature: *Swift*/BAT triggered on GRB 061006 at 16:45:50 UT on 6 October 2006. It did not trigger on the prompt but on the extended emission that had a duration of 130±10 s (Schady et al. 2006). Thanks to the Interplanetary Network, the early temporal profile of the burst was recorded. It showed a double-spiked morphology with a duration of T_{90} (20–200 keV) =0.42 s (Urata et al. 2006) and a fluence of $3.6 \pm 0.1 \times 10^{-6}$ erg cm^{-2} in the *Konus-Wind* energy window (30–400 keV; Krimm et al. 2006). A ground-based re-examination of the XRT data showed the presence of a faint afterglow at coordinates RA, Decl. (J2000) =07:24:06.36, −79:11:56.8, with an error circle of 6 arcsec (Troja et al. 2006). The final enhanced XRT position is at RA, Decl. (J2000) =07:24:07.66, −79:11:55.6 with an error circle of 1.″7 (Fig. 4.2).

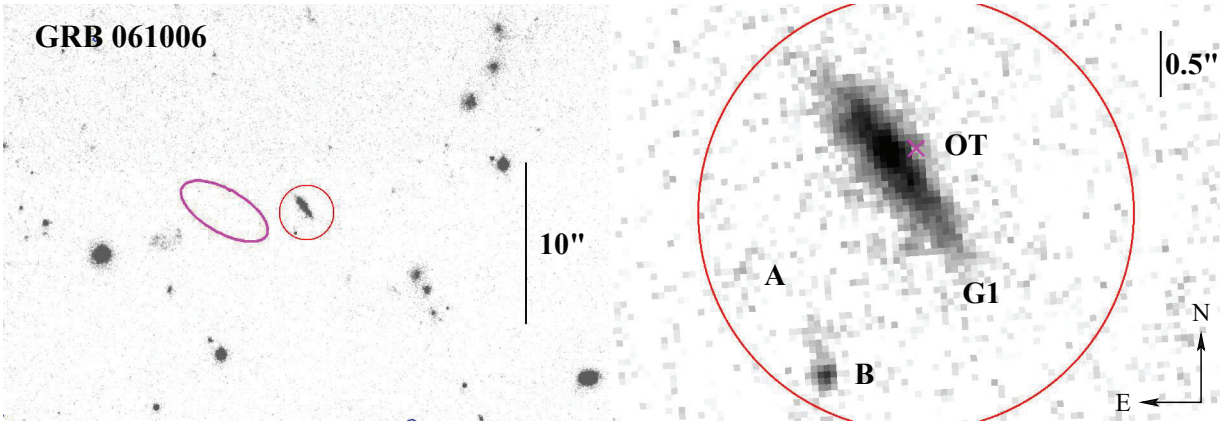

Fig. 4.2: *Left: HST*/F814W image (programme ID 10917, PI: D. Fox) of the field of GRB 061006. In red it is shown the final 1.″7 enhanced XRT error circle with a prominent galaxy inside. Though the field is rich in galaxies, no radio source is detected inside the shown field. In particular, neither is radio flux detected from the GRB explosion site, nor from the entire GRB host galaxy. In magenta is shown the size and position angle of the synthesized beam (3.″9 × 1.″7, position angle 150 deg). *Right:* Zoom-in of the suspected host, probably an edge-on spiral. The magenta cross shows the position of the OT west of the bulge of the galaxy (the OT is not visible anymore at the time when this image was taken with *HST*; note also that its positional error is ±0.5 arcsec; Malesani et al. 2006a). *A* and *B* designate two other objects inside the XRT error circle. Compared to *G1* they are much fainter and, hence, they are much less likely host-galaxy candidates.

Optical follow-up observations of the burst were performed using VLT/FORS1 around 14 hours after the GRB trigger and showed a single source inside the XRT error circle at coordinates RA, Decl. (J2000) =07:24:07.66, −79:11:55.1 (with an astrometric uncertainty of 0.5 arcsec; Malesani et al. 2006a). Using FORS1 an optical fading of the source by ∼0.5 mag was detected 1.6 days after the burst (Malesani et al. 2006b).

Host galaxy: The ESO archive contains several observations of the host of GRB 061006 with FORS1/2 and ISAAC (ESO programme 078.D-0809 and 177.A-0591; PI: S. Antonelli and J. Hjorth, respectively). On the VLT images the host galaxy appears as a faint (R_C ∼24.0) and fuzzy object (see also figure 1 in Berger et al. 2007a as well as Leibler & Berger 2010).

The Gemini-S telescope performed spectroscopic observations of the host galaxy of GRB 061006 in November 2006. GMOS was on target for about 3600 s using the R400 grating that goes from 4900 to 9200 Å, with a central wavelength at 7200 Å and a resolution of 7 Å. Weak emission lines of the [O III] doublet, Hβ, and [O II] were detected at a common redshift of $z = 0.4377 \pm 0.0002$ (see figure 5 in Berger et al. 2007a). The [O II] line has a flux of 4.1×10^{-17} erg s^{-1} cm^{-2}, which corresponds to a modest SFR of 0.02 M$_\odot$ yr^{-1} (Berger 2009).[2]

HST observed the field in several occasions betweeen October 2006 and November 2007

[2]At this redshift, the Hα line lies at 9435.85 Å and therefore outside the wavelength coverage of the R400 grating.

using the ACS in the NIR (filter F814W; programme ID 10917, PI: D. Fox). Figure 4.2 shows the combined (~6 hr) *HST*/F814W image of the field of GRB 061006. The host is an inclined, nearly edge-on spiral galaxy with a dimension of $2\farcs0 \times 0\farcs8$ (11.5×4.5 kpc^2). The optical afterglow (see blue cross) was located in the outskirts of its host galaxy (*G1*) close to the galactic bulge.

Next to the host galaxy of GRB 061006 and inside the XRT error circle lie two further and comparably much fainter objects (*A*, *B*; Fig. 4.2) which are visible on the *HST* but not on the VLT images. Both could be galaxies, too. Object *B* has a size of $0\farcs6 \times 0\farcs3$. It is located $1\farcs2$ south of the suspected host of GRB 061006 at coordinates RA, Decl. (J2000) = 07:24:07.9, −79:11:56.8. Object *A* has a fuzzy morphology and is barely visible. It is located $1\farcs4$ arcsec S-E of the suspected host at coordinates RA, Decl. (J2000) = 07:24:08.14, −79:11:56.1. No redshifts are known. The much fainter magnitude of these galaxies compared to *G1* as well as their notable larger angular distance from the OT does not define them as additional host-galaxy candidates.

Radio observations: Radio observations of the field were performed with *ATCA* on 20 June 2013 for about 7 hours (Table 2.4). Phase calibration was done by observing the quasar *PKS 0637-752* (redshift $z = 0.653$), which has a radio flux of $F_\nu(5.5\,\mathrm{GHz}) = 3.51$ Jy and $F_\nu(9.0\,\mathrm{GHz}) = 2.97$ Jy. The 1 σ_{rms} on the combined deconvolved radio images is between 7.3 and 7.8 μJy beam^{-1} at 5.5 GHz and between 8.1 and 9.3 μJy beam^{-1} at 9.0 GHz (Table 5.1). No radio flux is detected from the suspected host galaxy down to $F_\nu(5.5) < 22$ μJy and $F_\nu(9.0) < 25$ μJy (3 σ_{rms}). For the given redshift of *G1*, this translates into an upper limit for the SFR of $< 25\ M_\odot$ yr^{-1}. Compared with the reported optical SFR for this host (0.02 $M_\odot$ yr^{-1}; Berger 2009), these results are not very constraining. However, given that the redshift of this galaxy is comparable to the redshift of the host of GRB 071227 (Sect. 3.2), the radio data rule out that this is a similar starburst galaxy with a substantially hidden SFR.

4.3 GRB 061201: a very faint host galaxy

Observations reported in the literature: GRB 061201 was discovered by *Swift*/BAT at 15:58:36 UT on 1 Dezember 2006. It was also observed by the *Konus-Wind*satellite (Golenetskii et al. 2006). The burst had a duration of T_{90}(15–150 keV) = 0.9 ± 0.1 s. It consisted of two main spikes, the first starting at the time of the trigger and the second peaking at 0.8 s. The fluence in the BAT window (15–150 keV) was $3.4 \pm 0.2 \times 10^{-7}$ erg cm^{-2}, while in the *Konus-Wind* window (20–30 MeV) it was 5.3×10^{-6} erg cm^{-2}.

The GRB afterglow is in detail discussed in Stratta et al. (2007). *Swift*/XRT detected an

afterglow at coordinates RA, Decl. (J2000) = 22:08:19.0, −74:34:48.1 (error circle 3.″8). The final enhanced XRT error circle is located at RA, Decl. (J2000) = 22:08:32.31, −74:34:48.1, with an error radius of 1.″4.

Swift/UVOT observed the field and detected an optical transient in the *U, UVW1, UVM2, UVW2*, and *white-band* filter at coordinates RA, Decl. (J2000) = 22:08:32.21, −74:34:47.3 (with an astrometric uncertainty of 1 arcsec; Holland & Marshall 2006; Perri et al. 2006). Follow-up observations with VLT/FORS2 about 9 hours after the GRB trigger confirmed the UVOT source in a deep (900 s) *I*-band image (RA, Decl. (J2000) = 22:08:32.09, −74:34:47.8, ±0.″2; D'Avanzo et al. 2006). The optical transient was not detected anymore 1.4 days after the burst (D'Avanzo & Piranomonte 2006). The fading afterglow was also identified in the NIR bands (Haislip et al. 2006).

Host galaxy: The field was observed with VLT/FORS1 and FORS2 in six different epochs starting 9 hours after the GRB trigger up to May 2007 (ESO programme 078.D-0809 and 177.A-0591, PI: S. Antonelli and J. Horth, respectively). At the position of the optical afterglow there is no underlying galaxy down to R_C ∼26 mag. On the VLT images, the galaxy closest to the optical afterglow lies ∼17 arcsec N-W. It is an extended nearly edge-on spiral at coordinates RA, Decl. (J2000) = 22:08:29.1, −74:34:35.8 (*G1* in Fig. 4.3). Long-slit spectroscopy revealed emission lines from [O II] and Hα at a common redshift of $z = 0.111$ (Stratta et al. 2007). The projected spatial offset between *G1* and the afterglow is 35 kpc. Similar results were reported based on Magellan observations (Berger 2006). The SFR based on the Hα flux is 0.14 $M_\odot$ yr^{-1} (Stratta et al. 2007). Galaxy *G1* was considered by the latter authors as the most likely host-galaxy candidate.

The field was also observed by *HST* in three different epochs between 2007 and 2013 (programme ID 12502, PI: A. Fruchter). Using these publicely available data, I have selected the deepest observations (∼1.8 hr) which were performed using the F160W filter. Figure 4.3 shows in red the 1.″4 XRT error circle and with a black cross the position of the optical afterglow. On the *HST* image, the galaxy *G1* has a dimension of ∼ 12″ × 5″, corresponding to 25×10 kpc^2. Although the *HST* image goes deeper than the VLT image, at the position of the optical transient there is no evidence for an underlying galaxy. However, inside the 1.″4 XRT error circle lies a faint galaxy (*G2*) that is not visible on the VLT images, located ∼1.″8 S-E of the optical transient at coordinates RA, Decl. (J2000) = 22:08:32.5, −74:34:47.7 (r ∼25.5 mag; Fong et al. 2011). On the *HST* image, the morphology of *G2* resembles a spiral galaxy with its major axis parallel to the E-W direction. There is no redshift information for galaxy *G2*. Its position close to the optical transient classifies it as another host-galaxy candidate, though its chance probability value

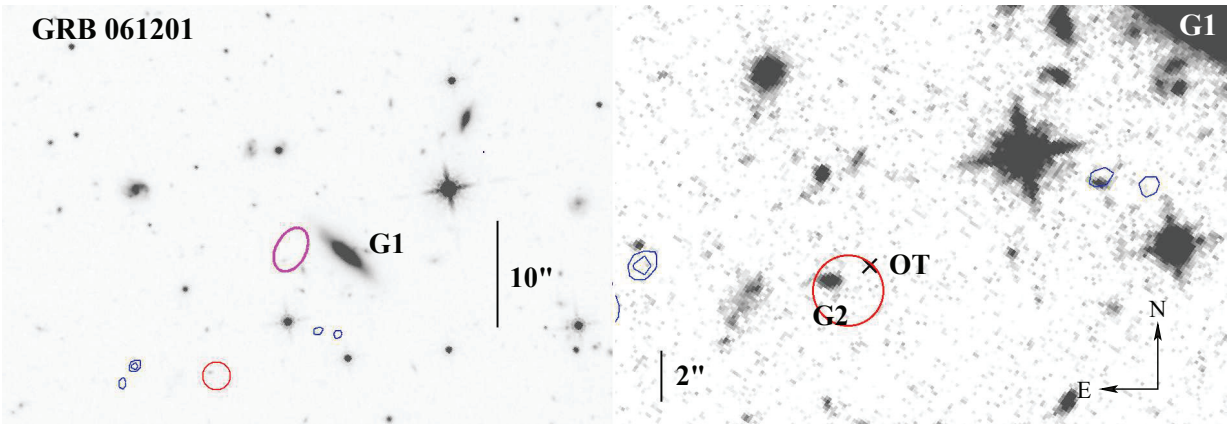

Fig. 4.3: *Left: HST*/F160W image (programme ID 12502, PI: A. Fruchter) of the field of GRB 061201. In red is shown the enhanced 1.″4 XRT error circle, in magenta the synthesized beam (2.″3 × 1.″5, position angle 62.1 deg). Based on VLT/FORS2 images, the spiral galaxy *G1* was originally considered as the most likely host-galaxy candidate (z = 0.111; Stratta et al. 2007). *ATCA* 5.5 GHz isolines are drawn in steps of 0.5 $\sigma_{\rm rms}$, starting at 3 $\sigma_{\rm rms}$ (Table 5.1). *Right: HST* imaging by Fong et al. (2011)) revealed the presence of a faint galaxy (*G2*) inside the XRT error circle, ∼1.″8 S-E to the position of the OT (black cross). Neither *G1* nor *G2* is detected by ATCA.

p (Eq. 1.1) is not as small as the one for *G1* (Table 2.3).

Radio observations: *ATCA* observed the field of GRB 061201 during three different visits in July 2013 for about 15.4 hours (Table 2.4). Phase calibration was performed by observing the quasar *PKS 2142-758* (redshift z = 1.139), which has a radio flux of F_ν(5.5 GHz) = 1.88 Jy and F_ν(9.0 GHz)=1.62 Jy. The final deconvolved radio image is the combination of all three observing runs. The 1 $\sigma_{\rm rms}$ on the combined deconvolved radio images is 5.1 ± 0.1 μJy beam^{-1} at 5.5 GHz and between 4.6 and 5.2 μJy beam^{-1} at 9.0 GHz (Table 5.1).

The *ATCA* data do not show any radio source either inside the XRT error circle (galaxy *G2*), or at the position of galaxy *G1* down to the following 3σ upper limits: $F_\nu(5.5) < 15$ μJy and $F_\nu(9.0) < 14$ μJy. This radio flux translates into an upper limit for the SFR in galaxy *G1* of 0.8 $M_\odot$ yr^{-1}. Compared to the reported optical SFR of 0.14 $M_\odot$ yr^{-1} (Stratta et al. 2007) this excludes the presence of a substantial amount of obscured star-formation activity. Concerning *G2*, its optical SFR is unknown. If this faint galaxy lies at z=1.0 then the 5.5 GHz upper limit implies an SFR of $\lesssim$ 110 $M_\odot$ yr^{-1}.

4.4 GRB 070729: three host-galaxy candidates

Observations reported in the literature: *Swift*/BAT triggered on GRB 070729 at 00:25:53 UT on 29 July 2007 (Guidorzi et al. 2007a). The burst was also seen by the *Konus* satellite

(Golenetskii et al. 2007b). It had a duration of T_{90}(15–350 keV) = 0.9 ± 0.1 s (Guidorzi et al. 2007c). An uncatalogued X-ray source was found by *Swift*/XRT, but no optical afterglow could be identified by *Swift*/UVOT (Guidorzi et al. 2007a). Inside the initial 5.″7 XRT error circle, Berger & Kaplan (2007) reported the detection of an extended object in the *K* band. A refined XRT error circle with a radius of r = 4.″5 was later reported by Guidorzi et al. (2007b). This error circle lies 3.″2 away from the initial XRT position. The position of the XRT afterglow was refined again in the year 2011 and shifted by about 5 arcsec in north-east direction while its error radius shrunk to r = 2.″5 (Evans 2011b,a). An inspection (Jan 2017) of the *Swift* webpage for the XRT enhanced positions shows that the XRT error circle was revised again and is now centered at RA, Decl. (J2000)= 03:45:15.98, −39:19:20.5, with an error radius of 2.6 arcsec.

GRB 070729 was the first short GRB observed with GROND after its commissioning in mid-2007. GROND observations started 6 hours after the burst and continued for 4.5 hours until sunrise. A second-epoch observation was performed the following night for 1 hr. No transient object between the two epochs was detected in any band (Küpcü Yoldaş et al. 2008). No optical afterglow was detected by any other ground-based observatory, no afterglow was detected in the radio band either (8.5 GHz, $F_\nu = -71 \pm 85$ μJy; Chandra & Frail 2007). The latter observations also constrain the radio flux of the underlying host galaxy.

Host galaxy: The field was observed with VLT/FORS2 in the $Z_{\rm Gunn}$ band and with *HAWKI* in the *H* band in mid 2013 (ESO programme ID 091.D-0904, PI: J. Horth). There is no galaxy inside the final XRT error circle (Fig. 4.4). Two faint objects (*G2*) lie at the western border of the error circle. The morphology of *G2* suggests two galactic nuclei, possibly a pair of merging galaxies. In the *HAWKI* *H*-band image *G2* seems to have only one nucleus. *G2* is the most likely host-galaxy candidate due to its proximity to the XRT error circle. No redshift for this object is known.

Two additional brighter galaxies lie close to the XRT error circle (*G1, G3*). They are in more detail discussed in Küpcü Yoldaş et al. (2008). Besides, the field was also studied in a comprehensive work by Leibler & Berger (2010). However, these authors did not publish finding charts or discussed these galaxies in detail. Galaxy *G1* lies around 10 arcsec north-east of the error circle. In the FORS2 $Z_{\rm Gunn}$-band optical image galaxy *G1* has an angular size of about 5″ × 4″. GROND observations showed that this is a red galaxy with $(r' - K)_{\rm AB} = 2.8 \pm 0.2$ mag. Galaxy *G3* is an even redder one with $(r' - K)_{\rm AB} = 3.2 \pm 0.2$ mag. It is located at a similar angular distance than galaxy *G1* but south-west of the XRT error circle. Its angular size is about 3.″5 × 2.″0. Neither *G1* nor *G3* seem to be elliptical galaxies. The fact that galaxies *G1* and *G3* are very red suggests that these are dusty star-forming galaxies. No spectroscopic redshifts are

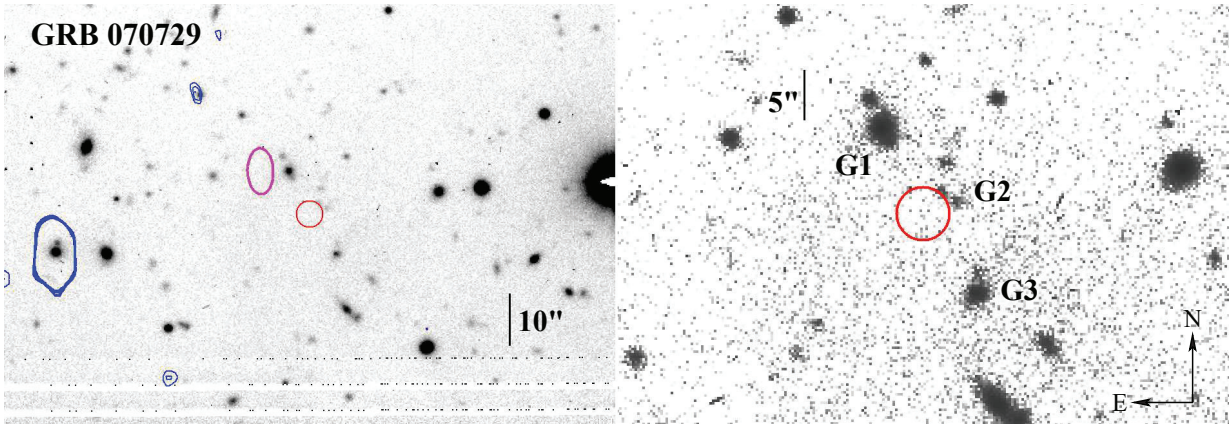

Fig. 4.4: *Left:* FORS2 $Z_{\rm Gunn}$-band image (archived data; ESO programme ID 091.D-0904, PI: J. Horth) of the field of GRB 070729. In red is shown the 2.″6 XRT error circle, in magenta the synthesized beam at 5.5 GHz (4.″5 × 2.″5, position angle 91.6 deg). The radio contours at 5.5 GHz are overplotted in blue colour. Contour lines are drawn in steps of 1/2 $\sigma_{\rm rms}$, starting at 3 $\sigma_{\rm rms}$ (1 $\sigma_{\rm rms}$ = 7.3 μJy beam^{-1}; Table 5.1). A bright radio source with an optical counterpart is located 50 arcsec east of the XRT error circle. *Right:* Zoom-in of the field showing *G1, G2*, and *G3* which are the galaxies nearest to the error circle. None of these galaxies is detected in the radio band.

known for galaxies *G1*, *G2* and *G3*.

Using `Le Phare` (Arnouts et al. 1999; Ilbert et al. 2006) [3], the GROND and WISE broad-band photometry of these faint galaxies is not sufficient to provide their redshifts. Even for the brightest galaxies, *G1* and *G3*, the redshift can only be constrained in a very wide range. Fixing the redshift to z=0.5 gives for *G1* an SFR of 100±50 M$_\odot$ yr^{-1} and for *G3* 5±4 M$_\odot$ yr^{-1}.

Radio observations: *ATCA* radio data of the field were obtained via remote observing from Lyon (France) on 24 September 2015. They lasted for about 11 hours. Phase calibration was performed by observing the Seyfert 2 galaxy *PKS 1934-63* at a redshift of z = 0.1812 which has a radio flux of F_ν(5.5 GHz) = 4.95 Jy and F_ν(9.0 GHz)=2.70 Jy. The 1 $\sigma_{\rm rms}$ on the deconvolved images is 7.3 μJy beam^{-1} at 5.5 GHz and 6.8 ± 0.1 μJy beam^{-1} at 9.0 GHz (Table 5.1).

There is no evidence for a radio source either inside the enhanced 2.″6 XRT error circle or at the position of galaxies *G1*, *G2*, and *G3* down to 3σ upper limits of F_ν(5.5) < 22 μJy and F_ν(9.0) < 21 μJy). Assuming a redshift of z=0.5, the *ATCA* data constrain the SFR for these galaxies to < 32 M$_\odot$ yr^{-1}. In the case of *G1* this is smaller than the result of the `Le Phare` fit, possibly indicating that here the adopted redshift is too small.

[3] `http://www.cfht.hawaii.edu/~arnouts/LEPHARE`

4.5 GRB 070809: two suspected host-galaxy candidates

Observations reported in the literature: GRB 070809 triggered *Swift*/BAT at 19:22:17 UT on 7 August 2007. The burst had a main spike with a duration of T_{90}(15–150 keV) = 1.3 ± 0.1 s. The fluence of the burst in the energy range of 15–150 keV was $1.0 \pm 0.1 \times 10^{-7}$ erg cm^{-2} (Krimm et al. 2007). The XRT started observations 71 seconds after the triger. A moderately bright X-ray afterglow was found at coordinates RA, Decl. (J2000) = 13:35:04.74, −22:08:29.9, with an error radius of 3.″6. *Swift*/UVOT performed observations in the *V* band simultaneously with XRT but did not detect any optical counterpart (Marshall et al. 2007), even though the Galactic reddening along the line of sight is small ($E(B-V)$ = 0.09 mag; Schlegel et al. 1998).

Keck follow-up observations performed around 10 hours after the GRB trigger revealed a fading optical afterglow at the edge of the XRT error circle, at coordinates RA, Decl. (J2000) = 13:35:04.5, −22:08:30.8, with a positional uncertainty of 0.4 arcsec (Perley et al. 2007, 2008). The optical afterglow had a magnitude of R∼24.0 mag. Close to the optical transient lies a bright ∼13 mag star that challenges the photometry of the afterglow (Fig. 4.5).

Host galaxy: Keck images obtained in 2008 do not show evidence for an underlying host galaxy either at the position of the optical afterglow or within the complete 3.″6 XRT error circle (Perley et al. 2008). On these Keck images, the galaxy nearest to the optical afterglow lies 6 arcsec N-W. It is an edge-on spiral at coordinates RA, Decl. (J2000) = 13:35:04.22, −22:08:27.4 (*G1*; Fig. 4.5). Additional Keck spectroscopy by these authors revealed the presence of bright emission lines from [O II] and [O III] at a common redshift of $z = 0.2187$. This galaxy lies at a projected distance of ∼ 22 kpc from the optical afterglow. The flux in the [O II] line is 2.0×10^{-16} erg s^{-1} cm^{-2}, corresponding to an optical SFR of 0.15 M$_\odot$ yr^{-1}.

A second galaxy (*G2*) lies 6 arsec west from the optical transient at coordinates RA, Decl. (J2000) = 13:35:04.14, −22:08:33.5. It is an E0 elliptical at a redshift of $z = 0.473$, with no evidence for star formation (Berger 2010a). The diameter of *G2* is about 3.″0, equivalent to 18 kpc. It has a magnitude of $r = 19.89 \pm 0.02$ (Leibler & Berger 2010). The field was also observed by *HST* at two different epochs (Aug 2009/May 2010) with two different filters (F606W/F160W; programme ID 12502, PI: A. Fruchter). At the position of the optical afterglow there is no underlying host galaxy either at the optical (>28.1 mag) or in the NIR (H >26.2 mag; Fong & Berger 2013). The *HST* observations reveal the presence of a faint background galaxy (*G3*) inside the XRT error circle (Fig. 4.5). Using Eq. 1.1, all three host-galaxy candidates have small p values, with the smallest chance coincidence probability for the elliptical galaxy *G2* (Tab. 2.3).

Radio observations: *ATCA* radio observations were performed on 19 June 2013 (Table 2.4).

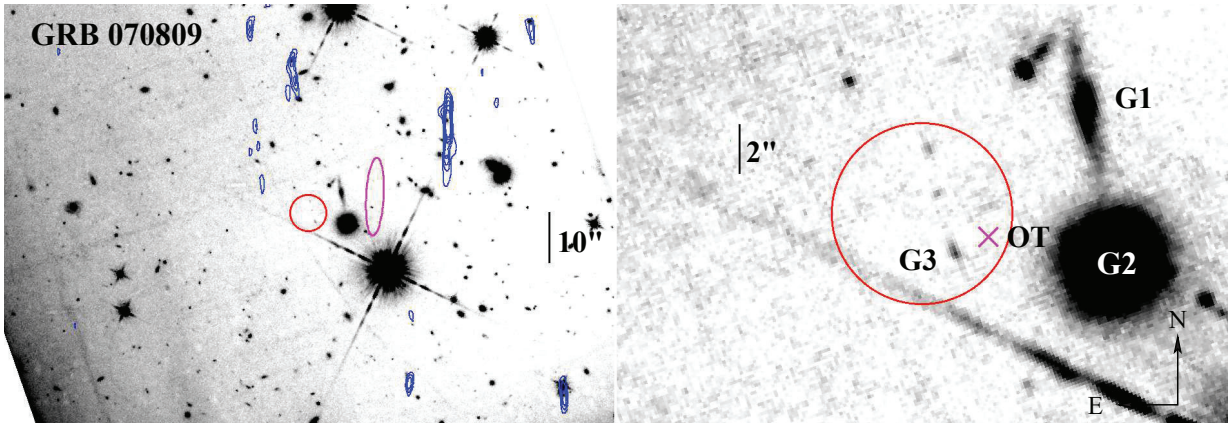

Fig. 4.5: *Left:* Archived *HST*/F606W image (programme ID 12502, PI: A. Fruchter) of the field of GRB 070809. In red is shown the 3.″6 XRT error circle, in magenta the size and position angle of the synthesized radio beam (7.″7 × 1.″7, position angle 87.9 deg). Radio contours at 5.5 GHz are drawn in blue color with steps of 1/2 $\sigma_{\rm rms}$, starting at 3 $\sigma_{\rm rms}$ (1 $\sigma_{\rm rms}$ = 6.0 μJy beam^{-1}; Table 5.1). *Right:* Zoom-in of the field. The cross indicates the position of the optical afterglow (not visible anymore). *G1* is an edge-on spiral close to the position of the OT (redshift z = 0.2187; Perley et al. 2008), *G2* is an elliptical at z = 0.473 (Berger 2010a). *G3* is faint background galaxy inside the XRT error circle. Its redshift is not known. No radio flux was detected either from any of the designated galaxies or from the position of the OT.

As a phase calibrator I used the radio galaxy *PKS 1308-220* (most commonly known as *3C 283*, redshift z=0.8, F_ν(5.5 GHz) = 1.02 Jy, F_ν(9.0 GHz)=0.51 Jy). The 1 $\sigma_{\rm rms}$ on the deconvolved images is between 6.0 μJy beam^{-1} and 7.3 μJy beam^{-1} at 5.5 GHz and between 6.1 μJy beam^{-1} and 6.4 μJy beam^{-1} at 9.0 GHz (Table 5.1). There is no radio source at the position of the optical transient down to 3σ upper limits of 18 μJy at 5.5 and 9.0 GHz. Besides, there is no detection of radio flux coming from *G1* or *G2*. In the case of *G1*, the 5.5 GHz upper limit constraints the SFR to < 4 M$_\odot$ yr^{-1}. For *G2*, the 5.5 GHz upper limit implies a SFR < 23 M$_\odot$ yr^{-1}. Given that this is an E0 galaxy, no sign of star-formation was expected. The radio data simply define this elliptical as a radio-quiet galaxy.

4.6 GRB 080123: a relatively bright host-galaxy candidate

Observations reported in the literature: The burst triggered *Swift*/BAT at 04:21:57 UT on January 23, 2008 (Ukwatta et al. 2008b). Its duration was T_{90}(15–150 keV) = 0.5 ± 0.1 s. The temporal profile showed a double-peaked structure with two well-separated peaks at 0.3 s and 0.6 s (Ukwatta et al. 2008b,b). *Swift*/XRT detected an X-ray afterglow during the first 10 ks after the GRB trigger. Its light curve showed a steep decay at early times and became flatter at later times. The enhanced XRT error circle is located at coordinates RA, Decl. (J2000) = 22:35:46.33, −64:54:02.7, with an uncertainty of 1.7 arcsec. *Swift*/UVOT started observations

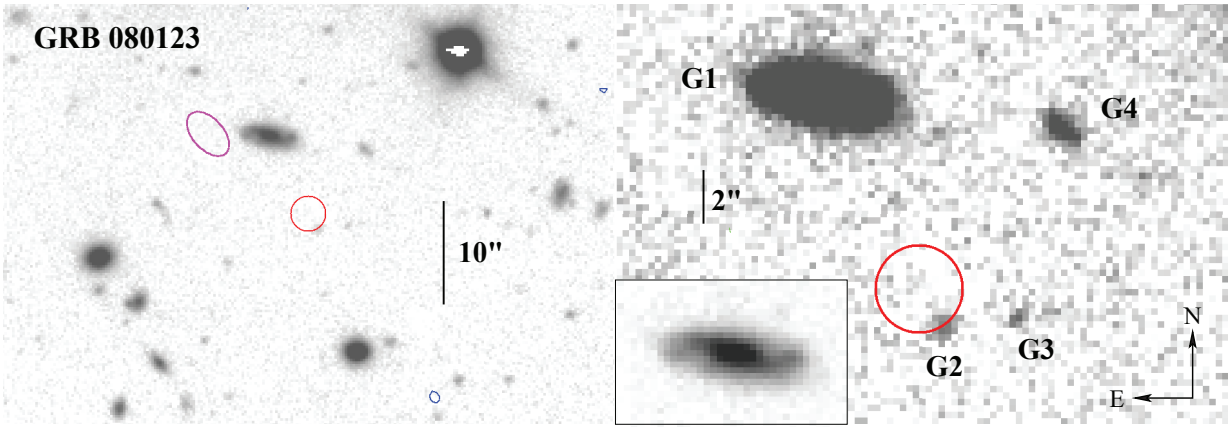

Fig. 4.6: *Left:* FORS2 image (ESO program ID 383.A-0399; PI: S. Klose) of the field of GRB 080123. In red it is shown the 1.″7 XRT error circle. In magenta it is shown the size and position angle of the synthesized radio beam (2.″6 × 1.″5, position angle 132.3 deg). No radio source was found in the field shown here (3 $\sigma_{\rm rms}$ upper limit = 19 μJy beam^{-1}; Table 5.1). *Right:* Zoom-in of the field showing the galaxies nearest to the XRT error circle. *G1* is the most likely host-galaxy candidate based on chance probability analysis (Leibler & Berger 2010). The inset shows the spiral structure of *G1* as it appears after changing the contrast parameters in the VLT image.

around 100 seconds after the trigger but no optical afterglow was detected (Ukwatta et al. 2008a), although the X-ray afterglow was still visible for *Swift*/XRT. No other optical/NIR observations are reported in the literature.

Host galaxy: In May 2009 we obtained VLT/FORS2 *R*-band (~90 min) as well as ISAAC K_s-band (~32 min) imaging data of the field of GRB 080123 (ESO program ID 383.A-0399; PI: S. Klose). Inside the 1.″7 XRT error circle, the VLT images do not reveal any source down to R_C = 27.0 and K_s = 23.3 mag. An optical faint source (*G2*) lies at the border of the XRT error circle, another source around 3 arcsec west of *G3* (Fig. 4.6). *G2* and *G3* are very faint in the R_c-band (~25.5 mag; Fig. 4.6) and not detected in the ISAAC K_s-band image down to K_s = 23.3 mag.

The most prominent object in the field is a galaxy (*G1*, z=0.496; R_C=19.6 mag) ~8 arcsec north-east of the center of the XRT error circle at coordinates RA, Decl. (J2000) = 22:35:46.92, −64:53:55.1 (Leibler & Berger (2010)). Besides, it is the most likely host-galaxy candidate (Table 2.3). The FORS2 R_C-band image reveals that this is an inclined, barred spiral with two symmetric spiral arms. Its central bar is relatively bright and extended. The major axis lies in the E-W direction and shows no signs of asymmetric distortions.

Additional long-slit spectroscopy of galaxy *G1* was obtained with VLT/FORS2 in October and November 2011 using the *GRIS 600B* and *GRIS 600RI* grism (PI: A. Nicuesa Guelbenzu, ESO programme ID 088.D-0657), covering the wavelength range from 3300 Å to 8450 Å. The

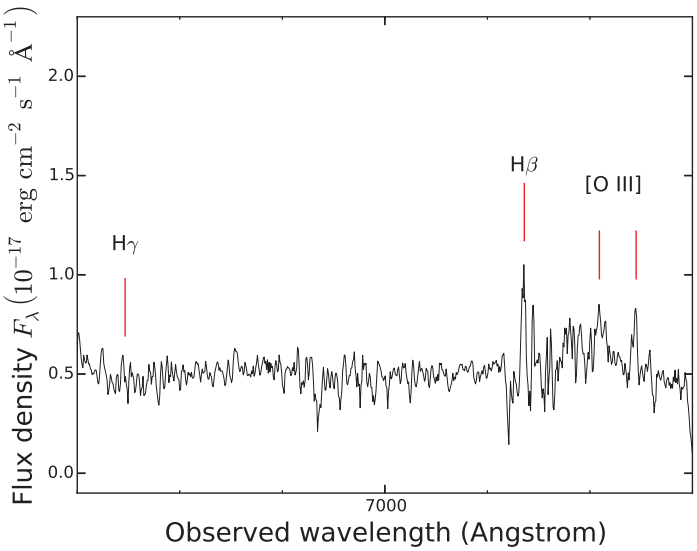

Fig. 4.7: FORS2 spectrum of the suspected host of GRB 080123 (*G1*) obtained with *GRIS 600RI* (ESO programme ID 088.D-0657, PI: A. Nicuesa Guelbenzu). It shows emission from the [O III] doublet, H*beta* and Hγ at a common redshift of z=0.496. When zooming-in the [O III] emission lines show a blue and a redshifted Doppler component due to the rotation of the disk (not shown here).

spectral slit was oriented along the major axis of the galaxy *G1* but the slit-width of 1 arcsec did not cover the complete minor axis which has a width of 2.5 arcsec. The spectrum (Fig. 4.7) shows emission lines of Hβ, Hγ, and [O III] at a common redshift of z=0.496, in agreement with what was reported by Leibler & Berger (2010). The blue spectrum obtained with the *GRIS 600B* is of less quality. I could not identify neither emission nor absorption lines.

At z=0.496 an angular distance of 1 arcsec corresponds to 6.2 kpc projected distance. Consequently, *G1* is a large galaxy ($\sim 37 \times 15$ kpc^2). Its SFR based on the measured Hβ line flux in the FORS2 spectrum is 0.7 M$_\odot$ yr^{-1}. In other words, in the optical the suspected host galaxy of the short GRB 080123 appears as a moderately star-forming, barred spiral galaxy.

Unfortunately, nothing can be said about *G2*. Although during the FORS2 observations the spectral slit was covering this galaxy, I could not identify any trace of this object. Its redshift remains unknown.

Radio observations: *ATCA* observations were performed on 25 July 2013 for 8.7 hours. Thereby, as a phase calibrator I observed the quasar *PKS 2353–686* (z = 1.716), which has a radio flux of F_ν(5.5 GHz) = 1.53 Jy and F_ν(9.0 GHz) = 1.47 Jy. The 1 $\sigma_{\rm rms}$ on the combined deconvolved radio image is 6.3 $\pm$0.1 μJy beam^{-1} at 5.5 GHz and between 6.1 and 6.6 μJy beam^{-1} at 9.0 GHz (Table 5.1). *ATCA* did not detect any radio flux at the position of the 1.″7 XRT error circle. Besides, the suspected GRB host galaxy *G1* is not detected either (F_ν(5.5 GHz) < 19 μJy, F_ν(9.0 GHz)< 18 μJy, 3 $\sigma_{\rm rms}$). At a redshift of z=0.496, this constraints the SFR to less than 27 M$_\odot$ yr^{-1}. Compared with the aforementioned optical SFR of 0.7 M$_\odot$ yr^{-1}, this still leaves open the possible presence of unobscured star-formation in *G1*.

4.7 GRB 080905A: a cosmologically nearby, face-on spiral host galaxy

Observations reported in the literature: *Swift*/BAT and *Fermi*/GBM triggered on GRB 080905A at 11:58:55 UT (Bissaldi et al. 2008; Pagani et al. 2008). The BAT light curve shows two peaks with a total duration of T_{90} (15–350 keV)=1.1 ± 0.1s (Cummings et al. 2008). A fading X-ray afterglow was found at coordinates RA, Decl. (J2000) =19:10:41.78, −18:52:48.5, with an error circle of 1.6 arcsec. However, no optical afterglow was detected with *Swift*/UVOT (Pagani et al. 2008). Even though the burst occured in a crowded stellar field, a faint optical afterglow candidate (R ∼24 mag) was discovered 8 hours after the GRB trigger with the Nordic Optical Telescope (NOT) on La Palma and with VLT/FORS2 at coordinates RA, Decl. (J2000) = 19:10:41.73, −18:52:47.3 (Malesani et al. 2008). Its fading was confirmed by follow-up observations with FORS2 1.5 days after the burst. A host-galaxy candidate was identified by de Ugarte Postigo et al. (2008).

GROND started observing the field of GRB 080905A about 17.5 hrs after the burst. Observations could be performed for only 11 min at a bad seeing of 2.″2. The combined $g'r'i'z'$-band image as well as the combined JHK_s-band image did not reveal the afterglow, even though it goes down to $g'r'i'z'JHK_s$= 23.0, 22.8, 22.3, 21.9, 20.4, 19.9, 19.6 (AB magnitudes; Nicuesa Guelbenzu et al. 2012). Published work showed that at the time of the *GROND* observations the magnitude of the afterglow was around $R_C = 24$, about 1 mag below our detection limit.

Host galaxy: Using VLT data, the afterglow and its host have been analyzed in detail by Rowlinson et al. (2010). The afterglow was located in the outer arm of a face-on spiral galaxy at a redshift of $z = 0.1218 \pm 0.0003$, the most nearby short GRB with an optical afterglow to date (Jan 2017). The host galaxy is centered at coordinates RA, Decl. (J2000) =19:10:41.95, −18:52:54.4, ∼8 arcsec S-E of the optical afterglow. On the VLT K_s-band image its spiral arms extend into the northern direction by more than 6 arcsec (13 kpc). The projected offset of the burst from the galaxy bulge is ∼18 kpc. Since there is no evidence for an underlying faint background galaxy, this suggests (but does not prove) that the GRB progenitor was in the process of escaping its host galaxy when it was exploding. Rowlinson et al. (2010) derived for this galaxy an absolute magnitude of $M_V = -21$ mag and a mass in old stars (based on the K_s-band data) of $(2 \pm 1) \times 10^{10}\,M_\odot$, i.e., this galaxy resembles the Milky Way galaxy. Because the field is crowded with Galactic foreground stars (see figure 3 in Rowlinson et al. 2010), no SFR could be derived for this galaxy by these authors based on the optical data.

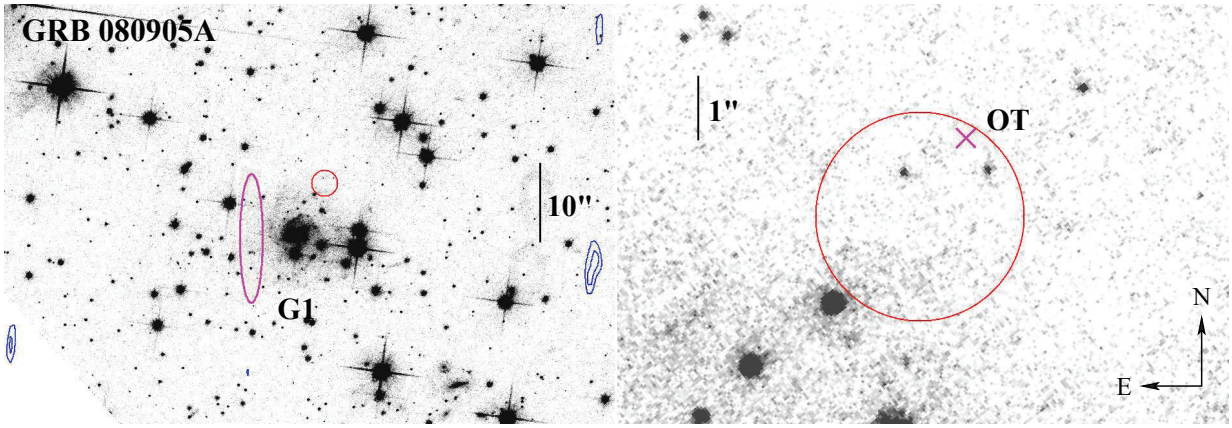

Fig. 4.8: *Left: HST*/F160W image (program ID 12502; PI: A. Fruchter) of the field of GRB 080905A. *G1* is the host galaxy of GRB 080905 at a redshift of $z = 0.1218 \pm 0.0003$. The optical transient (OT) was located 18 kpc (projected distance) from the center of its host galaxy. In red is shown the 1.″6 XRT error circle, in magenta the synthesized beam (7.″9 × 1.″4, position angle 89.9 deg). Blue contour lines correspond to 3 and 3.5 times the $\sigma_{\rm rms}$ (brighter radio sources are not visible in this image; 1 $\sigma_{\rm rms}$ = 5.7μJy beam^{-1}; Table 5.1). The field is rather sparse in radio sources at 5.5 GHz, *Right:* Zoom-in of the field. The red cross marks the position of the optical transient (not visible anymore). In red is drawn the XRT error circle.

The field was also observed by *HST* during four different occasions between the year 2011 and 2012 (programme ID 12502; PI: A. Fruchter). Figure 4.8 shows the deep (1.3 hr) *HST*/F160W image of the field where the spiral morphology of the galaxy appears in great detail (Fong & Berger 2013). Despite the small redshift, the galaxy is not detected by the *WISE* satellite in any band.

Radio data: Observations with *ATCA* were executed on 20 July 2013 and on 25 October 2015 with a total observing time of 10.5 hours. In both runs, phase calibration was performed by observing the quasar PKSB[4] *1908-201* (redshift $z = 1.119$) which has a radio flux of F_ν(5.5 GHz) = 2.79 Jy and F_ν(9.0 GHz)=3.0 Jy. The resulting 1 $\sigma_{\rm rms}$ of the deconvolved images is between 5.4 and 5.7 μJy beam^{-1} at 5.5 GHz and between 6.5 and 7.4 μJy beam^{-1} at 9.0 GHz (Table 5.1).

Given the angular distance between the bulge of the spiral galaxy and the position of the OT (~8 arcsec), the synthesized beam size was in principle small enough to decide whether a potential radio signal is coming from the position of the OT. Unfortunately, despite the small redshift no signal is detected, either from the galaxy as a whole or from the region where the OT was placed. The measured 3σ upper limits are $F_\nu(5.5) < 17$ μJy and $F_\nu(9.0) < 20$ μJy. At a redshift of $z = 0.1218$, the 5.5 GHz radio limit constraints the unobscured SFR within the smalles radio beam size 7.″9 × 1.″4 (the beam size for a robust parameter of 0.5; Table 7.2) to <1.1 M$_\odot$ yr^{-1}. In other words, this is the upper limit of the SFR in an aera of 18 × 3 kpc^2 around

[4] `Parkes Radio Catalog in B1950 coordinates`

the position of the OT.

4.8 GRB 130515A: a galaxy close to the XRT error circle

Observations reported in the literature: GRB 130515A was discovered by *Swift*/BAT at 01:21:17 UT on 13 May 2015. It consisted of a single short spike with a duration of T_{90}(15–150 keV) = 0.6 ± 0.1 s. *Swift*/XRT started observations 75 s later and found a faint X-ray afterglow at coordinates RA, Decl. (J2000) = 18:53:45.72, −54:16:45.9 (90% c.l. error circle 3.″1 radius[5]; Malesani et al. 2013). VLT imaging observations revealed one source inside the XRT error circle (*S1*; *R*=21.1, Xu et al. 2013) and two additional sources close to it (*S2, S3*, Fig 4.9; Xu et al. 2013). GROND follow-up observations started 50 min after the GRB trigger and confirmed the presence of the source inside the XRT error circle (*S1*; Schmidl et al. 2013). *Gemini* observations did not reveal the fading of any of these sources. Despite several optical follow-up campaigns, no optical afterglow could be found (Cenko & Cucchiara 2013; Levan & Tanvir 2013; Xu et al. 2013).

Host galaxy: VLT/FORS2 observed the field of GRB 130515A in photometric as well as in spectroscopic mode (ESO program ID 091.D-0558; PI: A. Levan). On the FORS2 R_C-band image, *S1, S2*, and *S3* have a point-like profile (Fig 4.9; Levan & Tanvir 2013). Spectroscopic observations revealed that *S1*, located at coordinates RA, Decl. (J2000) =18:53:45.82, −54:16:47.4, is an M dwarf star (Levan & Tanvir 2013). An inspection of the archived VLT data shows that during these observations the spectral slit did only cover *S1*.

Using the archived FORS2 R_C-band image, the only and most obvious galaxy closest to the 2.″2 XRT error circle is *G1* ($r'_{\rm AB}$ = 21.20 ± 0.05; Fig 4.9). It lies ∼6 arcsec south-west of the XRT position at coordinates RA, Decl. (J2000) = 18:53:44.88, −54:16:50.9 (Levan & Tanvir 2013). It is a faint galaxy with an angular diameter of about 5 arcsec. Its spectroscopic redshift is not known. The morphology of this galaxy in its eastern part appears to be slightly disturbed, possibly indicating signs of a galaxy-galaxy interaction. It is also possible that these are two galaxies very close togehter, which could not be resolved in the FORS2 image.

Figure 4.10 shows the broad-band SED of galaxy *G1* using *GROND* magnitudes (g', z', J, H, K_s) as well as VLT/FORS2 $R_{\rm special}$ and I_c. The SED is best described by a relatively young stellar population with a stellar age of $0.57^{+0.14}_{-0.10}$ Gyr, a stellar mass of $\log {\rm M}_\star/{\rm M}_\odot = 10^{+0.10}_{-0.13}$ and a SFR of 0.3–2.3 $\rm M_\odot\ yr^{-1}$. In the short-GRB host galaxy sample studied by Leibler & Berger (2010)

[5]The final enhanced XRT position is located at RA, Decl. (J2000) = 18:53:45.7, −54:16:45.7, with a 2.″2 error circle.

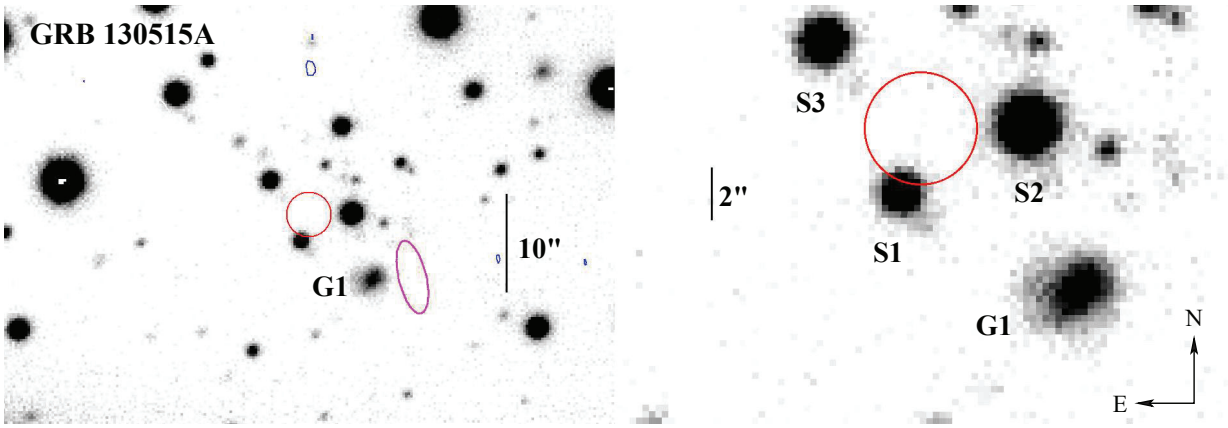

Fig. 4.9: *Left:* FORS2 R_C-band image (ESO program ID 091.D-0558; PI: A. Levan) of the field of GRB 130515A. In red is shown the 2.″2 XRT error circle, in magenta the synthesized beam (3.″6 × 1.″3, position angle 103.2 deg). The blue contour line line north of the XRT error circle shows the only radio source in the field (corresponding to 3 times the $\sigma_{\rm rms}$; 1 $\sigma_{\rm rms}$ = 6.2 μJy beam^{-1}; Table 5.1). *Right:* Zoom-in of the field. *S1, S2* and *S3* are stars (Levan & Tanvir 2013), *G1* is the most likely host-galaxy candidate.

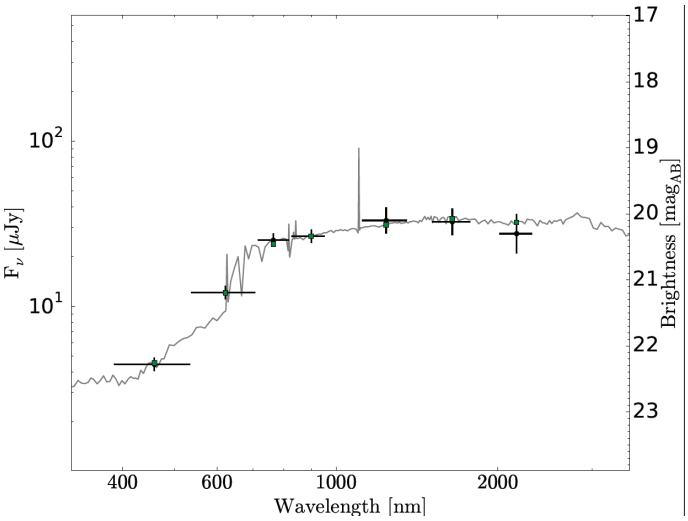

Fig. 4.10: Broad-band SED of the host galaxy of GRB 130515A based on *GROND* and FORS2 data and the best fit using the `Le Phare` package (χ^2=0.1).

the stellar mass was found to vary between log $M_\star/M_\odot$ = 8.8 and 10.6. Hence, the suspected host galaxy of GRB 130515A is quite massive member of its class. According to the `Le Phare` fit, the redshift of this galaxy is unfortunately not well constrained, $z = 0.68^{+0.77}_{-0.47}$.

If its redshift is z=0.5 then the GRB progenitor was exploding at a projected distance of $\sim$ 40 ± 15 kpc (where the error reflects the radius of the XRT error circle). This large distance from the center of its host could suggest that at the time of its explosion the GRB progenitor was escaping its host. Alternatively, it could have been exploding in an undetected satellite galaxy or in a globular cluster orbiting *G1*.

Radio observations: *ATCA* radio-continuum observations of the field were executed on 26 October 2015, about 2.5 years after the burst and lasted for about 7 hours. Phase calibration was performed by observing the quasar *PKS 1824–582* (redshift z = 1.531) which has a radio flux

of F_ν(5.5 GHz) = 1.44 Jy and F_ν(9.0 GHz)=2.06 Jy. The resulting 1 $\sigma_{\rm rms}$ of the deconvolved images is ~6.0 μJy beam^{-1} at 5.5 GHz and ~ 8 μJy beam^{-1} at 9.0 GHz (Table 5.1).

ATCA does not detect any radio source either inside the XRT error circle or at the position of the suspected host galaxy *G1* down to 3σ upper limits of F_ν(5.5 GHz) < 18 μJy and F_ν(9.0 GHz) < 21 μJy (Table 5.2). If *G1* lies at z = 0.5, then the 5.5 GHz radio data constrain its SFR to <26 $M_\odot$ yr^{-1}. If z=1 its SFR is <130 $M_\odot$ yr^{-1}.

4.9 GRB 150424A: a suspected bright and a suspected faint host

Observations reported in the literature: GRB 150424A was detected by *Swift*/BAT on 2015 April 25 at 07:42:57 UT. The gamma-ray emission consisted of multiple, very bright pulses with a duration of about 0.5 s followed by weak emission lasting up to 100 s. The *Swift*/XRT started observations 88 s after the burst and found a bright, fading X-ray source at coordinates RA, Decl. (J2000) = 10:09:13.35, −26:37:51.3, with a positional uncertainty of 1.4 arcsec. The GRB was also observed by the *Konus-Wind* satellite with a duration of about 0.4 seconds and emission up to 4 MeV was detected (Golenetskii et al. 2015). Optical follow-up observations with the Keck telescope 1.6 hours after the GRB trigger revealed the presence of an optical transient at coordinates RA, Decl. (J2000) = 10:09:13.38, −26:37:51.5 (Perley & McConnell 2015). The transient was also detected with the NOT telescope (Malesani et al. 2015) as well as with *Swift*/UVOT (Marshall & Beardmore 2015). Its rapid fading was confirmed by our group with GROND (Kann et al. 2015). A radio afterglow was detected with the VLA about 18 hours post burst at coordinates RA, Decl. (J2000) = 10:09:13.37, −26:37:51.5 (±0.″5) with a flux density of F_ν(9.8 GHz) = 31 μJy. Its transient nature was confirmed by additional VLA observations at 4.67 and 7.88 days (Fong 2015).

Host galaxy: Follow-up observations performed with the spanish GTC 10-m telescope (program ID GTC72-15A; PI: A. Castro-Tirado) revealed the presence of a spiral galaxy at coordinates RA, Decl. (J2000) = 10:09:13.00, −26:37:55.9, only 2 arcsec S-W to the optical transient (*G1*; Fig. 4.11). Observations were performed 15 hours after the GRB trigger when the optical transient was still visible. I downloaded these data and analyzed them again.

During the observations the spectral slit covered the location of the OT and the major axis of galaxy *G1*. The observations were performed using two different grisms, R1000B [6] and R2500I [7]

[6] wavelength coverage from 3630 to 7500 Å with a central λ at 5455 Å
[7] wavelength coverage from 7330 to 10000 Å with a central λ at 8650 Å

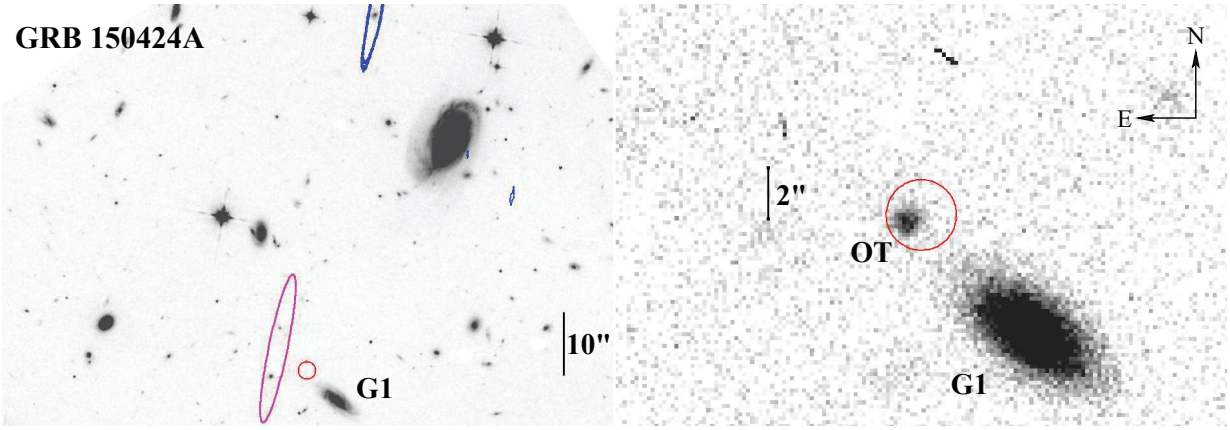

Fig. 4.11: *Left: HST* image (program ID 13830, PI: N. Tanvir) of the field of GRB 150424A. The red circle represents the r=1.″4 XRT error circle, in magenta is shown the synthesized beam (12.″0 × 1.″5, position angle 8.4 deg). Blue contour lines (left) represent the 5.5 GHz *ATCA* radio data (steps 0.5 $\sigma_{\rm rms}$, starting at 3.0 $\sigma_{\rm rms}$; 1 $\sigma_{\rm rms}$ = 7.1 μJy beam^{-1}; Table 5.1). These data were obtained 2 and 6 months after the burst. There is no evidence for a radio source at or close to the position of the burst or its originally suspected host galaxy *G1*. *Right:* GROND i'-band image of the field. The GROND data were taken 15.4 hours after the burst when the optical transient was still visible (Kann et al. 2015). *HST* observations by Tanvir et al. (2015) revealed a very faint galaxy at a position nearly coincident with the position of the OT (not visible here).

and a slit-width of 1 arcsec. The red grism R2500I has a resolving power of R = 2503 with a dispersion of 1.68 Å pixel^{-1}. The resolving power of grism R1000B is R = 1018 with a dispersion of 2.12 Å pixel^{-1}. Wavelength calibration was performed using HgAr+He+Xe calibration lamps. The bluer (R1000B) and redder (R2500I) spectra were flux-calibrated with the spectrophotometric standard star GD153.

Castro-Tirado et al. (2015) reported a redshift of z = 0.3 for *G1* based on the presence of emission lines from Hα and [O II]. I reanalyzed these data and found emission from Hα, [S II] as well as the [N II] doublet at a common redshift of z = 0.2981±0.0001 (Table 4.1). The flux in the Hα line is more prominent in the western part than in the eastern part of the galaxy (28 × 10^{-17} erg s^{-1} cm^{-2} vs. 13 × 10^{-17} erg s^{-1} cm^{-2}). In total its flux corresponds to a SFR of 0.15 M$_\odot$ yr^{-1} (Eq. 2.2). Since the spectral slit covered only 1/3 of the galaxy, a probably more realistic estimate of the optical SFR is 0.5 M$_\odot$ yr^{-1}.

On the GROND images *G1* has a size of ∼ 9.″3 × 4.″3. For the deduced redshift (z=0.298) this is equivalent to ∼ 42 × 20 kpc^2, a rather large galaxy. It was detected in all GROND bands (g' = 21.24 ± 0.05; r' = 20.15 ± 0.05; i' = 19.81 ± 0.05; z' = 19.57 ± 0.05; J = 18.8 ± 0.1; H = 18.5±0.1; K_s = 18.0±0.1). Figure 4.12 shows the broad-band SED of *G1* using the GROND data as well as the W1 and W2 *WISE* satellite data. Fixing the redshift to z=0.298, `Le Phare` finds that this is a star-forming galaxy (SFR ∼7 M$_\odot$ yr^{-1}) with an internal reddening of $E(B-V)_{\rm host}$=

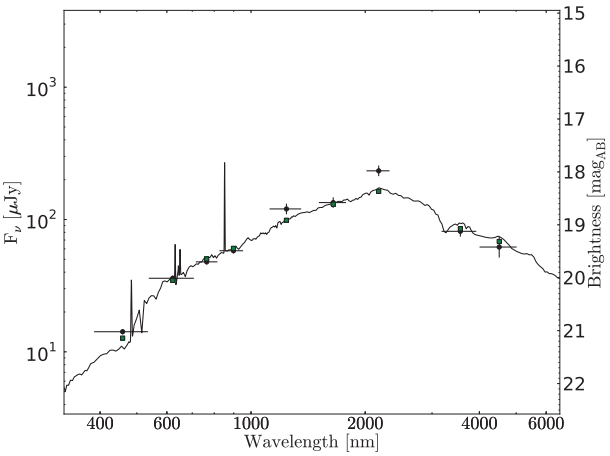

Fig. 4.12: GRB 150424A: `Le Phare` best fit of the broad-band SED of galaxy *G1* based on the *GROND* $g'r'i'z'JHK_s$-band as well as the publicely available *WISE* satellite data (corrected for a Galactic reddening along the line of sight of $E(B-V) = 0.06$ mag). The fit suggests that *G1* is a star-forming galaxy with a global reddening of $E(B-V)_{\rm host} = 0.25$ mag.

0.25 mag. Its mass in stars is rather high, about $10^{10} M_\odot$, its specific SFR is rather small, log sSFR ($M_\odot$ yr^{-1} per $M_\odot$) = −9.32.

Table 4.1: Emission lines in the spectrum of galaxy *G1*, the originally suspected host galaxy of GRB 150424A.

Line	Wavelength Å	z	Flux 10^{-17} erg s^{-1} cm^{-2}
[O III](4958.9)	6446.64	0.3000	4.9±0.3
[O III](5006.8)	6504.47	0.2991	6.1±0.6
Hα (6562.8)	8525.54	0.2979	12.1±1.0
[N II](6583.4)	8547.23	0.2982	1.2±0.1
[S II](6717.0)	8720.42	0.2981	5.03±0.3
[S II](6731.3)	8738.57	0.2981	1.3±0.1

Notes: The second column gives the observed wavelength, the third the corresponding redshift, the forth column the observed flux.

Follow-up observations with HST by Tanvir et al. (2015) later revealed the presence of a faint object underlying the position of the optical afterglow. According to these authors this is a faint galaxy at a redshift $z > 0.7$. This is the second host-galaxy candidate, *G2*.

Radio observations: *ATCA* observations were executed in June and October 2015, only 2 and respectively 6 months after the burst. The total observing time was 5 hours. In each observing run phase calibration was performed by observing the quasar *PKS 1034-293* (redshift $z = 0.312$, F_ν(5.5 GHz) = 1.44 Jy, F_ν(9.0 GHz)=1.48 Jy; Table 2.4). The 1 $\sigma_{\rm rms}$ on the combined deconvolved radio images is 7.2 ± 0.1 μJy beam^{-1} at 5.5 GHz and between 8.0 and 8.3 μJy beam^{-1} at 9.0 GHz (Table 5.1).

ATCA does not detect any radio source either at the position of the OT or at the position of *G1* down to 3σ upper limits of $F_\nu(5.5) < 21$ μJy and $F_\nu(9.0) < 24$ μJy. In case of *G1*, for a redshift of z=0.298 this constraints its SFR to $\lesssim 10$ $M_\odot$ yr^{-1}, a value which is close to the

SFR deduced from the `Le Phare` fit (Fig. 4.12). In other words, there is not much hidden star formation in this galaxy.

If the faint object which on the *HST* image is underlying the position of the OT is a galaxy at $z = 0.7$, then the *ATCA* data constrain its SFR to $< 66\ M_\odot\ \mathrm{yr}^{-1}$. If the redshift is larger, this upper limit would increase correspondingly.

4.10 Summary of Chapter 4

In this chapter I have summarized the *ATCA* radio observations for those nine short-GRB fields where the corresponding well known or suspected host-galaxy candidates were not detected in the radio band.

These galaxies cover a range in spectroscopic redshifts from z=0.1218 (GRB 080905A) to 0.496 (GRB 080123) and include photometric redshifts between z=0.5 and 1.0. The median observing time per field was around 9.5 hours, it was smallest for the field of GRB 150424A (5 hours).

For those galaxies with spectroscopic redshifts, the *ATCA* observations provide upper limits as low as 1 $\mathrm{M}_\odot\ \mathrm{yr}^{-1}$ for the most nearby hosts and ~30 $\mathrm{M}_\odot\ \mathrm{yr}^{-1}$ for the most distant ones. For the host galaxies and host-galaxy candidates where only photometric redshifts are known, the constraints on the SFR are larger in most cases and go up to ~150 $\mathrm{M}_\odot\ \mathrm{yr}^{-1}$ (if z=1 is adopted).

Thanks to its small redshift and large spatial extension the face-on, spiral host of GRB 080905 was a particularily interesting target since it has a well-defined optical afterglow position and a deep HST observation. Unfortunately, in this case the synthesized *ATCA* beam has an elongated shape. While its minor axis is substantially smaller than the angular size of this galaxy, its major axis is much bigger. The radio data constrain the SFR in an aera of $18 \times 3\ \mathrm{kpc}^2$ around the GRB explosion site to <1.1 $\mathrm{M}_\odot\ \mathrm{yr}^{-1}$.

When compared to the SFR derived via optical/infrared data, in several cases the presence of obscured star formation cannot be ruled out. Though, the data do show that short-GRB hosts with a SFR$\gtrsim$20 $\mathrm{M}_\odot\ \mathrm{yr}^{-1}$, i.e., cases like GRB 071227, are clearly the exception. The majority of short-GRB progenitors is not born in recent starbursts.

Chapter 5

Discussion

5.1 Data summary

RMS noise on the deconvolved images: Table 5.1 summarizes the achieved 1 $\sigma_{\rm rms}$ on the processed radio images at 5.5 and 9.0 GHz for different Briggs robust parameters.[1] The 1 $\sigma_{\rm rms}$ was measured using the Miriad command `imstat`. In most cases it refers to an area with a size of 200×200 pixels centered at the host-galaxy position, provided that there was no bright radio source in this field. Otherwise, I re-centered this area to exclude bright sources. The size of the primary beam was usually about 1300×1300 pixels^2, corresponding to about 530×530 arcsec^2.

The radio observations reached an RMS close to the expectations.[2] At 5.5 GHz, for a 10 hr observation on target, the theoretical RMS was $\sim 3\,\mu$Jy beam^{-1} for a robust parameter of `1` and `2`, while the achieved RMS was usually around $5\,\mu$Jy beam^{-1}. The same holds for 9.0 GHz, where the theoretical RMS was $\sim 4\,\mu$Jy beam^{-1} for a 10 hr observations, while the achieved RMS was around $5\,\mu$Jy beam^{-1} (Table 5.1).

Table 5.1 shows that the RMS on the deconvolved radio images does not strongly depend on the chosen Briggs robust parameter, at least for robust = `0.5`, `1.0` and `2.0`. For these values one obtains a very similar RMS. When varying the robust parameter the most obvious difference is the resulting size of the synthesized beam (Table 7.2). It increases by about 30% when going from robust = `0.5` to robust = `2.0`.

Synthesized beam size: Thanks to the chosen 6 km baseline, in most cases the size of the minor axis of the synthesized beam at 5.5 GHz was very small. For a robust parameter of `0.5` it mostly reached a value between 1.5 and 1.7 arcsec (Table 7.2), i.e., it was comparable to the

[1] see Sect. 7.3.3

[2] see the *ATCA* sensitivity calculator at http://www.narrabri.atnf.csiro.au/myatca/interactive_senscalc.html

Table 5.1: *ATCA* 1 $\sigma_{\rm rms}$ values (in μJy beam^{-1}) for different Briggs robust parameters.

GRB	$t_{\rm obs}$ hours	5.5 GHz 0.5	5.5 GHz 1.0	5.5 GHz 2.0	9.0 GHz 0.5	9.0 GHz 1.0	9.0 GHz 2.0
050709	10.4	5.3	5.1	5.0	5.1	5.0	5.3
050724	10.4	5.0	4.8	4.8	5.2	4.8	4.8
061006	7.0	7.8	7.3	7.3	9.3	8.3	8.1
061201	15.4	5.2	5.0	5.0	5.2	4.8	4.6
070729	11.0	7.3	7.4	7.4	6.9	6.7	6.7
070809	9.5	6.0	6.4	7.3	6.4	6.2	6.1
071227	11.3	5.1	4.7	4.6	8.7	8.6	8.8
080123	8.7	6.4	6.2	6.2	6.6	6.1	6.1
080905A	10.5	5.7	5.4	5.5	7.4	6.6	6.5
100628A	10.8	5.1	5.3	5.7	6.0	6.1	6.2
130515A	7.1	6.2	6.0	6.0	7.3	6.8	6.8
150424A	5.0	7.1	7.2	7.3	8.0	8.0	8.3

Notes: Briggs robust parameters (0.5, 1.0, and 2.0) are given in the bottom line in the table header. The time listed in the second column is the complete telescope time, including the observations of the bandpass and phase calibrator. The time on target is typically 80 to 90% of this value.

angular size of the targeted galaxies. For the three cosmologically nearest hosts and host-galaxy candidates which lie at a redshift of z ~0.1 (GRB 061201, 080905A, 100628A) the beam size was even notably smaller than the size of the primary targets. In these cases the size of the minor axis of the beam corresponds to a projected distance of only 3 to 4 kpc in the host frame. The major axis of the synthesized beam was often much larger, however, depending on the altitude of the targeted fields during the observing run and the finally achieved *uv* coverage.

5.2 Radio-derived star formation rates

As noted in Sect. 2.1, the targeted fields were selected such that the GRB host galaxy or the primary host-galaxy candidate is not an elliptical galaxy. Later on, in some cases early-type galaxies entered the discussion either because they were discovered based on the *ATCA* radio data as a second host-galaxy candidate (GRB 100628A, galaxy D; Sect. 3.3) or they are simply close to the position of a suspected (non-elliptical) host-galaxy candidate (GRB 070809, galaxy G2; Sect. 4.5). Even though the host of GRB 050724 has a dominating bulge component, and is often referred to as an elliptical galaxy, it has an additional faint spiral disk (Sect. 4.1).

Among the observed fields, in four cases the suspected star-forming hosts show signs of galaxy-galaxy interaction (GRB 050709, galaxy G2 in 070729, galaxies C-K in 100628A, galaxy G1 in 130515A). Isolated spiral galaxies and interacting, morphologically disturbed galaxies,

could harbour optically obscured star-forming activity which can be revealed by radio-continuum observations.

Table 5.2 summarizes the optical and radio SFR of all targets discussed in chapters 3 and 4. The radio SFR was derived according to Eq. (2.1), adopting a ΛCDM cosmology with a Hubble constant $H_0 = 68$ km s^{-1} Mpc^{-1} and density parameters $\Omega_M = 0.31$ and $\Omega_\Lambda = 0.69$ (Planck Collaboration et al. 2016). In all cases it is best constrained at 5.0 GHz and therefore these values are used in the following.

For this hosts of GRB 070729, 080123, 100628A, 130515A and 150424A, the optical SFR has been derived in this work either from long-slit spectroscopy or based on a broad-band SED fitting. Otherwise the optical SFR was taken from the literature. In all those cases where the optical SFR was derived via spectroscopy, it is at most 1 $M_\odot$ yr^{-1}. A special case are the host-galaxy candidates G1 and G3 associated with GRB 070729. Both galaxies are very red, $(r' - K)_{AB} = 3$ mag. A `Le Phare` fit implies a SFR of about 100 and 10 $M_\odot$ yr^{-1}, respectively, if their redshift is z=0.5. Among the 10 galaxies with reliable spectroscopic redshift listed in Table 5.2, eight galaxies have a SFR of less than 25 $M_\odot$ yr^{-1}.

For altogether five GRBs the radio SFR of the host galaxy or the host-galaxy candidate is less than 10 $M_\odot$ yr^{-1}. In some cases the *ATCA* radio upper limits are quite deep and the corresponding SFR goes down to less than 2 $M_\odot$ yr^{-1} (GRB 061201, 080905A, 100628A), excluding the presence of substantial unobscure star-formation in these galaxies.

Figure 5.1 summarizes the radio-derived SFRs and brings them into context with the so far available data base of short-GRB host galaxies published in the literature (Fong et al. 2015, their table 8; Fong et al. 2016, their table 1). It should be noted that these published data were actually not obtained with the goal to measure or constrain the permanent radio flux of short-GRB host galaxies due to SFR activity.

The data provided in Fong et al. (2015) are a summary of all reported observations (detections or $3\sigma_{rms}$ upper limits) of the radio flux of the corresponding GRB afterglows, while the data published in Fong et al. (2016) were taken to search for the predicted (Margalit & Piran 2015, and references therein) long-lasting radio emission (transients) following a NS-NS merger due to the slow-down of the relativistic ejecta from the merger in the circumburster interstellar medium.

Nevertheless, all these non-detections are also upper limits for the permanent radio flux of the corresponding host galaxy due to star-formation activity. Since the data summarized in Fong et al. (2015) refer to observations performed at different radio frequencies, and all data reported in Fong et al. (2016) refer to 6.0 GHz, all upper limits reported by these authors have been transformed correspondingly to an observing frequency of 5.5 GHz, assuming a spectral index

Table 5.2: Star formation rates based on the ATCA radio data.

GRB	Gal.	z	$\text{Flux}_{5.5}$ μJy	$\text{Flux}_{9.0}$ μJy	$\text{SFR}_{5.5}$ $M_\odot$/yr	$\text{SFR}_{9.0}$ $M_\odot$/yr	$\text{SFR}_{\text{optical}}$ $M_\odot$/yr	Ref.	ratio	diff. $M_\odot$/yr
(1)	(2)	(3)	(4)	(5)	(6)	(7)	(8)	(9)	(10)	(11)
050709		0.1606	24 ± 7	<15	2.8±0.8	<2.5	0.1	[1]	28±8	2.7±0.8
050724	G1	0.258	<15	<15	<4.9	<6.9	0.05	[2]	<100	<4.9
061006	G1	0.4377	<22	<25	<24	<38	0.02	[3]	<1200	<24
061201	G1	0.111	<15	<14	<0.8	<1.0	0.14	[4]	<6	<0.65
	G2	1.0 as	<15	<14	<108	<143	–	–	–	–
070729	G1	0.5 as	<22	<21	<32	<43	100±50	[7]	–	–
	G3	0.5 as	<22	<21	<32	<43	5±4	[7]	<32	<31
070809	G1	0.2187	<18	<18	<4.1	<5.8	0.15	[5]	<27	<4
071227		0.381	43 ± 11	<26	34±10	<29	0.6	[6]	57 ± 16	33±10
080123	G1	0.496	<19	<18	<27	<36	0.7	[7]	<39	<26
080905A	G1	0.1218	<17	<20	<1.1	<1.8	–	–	–	–
100628A	C	0.102	<16	<18	<0.7	<1.1	0.1	[8]	<7	<0.6
	K	0.102	46 ± 16	<18	2±0.8	<1.1	0.3	[8]	7 ± 3	1.7±0.8
130515A	G1	0.5 as	<18	<21	<26	<43	0.3–2.3	[7]	<90	<25
150424A	G1	0.2981	<21	<24	<10	<15	0.15–7	[7]	<67	<10
	G2	0.7 as	<21	<24	<66	<107	–	–	–	–

Notes: The color coding of the rows separates different GRB fields. Column #2 gives the designation of the suspected host (if there is more than one; see Fig. 2.2). Column #3 provides the redshift. An 'as' stands for 'assumed'. In this case no spectroscopic redshift is known. Radio flux upper limits (columns #4 and #5) refer to $3\sigma_{\text{rms}}$ (Table 5.1). Columns #6 and #7 give the radio-derived SFR at 5.5 and 9.0 GHz using Eq. (2.1). Column #8 provides the optical SFR, column #9 the corresponding reference. Column #10 gives the ratio between the radio (5.5 GHz) and the optically derived SFR, column #11 the difference. *Notes to individual sources:* GRB 050709: the SFR values have to be taken with care since this is an interacting galaxy (see Sect. 3.1). GRB 061201: the data refer to two host-galaxy candidates (G1 and G2). GRB 070729: the data refer to two host-galaxy candidates (G1 and G3). For G1 the constraint set on the SFR by the radio observations is smaller than the SFR based on the `Le Phare` fit. Therefore, no results are given in columns #10 and #11. GRB 070809: the data refer to the host-galaxy candidate G1. G2 is not included here as it is an elliptical galaxy. GRB 100628A: the data refer to two objects inside the *Swift*/XRT error circle (C and K). Both are at the same redshift. Object D, the second host-galaxy candidate is not listed here since it is an elliptical. GRB 130515A: the SFR is based on `Le Phare`. GRB 150424A: the optical SFR based on spectroscopy is 0.15 $M_\odot$ yr^{-1}, while the SFR based on `Le Phare` is 7 $M_\odot$ yr^{-1}. *References:* [1] Hjorth et al. (2005b); Covino et al. (2006), [2] Malesani et al. (2007); Gorosabel et al. (2006), [3] Berger (2009), [4] Stratta et al. (2007), [5] Perley et al. (2008), [6] D'Avanzo et al. (2009), [7] this work, [8] Nicuesa Guelbenzu et al. (2015).

of 0.7. Thereby, in those cases where in Fong et al. (2015) several observations with different upper limits were reported for the same host, then in Fig. 5.1 only the most constraining data is plotted.[3] In four cases, these additional data overlap with my sample but my *ATCA* upper limits

[3]Some upper limits are rather high (up to >1000 $M_\odot$ yr^{-1}; GRB 070429B at z=0.904 and GRB 070714B at z=0.920) since these observations refer to a radio afterglow follow-up and did not went very deep. They are not shown in Fig. 5.1.

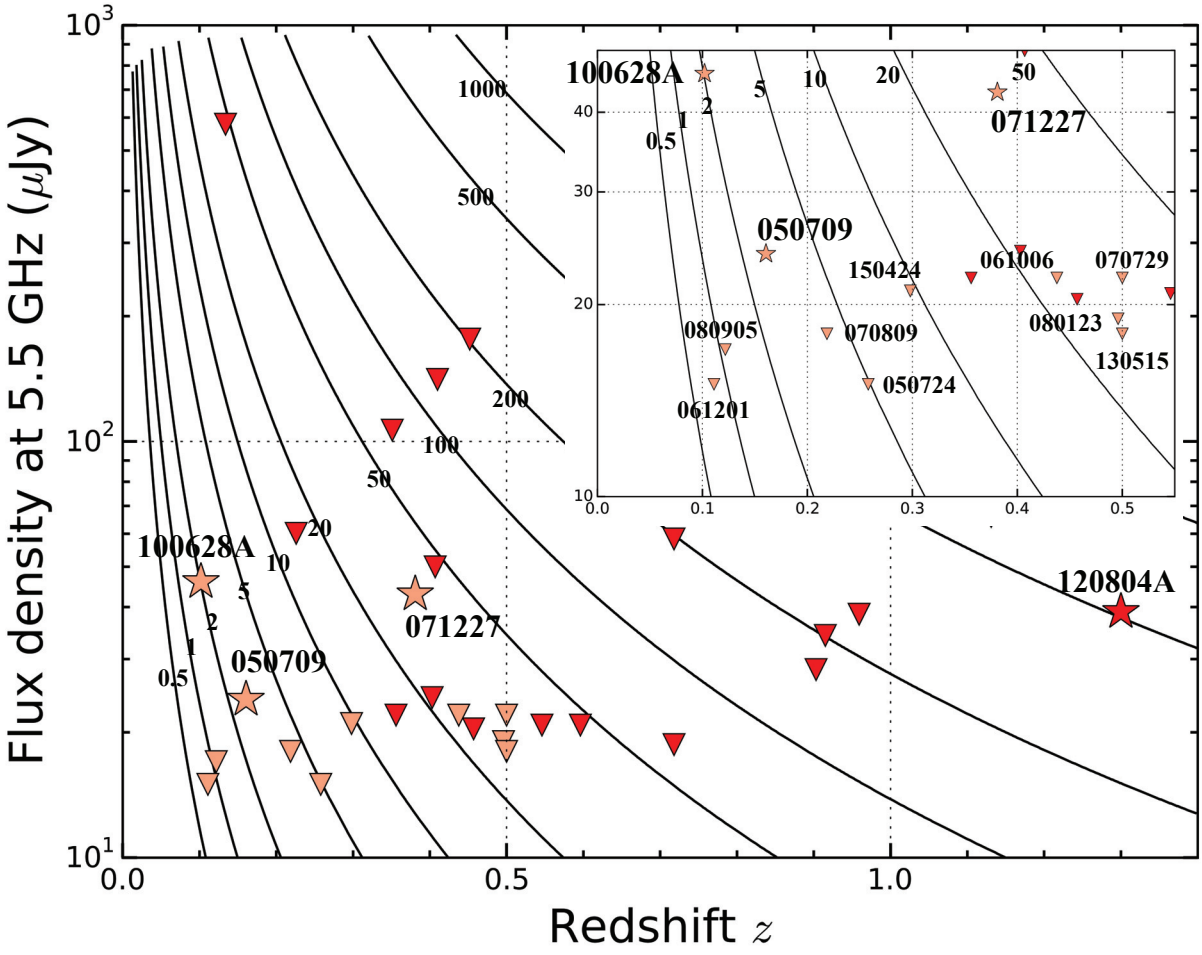

Fig. 5.1: Summary of the present data base on the radio flux from short-GRB host galaxies and the corresponding radio-derived star-formation rates. In light red are shown the *ATCA* data presented here, in red the data taken from Fong et al. (2015) and Fong et al. (2016) (see the text for details). Isolines correspond to different SFRs (in units of $M_\odot$ yr^{-1}). Downward pointing triangles are upper limits, stars refer to detections (GRB 071227, Nicuesa Guelbenzu et al. 2014; GRB 100628A, Nicuesa Guelbenzu et al. 2015; GRB 120804A, Berger et al. 2013b). If there is more than one host-galaxy candidate in the field (Table 5.2), then the data for the galaxy with the tightest constraint on the SFR is plotted. Note that GRB 050709 is included here, even though the spectroscopic data suggest that the line emission is not due to star-formation activity (Sect. 3.1). All data refer to 5.5 GHz, upper limits are $3\sigma_{\rm rms}$. The zoom-in shows the redshift range explored in this work, i.e., all targets with $z \leq 0.5$.

are deeper in all cases, therefore I do not plot the data from these authors.[4]

Figure 5.1 shows that the *ATCA* sample provides the so far deepest radio constraints on the SFR in short-GRB hosts, going down to <1 $M_\odot$ yr^{-1}. Previous radio samples did not go below about 15 $M_\odot$ yr^{-1}. The reason for this success is the comparably small redshift of the studied hosts here as well as the deep sensitivity limit I could achieve. In particular, the two

[4] A similar plot is shown in Stanway et al. (2014) but for some long-GRB host galaxies. Since these authors use a slightly different equation for the transformation of radio flux into SFR, their curves SFR(z, F_ν) do not perfectly match with the one shown here.

radio detections demonstrate that at low reshifts individual galaxy components can be localized at the 1 arcsec accuracy level. In case of a radio detection, the GRB explosion sites can be tested in this way at the kpc scale. In other words, the radio band can be used to search for star-forming activity at the position of the optical transient in a more sophisticated way than previous methods.

5.3 Radio SFRs in long and short-GRB host galaxies

Figure 5.2 shows the radio-derived SFR for the present world sample of 60 long and 32 short-GRB host galaxies which have been observed in the radio band. The former sample is again from Greiner et al. (2016), the latter sample includes the 12 GRB fields studied here (Table 5.2) as well as the data listed in Fong et al. (2015) and Fong et al. (2016) (in total 1 detection, GRB 120804A, and 19 non-detections).[5] In the case of short GRBs this includes the upper limits and detections for the corresponding host-galaxy candidates, while in the case of long bursts all hosts might have a secure identification. In this figure I have also included the two events for which I have no secure redshift information (GRB 070729 and 130515A), and adopted a redshift of z=0.5. The long-GRB sample, on the other hand, contains only hosts with a known spectroscopic redshift.

Among the long-GRB hosts sample, 17 targets (~30%) have a detection, while among the short-GRB hosts sample only 2 targets (~ 5%) have a detection (Fig. 5.2). The cosmologically nearest long-GRB hosts with a detection are the hosts of GRB 980425/SN 1998bw (z=0.0085) and GRB 111005A (z=0.013). With the exception of one target, all long-GRB hosts at a redshift of $z < 0.1$ have been detected in the radio band. The non-detected host belongs to GRB 060218/SN 2006aj (z=0.033). It is a dwarf galaxy with a very small SFR of (based on Hα) 0.065±0.005 $M_\odot$ yr^{-1} but a high specific SFR as its mass in stars is only 10^7 $M_\odot$ (Wiersema et al. 2007). There are radio detections of long-GRB host up to a redshift of 6. Contrary to long GRBs, no short-GRB closer than $z < 0.1$ is known. If I select the redshift range from 0.1 to 0.5 that was covered by this work, then there are observations of 16 long-GRB hosts of which 3 (~20%) have a radio detection detection.

One has to keep in mind that both radio samples, the long-GRB and the short-GRB host galaxy sample, are the results of different observing strategies, telescopes, exposure times and target selection criteria. Also the short-GRB sample is still rather small, in other words general conclusions are affected by low-number statistics. As such a comparison between both datasets has to be taken with care.

[5]Not included are bursts where my *ATCA* data provide deeper upper limits. As stated beforehand, from Fong et al. (2016) and Fong et al. (2015) I included upper limits from GRB radio afterglow observations and magnetar searches.

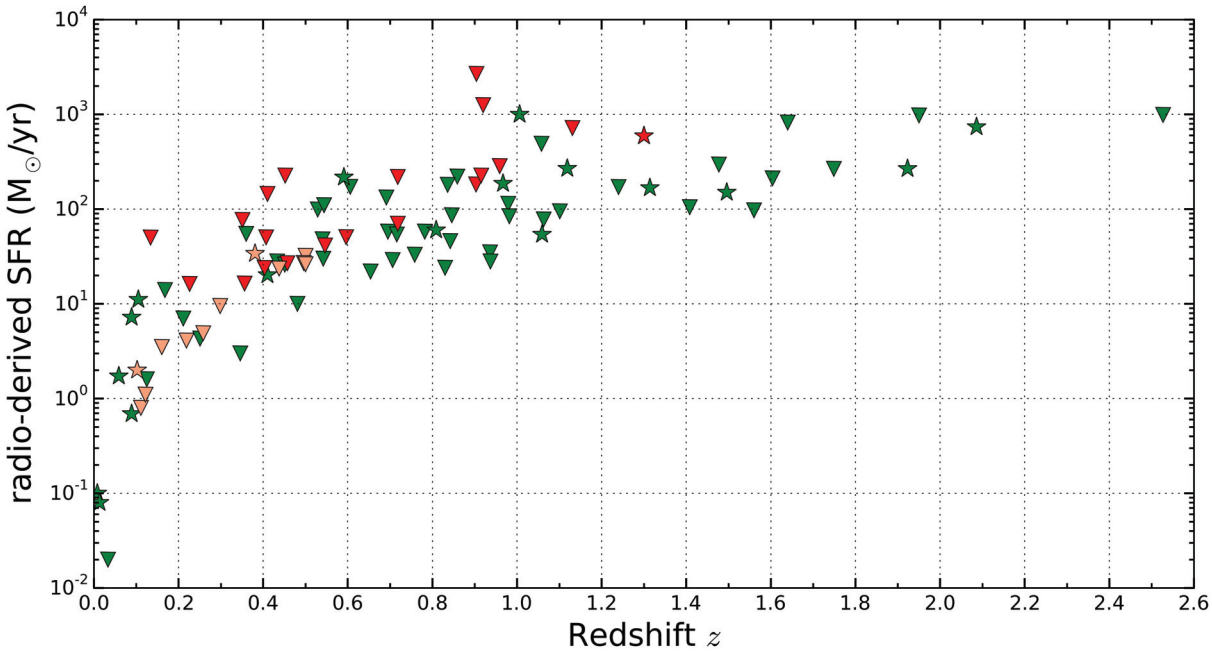

Fig. 5.2: The radio-derived SFR for long-GRB hosts (green color) and short-GRB hosts (in red and light red). The red color refers to data taken from Fong et al. (2016) and Fong et al. (2015), in light red are shown the data based on this work. Downwards pointing triangles refer to upper limits (43 long-GRB hosts, 32 short-GRB hosts) while stars are detections (17 long-GRB hosts, 3 short-GRB hosts). Note that the apparent trend of the SFR's upper limit with redshift is just a reflection of the general $3\sigma_{\rm rms}$ sensitivity limit of typically 20 μJy (see Fig. 2.3).

5.4 Radio vs. optical SFRs in long and short-GRB hosts

Figure 5.3 provides a summary of the measured SFR for all long (Greiner et al. 2016) and short-GRB host galaxies with known redshift for which an optical *and* a radio-SFR has been published. In addition to the short-GRB hosts discussed in this work, I have included here an additional set of six short-GRB hosts for which such data are available in the literature (GRB 051221 at z=0.546, 070724 at z=0.457, 090510 at z=0.903, 100206 at z=0.407, 101219 at z=0.718, 130603 at z=0.356; all radio data come from observations with the VLA).[6] Short-GRB hosts that are identified as elliptical galaxies are not included in this plot. For short-GRB hosts there are only 3 radio detections (GRB 050709, 071227, 100628A). As stressed beforehand (see the figure caption in Fig. 5.1), the radio-SFR for GRB 050709 has to be taken with care since the radio flux is dominated by flux from shocked gas. As noted in Table 5.2, all plotted upper limits for short-GRB hosts refer to 3 $\sigma_{\rm rms}$. Since Greiner et al. (2016) give radio-derived upper limits based

[6] GRB 051221A: Soderberg et al. (2006); Fong et al. (2016); GRB 070724A: Berger et al. (2009); Fong et al. (2016); GRB 090510: McBreen et al. (2010); Fong et al. (2016); GRB 100206A: Perley et al. (2012); Berger et al. (2013b); GRB 101219A: Fong et al. (2013, 2016); GRB 130603B: de Ugarte Postigo et al. (2014); Fong et al. (2016)

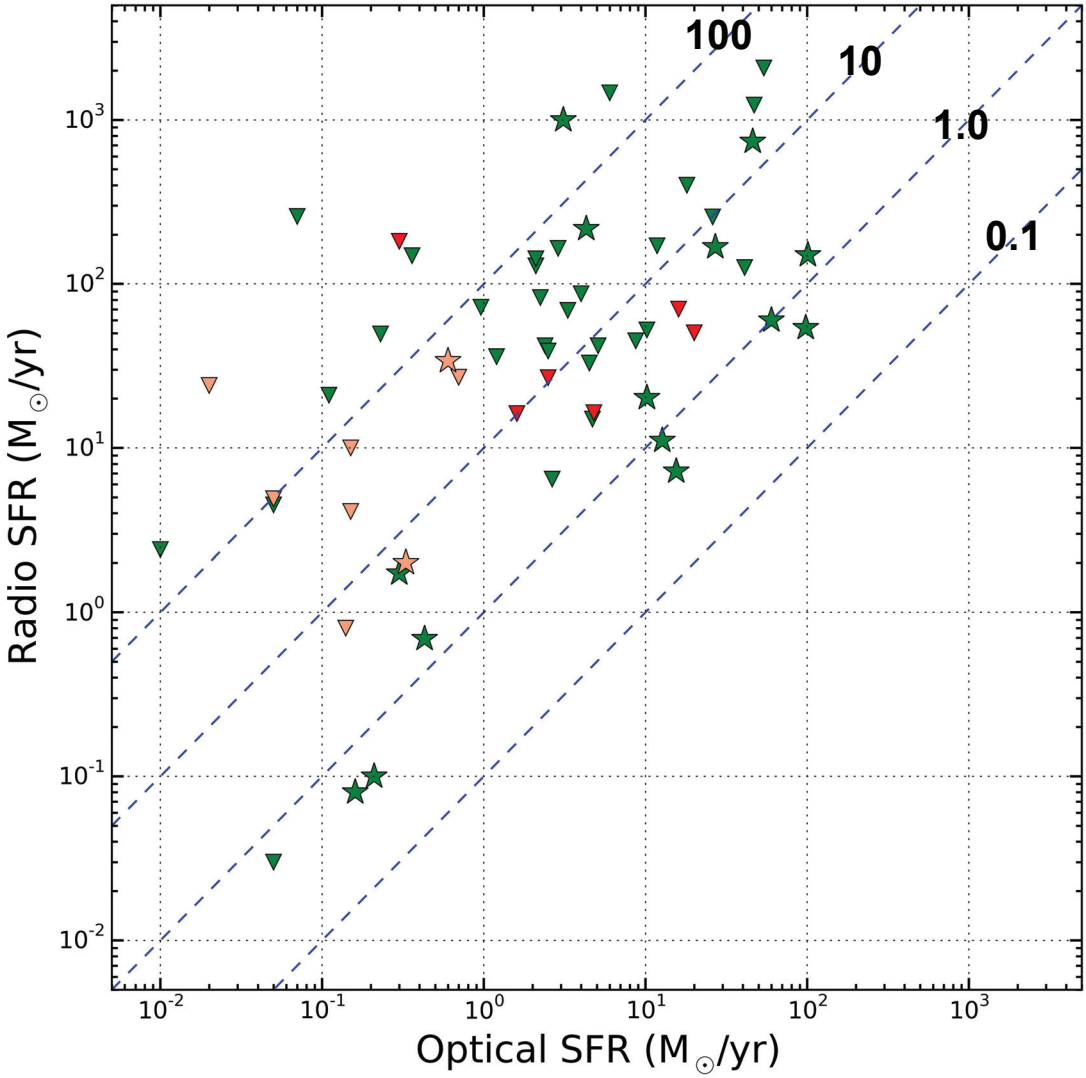

Fig. 5.3: The radio and optical SFR for 44 long (green; Greiner et al. 2016) and 15 short-GRB host galaxies (light red: 9 data points from this work; red: 6 data points from the literature, see text). Included are only short-GRB hosts with a spectroscopic redshift and a known optical SFR. This excluded GRB 070729, 080905A, and 130515A. Also excluded is GRB 050709 (see Table 5.2). Downwards pointing triangles refer to upper limits while stars are detections. Broken lines refer to different ratios SFR(radio)/SFR(Hα). Note that the optical SFRs are not extinction-corrected. Note also that contrary to the radio data, the optical data are always detections. The two short-GRB hosts with an optical SFR >10 M$_\odot$ yr^{-1} are GRB 100206A and 101219A.

on 2 $\sigma_{\rm rms}$, all radio-SFR upper limits reported by these authors have been re-scaled by a factor of 3/2.

Figure 5.3 compares radio-derived SFRs with optical SFRs. The former are unaffected by extinction by cosmic dust but the latter are. As such, if optical and radio detections exist, then a ratio η = SFR(radio)/SFR(Hα)>1 implies optially hidden star-forming activity. In principle, cases with η <1 should not exist but some long-GRB hosts lie in this region. Given that I have

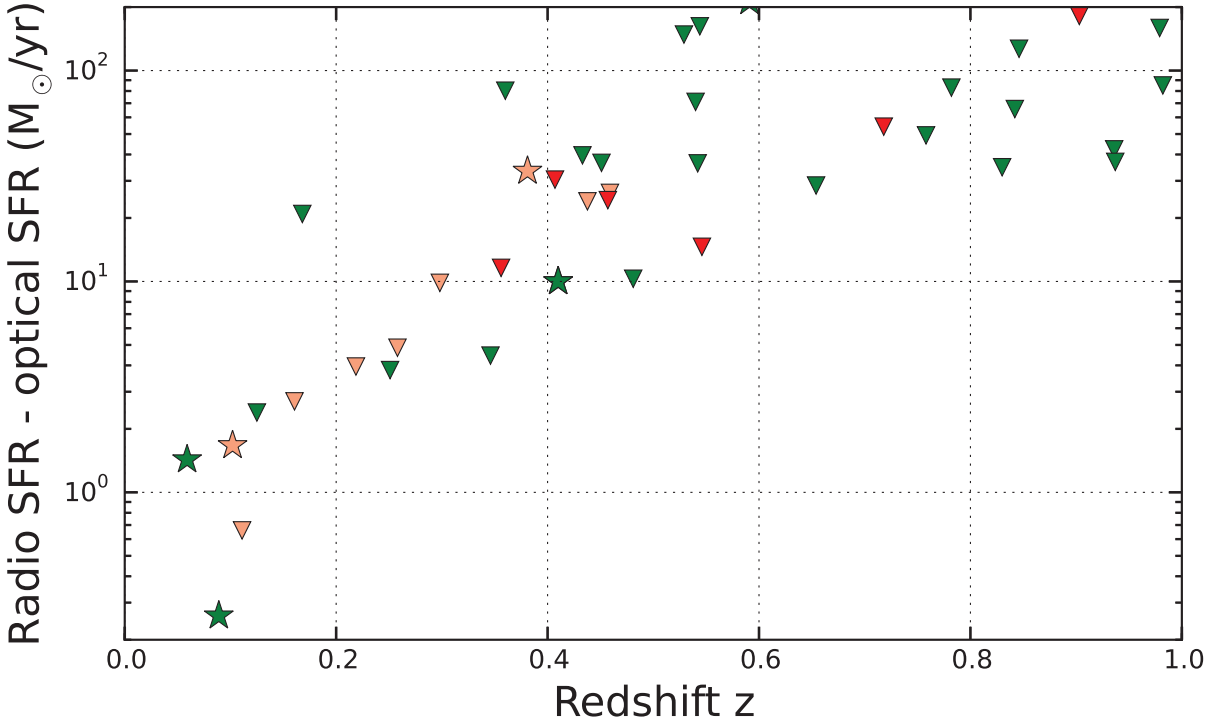

Fig. 5.4: The difference between the radio and the optical SFR for long and short-GRB host galaxies. Symbols follow Fig. 5.3. The radio upper limits rule out that in the local universe (z <0.3; d_L=1.5 Gpc) short-GRB hosts are on average forming stars at a high rate.

not included error bars in this plot and given that these SFR ratios are still relatively close to 1.0, these cases should not be overinterpreted.

What is immediately apparent in Fig. 5.3 is that most GRB host galaxies (long and short) with an optically measured SFR have no detection in the radio bands. In many of these cases, optially hidden star formation is not excluded because the radio observations did not go deep enough. In particular, a substantial fraction of long-GRB hosts have radio upper limits which are rather high (say, > 30 $M_\odot$ yr^{-1}), i.e., the radio observations were not much constraining. The main reason in these cases is the on average high redshift of these hosts ($z \gtrsim$1.0), In particular, in case of *ATCA*, a 10-hour radio observation can not be used to constrain deep SFR limits (Greiner et al. 2016).

Some long-GRB hosts with radio detection have a relatively high SFR(radio)/SFR(Hα) ratio with two hosts in the range of $10 < \eta < 100$ *and* just one host in the range of $\eta > 100$ (GRB 021211). Such high values are obviously not excluded in nature, but most hosts have $\eta < 10$. The number of radio-detected hosts with $\eta \sim 1$ (equivalent to negligible obscured star formation) is clearly dominating in number.

How much optically hidden star formation is there? While Fig. 5.3 provides an estimate about the maximum fraction of obscured SFR, Fig. 5.4 brings these results to absolute values.

For example, for GRB 050724 the ratio of radio to optical SFR can be as high as 100, but the radio observations have told us that the optically hidden SFR can be at most 4.9 $M_\odot$ yr^{-1}.

Figure 5.4 shows that all short-GRB hosts with $z < 0.3$ have an optically obscured SFR of less than 10 $M_\odot$ yr^{-1}. For the most nearby events (GRB 061201, z=0.111; 080905A, z=0.1218, 100628A, z=0.102) the *ATCA* radio data exclude the presence of substantial optically hidden star-formation activity, it can be at most 3 $M_\odot$ yr^{-1}. At least in the local universe (z <0.3) short-GRB host galaxies are not forming stars at a high rate. There is no big observational evidence for optically obscured star formation in short-GRB hosts. At higher redshifts this cannot yet be ruled out since in most cases the radio data do not go deep enough.

5.5 The most actively star-forming short-GRB hosts

GRB 071227 is the only short GRB in my sample with a clear presence of obscured star-formation. Figure 5.3 shows that star formation rates found for the hosts of *long* GRBs range between about 0.1 and 100 solar masses per year. The radio-SFR found for the host of the short GRB 071227 ($\sim$ 30 $M_\odot$ yr^{-1}) would be even a high SFR for a long-GRB host.

The high SFR puts the host of GRB 071227 in line with the hosts of the short GRBs 100206A (SFR$\sim$30 $M_\odot$ yr^{-1}, z=0.407; Perley et al. 2012) and 120804A (SFR$\sim$300 $M_\odot$ yr^{-1}, z $\sim$1.3; Berger et al. 2013b). It is the third known luminous infrared galaxy (LIRG) that hosted a short GRB.

As I have noted in Sect. 2.1.2, there are only five short-GRB hosts that have a detection in the *WISE* W1, W2, *and* W3 bands. This includes GRB 071227 and 100206A. The starburst host of GRB 120804A (z=1.3) is not detected by *WISE* in any band, likely due to its high redshift.

While a *WISE* detection naturally favors low-z galaxies, a comparison of the properties of long-burst hosts with galaxies hosting short bursts is worthwhile. In Nicuesa Guelbenzu et al. (2014) we found that only one out of five $z < 0.5$ *long-burst* host galaxies in the TOUGH host galaxy survey (Hjorth et al. 2012; see Sect. 1.2.3) has detections in W1, W2 *and* W3. The comparably high percentage of WISE-detected short-burst host galaxies could be indicative that a fraction of short-GRB progenitors is indeed linked to recent starbursts and may have short merger timescales. As it has been shown in this work, finding evidence for such a relation remains a challenge (particular examples are the hosts of GRB 050709 and 080905). The question if the progenitor of GRB 071227 was a young NS-NS binary remains unanswered as with *ATCA* no evidence for star-forming activity was found in the vicinity of the GRB explosion site.

Among the 25 short-burst host galaxies compiled and listed in Berger (2014) which have a measured SFR (bursts from mid 2005 to 2010), 19 hosts have an optical SFR $\lesssim$ 2.5 $M_\odot$ yr^{-1}

(in his list GRB 071227 has 0.6 $M_\odot$ yr^{-1}). The remaining seven hosts have an SFR between 2.5 and 30 $M_\odot$ yr^{-1}. Only the hosts of GRB 100206A (30 $M_\odot$ yr^{-1}) and 101219A (16 $M_\odot$ yr^{-1}) lie above 10 $M_\odot$ yr^{-1}. In other words, the *ATCA* observations revealed that the host of GRB 071227 belongs to the most actively star-forming short-GRB host galaxies known to date.

The fact that at least 4 out of about 40 known short-GRB hosts have a relatively high SFR (GRB 071227, 100206A, 101219A, 120804A) implies that these kind of galaxies represent a notable fraction of the short-GRB host-galaxy ensemble. It can indicate to a link between recent star formation and the formation of short-lived short-GRB progenitors. At least 3 of these 4 hosts are characterized by a relatively large mass in stars. This fact could also indicate that it is just the large number in stars which increases the probability of a NS-NS to occur in such a galaxy. A final conclusion in this respect might have to await a substantial increase in radio observations of short-GRB hosts. Given that there are only about 40 short bursts with a well-known host or a host-galaxy candidate, and taking into account that at present the number of these known galaxies is increasing by just about 1 to 2 per year, progress in this respect could be fast. A complete survey of all known hosts in the radio band could in principle be finished within the next 3 to 5 years.

5.6 Future radio observations

Table 5.3 lists all short GRBs in the southern sky at declination < -15 deg with (i) a *Swift*/XRT detection, i.e., where an X-ray afterglow was found and consequently an arcsec-precise localization was possible (typically 3 arcsec radius, 90% c.l.), (ii) where a GRB host galaxy is known or a host-galaxy candidate could be identified, and (iii) the redshift of which is $z \lesssim 0.5$.

This table includes those cases where later deep HST or VLT/FORS2 observations finally suggest a much fainter host at probably much higher redshift (GRBs 061201, 070729, 070809, 080123, 150424A). The reason is that these deeper observations do not rule out the previously identified host-galaxy candidates. At least in these cases no afterglow spectroscopy could be performed so that no redshift of the pure afterglow was measured. So far, for a short burst such an afterglow spectroscopy was only possible in the case of GRB 130606B (Cucchiara et al. 2013; de Ugarte Postigo et al. 2014) and GRB 140903A (Troja et al. 2016), but these two fields do not enter this *ATCA* list with the aforementioned selection criteria.

With the exception of GRB 070724, which was never scheduled by the *ATCA* Time Allocation Committee, my observations basically cover all possible *ATCA* targets (until early 2017). In my sample the mean observing time per target was about 9.2 hours (including the observation

of the calibrator, which ususally counts about 10% of the time). The observing time was shortest for the field of GRB 150424A (4.4 hours). In basically all other cases it was larger than 8 hours and the 1 $\sigma_{\rm rms}$ goes down to flux limits of 5 to 10 μJy rms/beam. Notably deeper 5.5 GHz *ATCA* observations are hardly possible in the near future, however, if one takes into account that the sensitivity of an interferometer (more precisely, the RMS) is proportional to $t^{-1/2}$, where t the integration time (Condon & Ransom 2016).

Alternatively, one might consider to observe with *ATCA* in the 2.1 GHz band. Assuming synchrotron radiation with a spectral index of 0.7, a star-forming region will be more luminous at 2.1 GHz by a factor of $(5.5/2.1)^{0.7} = 2$. Radio-continuum observations of long-GRB host galaxies with *ATCA* at 2.1 GHz by Greiner et al. (2016) have shown however that the detection percentage of GRB hosts remains very small. In addition, the fields become much more crowded with bright radio sources, often making the data reduction more challenging. It is for sure worth to observe at 2.1 GHz, but probably getting additional 10 hour blocks of extra observing time to re-observe the same targets might be challenging.

Table 5.3: All well-localized short GRBs at Decl. ≤ -15 deg.

GRB (1)	obs.? (2)	excl.? (3)	RA, Decl.(J2000) (4)	z (5)	Gal. type (6)	OT? (7)
050709	Y		23:01:30, −38:59	0.161	L	yes
050724A	Y		16:24:51, −27:31	0.257		yes
051210	–	z	22:00:47, −57:38			
061006	Y		07:24:22, −79:12	0.438	L	yes
061201	Y		22:07:53, −74:36	0.111		yes
061217	–	z	10:41:46, −21:07	0.827	L	
070429B	–	z	21:52:06, −38:51	0.902	L	
070707	–	z	17:51:23, −68:54			yes
070724A	tbd		01:51:16, −18:37	0.457	L	
070729	Y		03:45:17, −35:19	0.5?		
070809	Y		13:35:08, −22:08	0.219		yes
071227	Y		03:52:29, −55:57	0.381	L	yes
080123	Y		22:35:43, −64:53	0.496	L	
080905A	Y		19:10:39, −18:53	0.122	L	yes
080919A	–	z	17:41:09, −42:24			
081226A	–	z	08:02:06, −69:00			
090305	–	z	16:07:02, −31:34			yes
090510	–	z	22:14:13, −26:36	0.903	L	yes
091109B	–	z	07:31:00, −54:06			yes
100625A	–	E	01:03:05, −39:05	0.452	E	
100628A	Y		15:03:52, −31:40	0.102	L	
100702A	–	z	16:22:49, −56:32			
111020A	–	z	19:08:06, −37:59			
111121A	–	z	10:19:00, −46:38			
120521A	–	z	09:54:46, −49:25			
120804A	–	z	15:35:43, −28:46	1.3	L	
121226A	–	z	11:14:38, −30:25			yes
130515A	Y		18:53:41, −54:17	0.5?		
150301A	–	z	16:17:09, −48:42			
150424A	Y		10:09:15, −26:39	0.298		yes
150831A	–	z	14:44:05, −25:39			
151127A	–	z	01:19:07, −82:46			
151229A	–	z	21:57:31, −20:44			
160411A	–	z	23:17:27, −40:16			yes
170127B	–	z	01:19:47, −30:20			

Notes: Listed here are those 35 short GRBs which occurred at a declination ≤ -15 deg and where at least an arcsec-precise X-ray afterglow localization was possible (by early 2017). Column #1: GRB data were taken from the tables provided in Berger (2014) and Fong et al. (2015). Column #2: An Y means that this target was observed during this work. One target (GRB 070724) was not scheduled (to be done, tbd). All other targets are at present no promising targets (–). Column #3 provides an argument why this field at present does not appear to be a promising target. z: the redshift is unknown or larger than 0.5; E: the suspected host galaxy is an elliptical. Coordinates in column #4 were collected from J. Greiner's www page at http://www.mpe.mpg.de/jcg/grbgen.html. Column #5 gives the redshift and #6 the morphological type of the suspected host (taken from Berger 2014). In the last column a 'yes' means that an optical transient (OT; afterglow) was detected.

Chapter 6

Summary and conclusions

I have reported about *ATCA*/CABB 5.5 and 9.0 GHz radio-continuum observations of a sample of 12 short-GRB host galaxies at the southern sky. It is the most comprehensive and deepest radio survey of this class of galaxies to date, representing about 1/4 of the present world-sample of known short-GRB host galaxies. Exposure times were usually around 10 hours, going deep to a $1\sigma_{\rm rms}$ between 5 and 7 μJy beam^{-1} in the 5.5 GHz band. The immediate objective was to use the radio observations to measure or to constrain the SFR in these galaxies and to figure out if the radio data point to optically hidden star-formation activity in these galaxies, in particular at or close to the GRB explosion sites (at kpc scales). This study was triggered by theoretical work, according to which a subpopulation of young short-GRB progenitors (NS-NS binaries) should exist (Voss & Tauris 2003; Belczynski et al. 2006), which might still lie close to or even inside their birth places when they merge and explode.

In three cases radio flux from a GRB host galaxy was detected (GRB 050709 at z=0.1606, GRB 071227 at z=0.381, GRB 100628A at z=0.102). For the remaining nine targets only upper limits could be established, typically smaller than 20μ Jy at 5.5 GHz (3 $\sigma_{\rm rms}$), in most cases corresponding to SFR limits between ~1 and 30 M$_\odot$ yr^{-1}. This includes the nearest known short-GRB host galaxy at z=0.122 (GRB 080905A), which has a well-defined afterglow position, for which the radio data imply a SFR< 1.1 M$_\odot$ yr^{-1}.

Among the three hosts with *ATCA* radio detection, strong evidence for optically hidden star-formation activity was only found for the host of GRB 071227 (z=0.381), a galaxy that is also a bright infrared source in the *WISE* catalog. The radio flux comes from the central bulge of the host (radio-SFR ~30 M$_\odot$ yr^{-1}), an edge-on spiral. The radio source lies in projection 15 kpc away from the optical afterglow position. No radio flux was detected at the GRB explosion site.

Although the cosmologically nearest known short-GRB hosts with redshifts $z \sim 0.1$ were included in this study and the spatial resolution of the radio telescope and the detection sensitivity

were best, no mounting evidence for star-formation close to the corresponding GRB explosion site was found. In the case of the short GRB 100628A I found a radio source inside the r=7 arcsec *Swift*/XRT error circle, probably located in a tidal arm of an interacting spiral galaxy. If the flux is due to star-formation activity, then it is in the order of 2 $M_{\odot}$ yr^{-1}. A second host galaxy candidate was identified thanks to the radio data. It is a radio-bright giant elliptical at a redshift of z = 0.311 that is located outside the XRT error circle.. Due to the lack of secure redshift for this event, I can not conclude which one is the real host galaxy for this event.

The observationally most promising case was GRB 050709 for which an optical afterglow was discovered. Indeed, here I did detect diffuse 5.5 GHz radio emission from the eastern part of the host, where the optical afterglow was placed. Since this is an interacting galaxy-galaxy system, it remains open the question if the source of this radio emission is star-forming activity or shocked gas. Further studies are needed here.

With only two radio detections of optically hidden star-forming activity (GRB 071227, 100628A), the data-in-hand do not push towards the idea that a large percentage of short-GRB hosts is characterized by obscured star formation. It does indeed exist in some cases, but more and better data (more hosts, deeper sensitivity limits) are required here in order to draw definite conclusions.

In spite of these unfortunately inconclusive results, the ATCA observations have shown that for the cosmologically nearest short GRBs radio observations can probe their host galaxies at the kpc scale. As such it is just a question of time when a suited short GRB is found in a nearby host (say, z <0.3) and radio observations can identify and probe the GRB explosion site. Future *MUSE* observations might provide further insights here.

In conclusion, in my observations I do not find the Roesetta Stone which does reveal a link between recent ($\lesssim$100 million years) star-formation activity and the formation of young, merging NS-NS binaries. The data are in line with the picture that most short-GRB progenitors are members of an old stellar population, i.e., the star-formation activity which produced these progenitors stopped long time ago. However, the radio data do not rule out that a population of young short-GRB progenitors might exist. The ultimate observational proof or disproof of this concept needs still to be done.

Future work will focus on VLA observations of northern short-GRB hosts. The goal is to observe at least ten more targets. It would bring the total number of short-GRB host galaxies with deep radio-continuum observations to >20, which would represen ~50% of the present world sample of well-localized short-GRB hosts. Additional ALMA millimeter and Integral Field Unit spectroscopic observations are also planned.

Chapter 7

Appendix

7.1 Supplementary tables and figures

Table 7.1: Host galaxy redshifts, luminosity distances, and lookback times.

GRB	z	d_L 10^{27} cm	1 arcsec kpc	look back Gyr
(1)	(2)	(3)	(4)	(5)
050709	0.1606	2.44	2.84	2.06
050724 G1	0.2580	4.14	4.11	3.10
061006 G1	0.4377	7.65	5.82	4.70
061201 G1	0.111	1.63	2.08	1.47
061201 G2	1.0	2.08	8.20	7.90
070729 G1/2	0.5	8.97	6.26	5.17
070729 G1/2	1.0	2.08	8.20	7.90
070809 G1	0.2187	3.43	3.63	2.70
070809 G2	0.473	8.40	6.08	4.97
071227	0.381	6.54	5.37	4.25
080123 G1	0.496	8.89	6.24	5.14
080905A G1	0.1218	1.80	2.25	1.60
090426	2.609	6.76	8.16	11.24
090510	0.903	1.84	7.99	7.49
090927	1.37	3.08	8.61	9.14
100117A	0.915	1.87	8.02	7.54
100206A	0.41	7.09	5.60	4.48
100625A	0.452	7.96	5.93	4.81
100628A C	0.102	1.49	1.93	1.36
100628A D	0.311	5.13	4.69	3.61
101219A	0.718	1.39	7.40	6.56
130515A G1	0.5	8.97	6.26	5.17
150424A G1	0.298	4.89	4.56	3.49
150424A G2	0.7	1.34	7.32	6.46

Notes: If GRBs are given twice then no precise redshift is known and two possibilities are discussed in the text. Column #3 lists the luminosity distance, column #4 the equivalent of 1 arcsec projected distance and column #5 the lookback time. The data assume a ΛCDM cosmology with $H_0 = 68$ km s^{-1} Mpc^{-1}, $\Omega_M = 0.31$, and $\Omega_\Lambda = 0.69$ (Planck Collaboration et al. 2016). References for the redshifts are provided in the corresponding sections.

Table 7.2: *ATCA* synthesized beam size (arcsec) for the different Briggs robust parameters.

GRB (1)	5.5 GHz/0.5 (2)	5.5 GHz/1.0 (3)	5.5 GHz/2.0 (4)	9.0 GHz/0.5 (5)	9.0 GHz/1.0 (6)	9.0 GHz/2.0 (7)
050709	3.15 × 1.59	4.08 × 2.05	4.55 × 2.26	2.01 × 0.95	2.57 × 1.20	2.87 × 1.33
050724	4.36 × 1.54	5.74 × 2.00	6.40 × 2.21	2.67 × 0.94	3.46 × 1.21	3.87 × 1.34
061006	3.03 × 1.34	3.95 × 1.71	4.43 × 1.89	1.85 × 0.82	2.38 × 1.04	2.67 × 1.14
061201	2.32 × 1.49	3.20 × 1.83	3.68 × 1.98	1.43 × 0.91	1.93 × 1.10	2.22 × 1.20
070729	4.47 × 2.52	5.44 × 3.03	5.92 × 3.27	2.69 × 1.53	3.25 × 1.83	3.55 × 1.98
070809	7.72 × 1.74	8.90 × 1.98	10.00 × 2.18	4.66 × 1.05	5.39 × 1.19	6.06 × 1.32
071227	2.23 × 1.68	2.89 × 2.16	3.21 × 2.39	1.37 × 1.03	1.74 × 1.30	1.94 × 1.45
080123	2.56 × 1.49	3.33 × 1.91	3.72 × 2.11	1.56 × 0.91	2.00 × 1.15	2.25 × 1.27
080905	7.90 × 1.40	10.22 × 1.79	11.40 × 1.97	4.82 × 0.86	6.15 × 1.08	6.89 × 1.19
100628	3.87 × 1.57	5.02 × 2.02	5.59 × 2.23	2.36 × 0.97	3.02 × 1.22	3.38 × 1.35
130515	3.64 × 1.34	4.75 × 1.72	5.32 × 1.89	2.23 × 0.82	2.88 × 1.03	3.24 × 1.14
150424	12.00 × 1.48	14.61 × 1.76	15.94 × 1.90	7.31 × 0.90	8.79 × 1.06	9.59 × 1.14

Notes: The beam size follows from the Miriad `imfit` command.

Table 7.3: Galaxie coordinates, morphological types, and dimensions.

GRB (1)	Galaxy (2)	RA (3)	Decl. (J2000) (4)	morphol. type (5)	maj. axis (6)	min. axis (7)	z (8)
050709		23:01:26.81	−38:58:39.9	Irr	3.1	2.7	0.1606
050724	G1	16:24:44.40	−27:32:26.4	L	4.7	4.1	0.258
061006	G1	07:24:07.71	−79:11:55.2	L	2.1	0.75	0.4377
061201	G1	22:08:29.10	−74:34:35.8	L	11.5	5	0.111
061201	G2	22:08:32.50	−74:34:47.7	L	1.5	0.9	1.0
070729	G1	03:45:16.32	−39:19:12.3	L	4.0	2.4	0.5 ass.
070729	G2	03:45:15.70	−39:19:18.9	Irr	2.9	1.2	0.5 ass.
070729	G3	03:45:15.50	−39:19:28.5	L	4.1	3.0	0.5 ass.
070809	G1	13:35:04.22	−22:08:27.4	L	5.7	0.7	0.2187
070809	G2	13:35:04.14	−22:08:33.5	E	5.5	5.3	0.473
070809	G3	13:35:04.64	−22:08:31.8	L	0.7	0.4	–
071227		03:52:30.12	−55:59:00.2	L	8.2	3.2	0.381
080123	G1	22:35:46.92	−64:53:55.1	L	6.8	3.2	0.496
080123	G2	22:35:46.18	−64:54:04.2	L/Irr	1.4	1.0	–
080123	G3	22:35:45.73	−64:54:53.8	L/Irr	0.8	0.5	–
080123	G4	22:35:45.48	−64:53:56.4	L	1.8	0.9	–
080905	G1	19:10:42.09	−18:52:55.0	L	13.6	5.8	0.1218
100628A	C	15:03:52.81	−31:39:33.6	L	4.0	1.7	0.102
100628A	K	15:03:52.80	−31:39:28.8	Irr	1.2	0.9	0.102
100628A	D	15:03:53.59	−31:39:37.8	E	4.7	4.4	0.311
130515A	G1	18:53:44.88	−54:16:50.9	L/Irr	4.1	2.3	0.5 ass.
150424A	G1	10:09:13.00	−26:37:55.9	L	9.6	4.0	0.2981
150424A	G2	10:09:13.37	−26:37:51.3	L	0.9	0.6	>0.7

Notes: Most columns are self-explanatory. Column #5: The morphological type is given as: Irr = irregular, E = elliptical, L = lenticular. Column #6: The galaxy dimensions are given in arcsec and were measured on the images which were also used when overplotting the corresponding radio contours (Sect. 3 and 4).

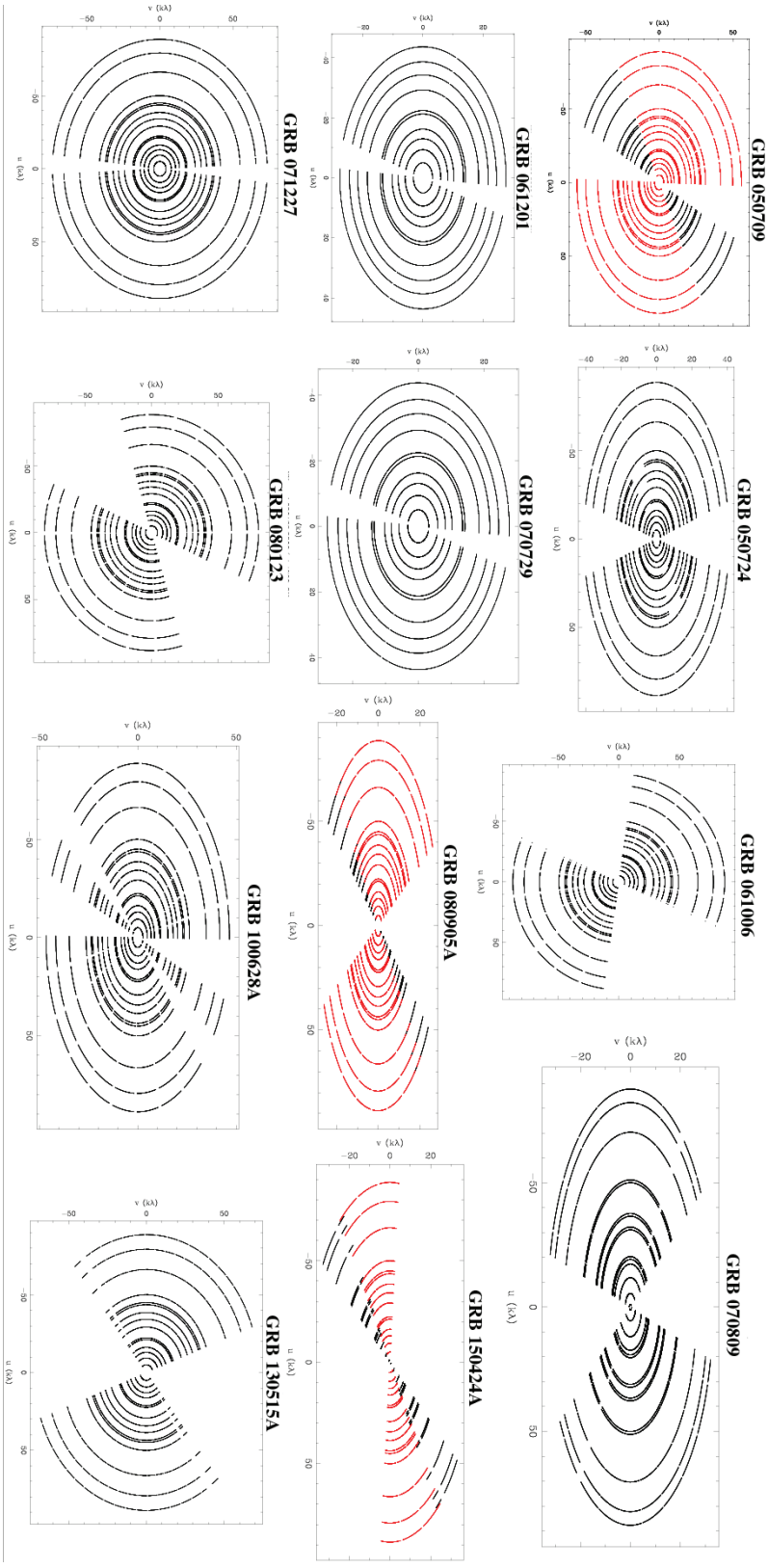

Fig. 7.1: *uv* plane coverage for the different *ATCA* observations. An additional red color indicates cases where the final data set is the sum of two observing runs.

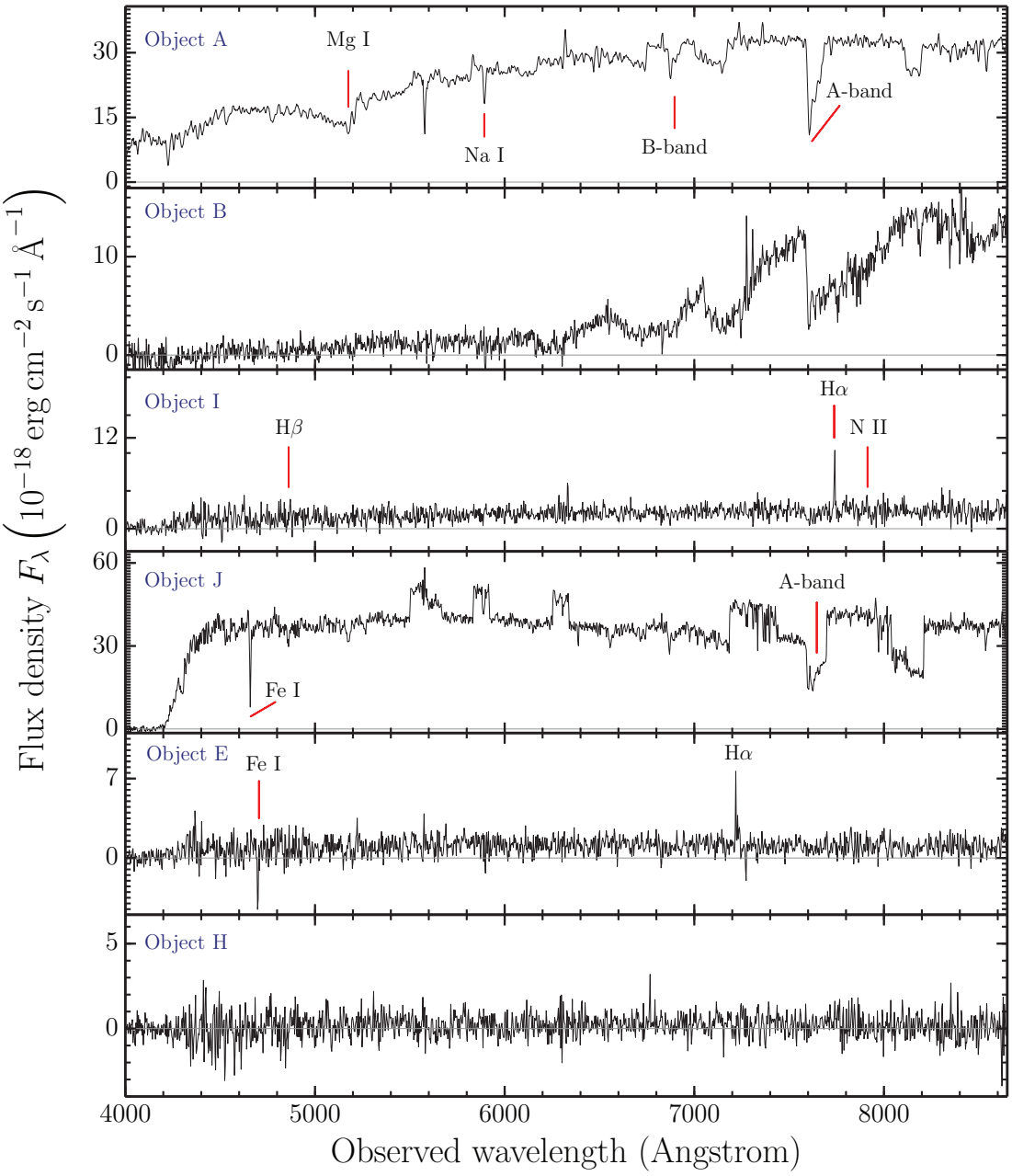

Fig. 7.2: Additional spectra of six objects inside or close to the *Swift*/XRT error cricle of GRB 100628A. For the designation see Fig. 3.6 in Sect. 3.3. For the magnitudes, coordinates, and redshifts see Table 7.4 in Sect. 7.

Table 7.4: GRB 100628A: Objects inside and close to the XRT error circle.

Object	RA (J2000)	Decl.	i_{AB}	redshift z
A	15:03:52.34	−31:39:33.9	20.8	K star
B1	15:03:52.86	−31:39:35.4	22.1	M star
B2	15:03:52.86	−31:39:36.7	22.3	star
C	15:03:52.81	−31:39:33.6	∼21.5	0.102
D	15:03:53.598	−31:39:37.89	20.2	0.311
E	15:03:53.61	−31:39:30.9	24.5	0.099
F	15:03:52.80	−31:39:28.8	24.1	0.406
G	15:03:52.02	−31:39:32.3	23.8	galaxy
H	15:03:51.96	−31:39:36.3	23.7	galaxy
I	15:03:51.50	−31:39:38.9	23.1	0.179
J	15:03:53.36	−31:39:22.6	17.6	star
K	15:03:52.45	−31:39:34.7	23.8	0.102

Notes: For object D the coordinates are based on the *ATCA* radio data at 9.0 GHz. Redshifts, when measured, are given with an accuracy of ±0.001 (see also Fig. 7.2). *i*-band AB magnitudes were measured on the combined Gemini-S/GMOS frames.

Table 7.5: 100628A: Log of the observations.

Date	Telescope	Instrument	Exposure
2010 Jun 29	2.2 m	GROND/$g'r'i'z'JHK_s$	1.5 hours
2010 Jun 29	Gemini-S	GMOS-S/i band	12×120 s
2011 Apr 11	VLT/UT1	FORS2/GRIS 300V+10	2×1240 s
2011 May 26	VLT/UT1	FORS2/GRIS 300V+10	2×1240 s
2013 Mar 20	VLT/UT2	X-shooter	4×940 s
2013 Apr 03	VLT/UT1	FORS2/GRIS 300V+10	2×1240 s
2013 Jul 23	ATCA	CABB	11 hours

Notes: Gemini data were obtained from the public archive. All other observations were performed during this work.

Fig. 7.3: The *ATCA* radio telescope. This Image was taken during my observing run in June 2013. Only three of the six antennas are visible.

7.2 The Australia Telescope Compact Array

The Australia Telescope Compact Array (ATCA)[1] is located at Paul Wild Observatory in Culgoora, around 25 km west of the small town Narrabri in Australia (550 northwest of Sydney, around eight hours by car). *ATCA* is operated by the Australian Telescope National Facility (ATNF) and is managed by the Commonwealth Scientific and Industrial Research Organization (CSIRO). The ATNF headquarter is in Marsfield/Epping, a suburb of Sydney. At the time of my first observing run (June 2013), I conducted the observations directly at the radio telescope at Paul Wild Observatory. This policy changed due to general budge-cuts of the CSIRO in mid 2015. Nowadays, the visitor has to perform the observations remotely from the ATNF headquarter in Sydney.

Since its inauguration in 1988, *ATCA* s still the biggest radio telescope array in the southern hemisphere. ASKAP[2], the Australian SKA pathfinder (also part of CSIRO), has recently started to be operational and will be ATNF's prime radio telescope in the near future

ATCA consists of an array of six antennas, each with a 22 m diameter dish (Frater et al. 1992). The antennas are designed as CA01 to CA06 and produce 15 baselines, with the longest having 6 km and the smallest 375 m. CA06 is the only fixed antenna, located at a distance of 3 km from the western end of the track. The other five dishes can be repositioned along a three

[1] `http://www.csiro.au/en/Research/Facilities/ ATNF/Australia-Telescope-Compact-Array`
[2] `http://www.atnf.csiro.au/projects/askap/index.html`

kilometer railway track and a 214 m long north-south spur.

ATCA was designed to perform observations at cm wavelengths on sources with declinations < -25 deg. Having this in mind, an east-west array, with a few number of antennas that could stay around ~ 12 hours on target, provided a suitable solution to achieve a good coverage of the *uv* plain.

In April 2009 the original *ATCA* correlator was replaced by the Compact Array Broadband Backend (CABB) correlator (Wilson et al. 2011), providing a bandwidth of 2048 MHz. *ATCA* can observe in seven different frequency bands (Moorey et al. 2008):

- 2.1 GHz in the 16 cm band,
- 5.5 GHz and 9.0 GHz in the 4 cm band,
- 16.7 GHz and 21.2 GHz in the 15 mm band,
- 33 GHz and 35 GHz in the 7 mm LSB band,
- 43 GHz and 45 GHz in the 7 mm USB band,
- 93 GHz and 95 GHz in the 3 mm band.

For more details see `http://www.narrabri.atnf.csiro.au/observing/users-guide/html/atug.html# Choosing-an-Observing-Frequency`.

7.3 Data reduction: *ATCA* radio data

In the following, I briefly outline the Miriad data reduction procedure by considering the *ATCA* observations of the field of the short GRB 100628A.

7.3.1 General

`RPFITS` is a data-recording format that is used to store the radio synthesis visibility data from the telescopes that are managed by the Australian ATNF (Sect. 7.2). As a first step, the *ATCA* radio continuum data has to be transformed into the Miriad format. This is done with the `atlod` command. It is recommended to run it with the 'birdle' option to remove self-interference and discard the autocorrelation data.

There can be several problems during the observations like the presence of RFI having its origin in different (non astronomical) radio emitters, potential telescope off-source data, or the interruption of the transmission from one of the six antennas. The non-identification of such bad data would have the consequence of a higher noise in the final image, which would result into a

less S/N ratio. In particular, during the observations in June 2013 I was affected by RFI due to military activities in the area.

An observing-log of the data-set is provided with the Miriad task `prrhd`. It allows the observer to perform a first inspection of the data by plotting the complete data set for an observing run in different formats. Figure 7.4 shows the complete dataset of the field of GRB 100628A spanning 11 hours of observations from 4 to 15 UT on July 23, 2013. The amplitudes of the science target together with the bandpass and the flux calibrator are shown as a function of time. I used two different flux calibrators, at the begin of the observations 0823-500 and a the end PKS B1934–638. The latter source is the main *ATCA* flux calibrator and was finally used (see Sect. 7.3.2) during the data reduction. The phase calibrator was the radio source 1451–375, which was observed for 7 min each hour, it is shown in yellow-white colors. The plot reveals a strong radio-frequency interference (RFI) around 12:18 UT, reaching an amplitude of >6 Jy.

Cleaning the data from RFI can be performed by using the automatic `pgflag` routine. It requires no human intervention, though the result can be edited by hand if outliers would still be apparent in the flagged data set (which can be easily identify via the Miriad displayer `uvplot`). My experience, however, is that the `pgflag` routine worked very well. In addition to a search for bad data, on every side of the bandpass there are two regions of ~32 MHz width that are less sensitive. These areas are flagged by default. As a consequence of this procedure 12.4% of the data were flagged, resulting in a corresponding reduction of the effective bandwidth from 2048 to to 1794 MHz. In all other observations, the flagging was always around 12%.

The GRB 100628A observing run lasted for about 11 hours, including the science target, the bandpass or flux calibrator, and the secondary or phase calibrator. Thereby, the data stream was ~ 1 Gbyte per hour. The complete data set was then split into the three individual targets with the task `uvsplit`. The final reduced data set has a size of about ~33 Gbyte.

7.3.2 Bandpass, flux and phase calibrations

Bandpass and flux calibrations were performed by observing the Seyfert 2 galaxy PKS B1934–638. Because the flux of the main calibrator has a constant flux as a function of frequency, it is used to adjust the gain of the array. This is done with the Miriad task `gpcal`.

Similar to optical observations where, depending from band to band, the detector does not respond uniformly to a homogeneous amount of light, in radio observations one needs to correct for the different response of the radio array in frequency and time domain, the so-called gain. Since the science target was observed for ~11 hours, its altitude in the sky was very much chang-

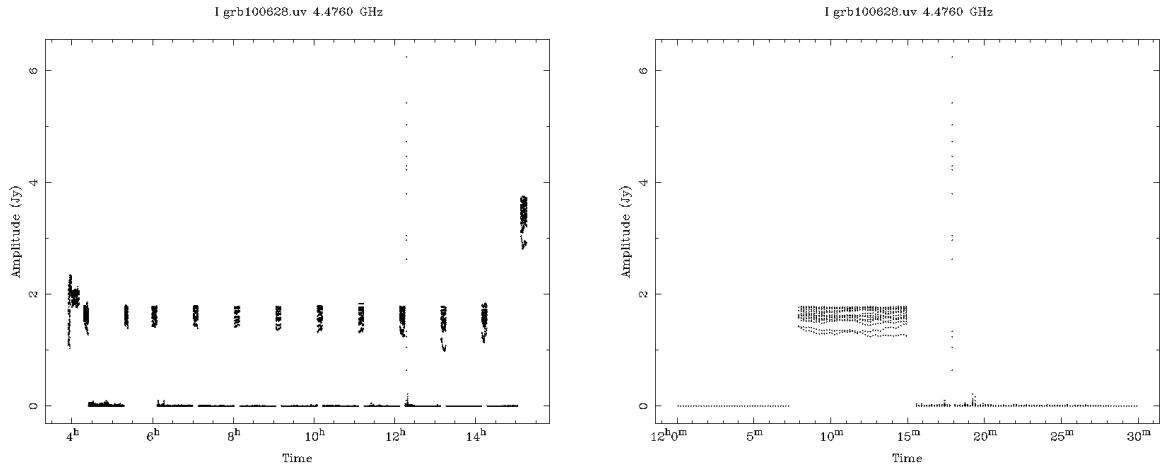

Fig. 7.4: Amplitude versus time. Plot of the complete data set (science target, flux and phase calibrator) of the ∼11 hour *ATCA* observations at 5.5 and 9.0 GHz of the field of GRB 100628A. Note the strong radio-frequency interference (RFI) around 12:18 pm which was orders of magnitudes above the finally achieved $1\sigma_{\rm rms}$ of some μJy. The RFI was finally flagged and removed from the data. This plot was obtained by using the Miriad command `uvplt`.

ing. Consequently, the gain solution calculated at the beginning of the observation is not valid anymore along the observations. Therefore, a secondary or phase calibrator was observed for 7 min at the beginning of each hour. Typically a good phase calibrator has to be a strong radio source located only a few degrees away from the science target during the observations. In case of GRB 100628A, I observed 1451–375. A detailed description of the calibration process can be found in Fomalont & Perley (1999).

7.3.3 Image reconstruction

When producing a radio image the first step is to produce a so-called dirty image from the calibrated (gain, flux, phase) visibility data by applying some kind of weighting procedures. The second step is the improvement of this result by additional image processing.

Different weighting schemes have been introduced for the first step in the image reconstruction.[3] In case of the so-called *natural weighting*, the same weight is given to all data points in the *uv* plane, i.e., to all baselines. This produces a maximum sensitivity but the synthesised beam shape is less good. Since the density of data points in the *uv* plane is however larger for small baselines, and alternative weighting scheme has been introduced. If more weight is given to areas in the *uv* plane where the density of data points is higher, this is called *uniform weighting*. It improves the angular resolution but degrades the noise level.

[3] see `http://www.atnf.csiro.au/computing/software/miriad/userguide/node97.html`

The so-called robust weighting scheme was introduced by Briggs (1995) as a compromise between natural and uniform weighting and since then it is commonly used in Miriad. Robust weighting is parametrised by the so-called robust parameter. As explained in the aforementioned *ATCA* webpage, robust values less than about −2 correspond essentially to minimising sidelobes, whereas values greater than +2 are just minimising the noise.

The Briggs robust parameter is selected in the Miriad command `invert`. In this work I varied it between `0.5` and `2.0`. A value of `0.5` is closer to uniform weighting while a value of `2.0` is close to natural weighting.

The final step is then to run the Miriad commands `mfclean` and `restor`. Thereby, the cleaning region was usually set to 880×880 pixels (about $6' \times 6'$) centered around the image center. The `mfclean` task was halted when the 1 $\sigma_{\rm rms}$ noise did not change significantly from iteration to iteration. After applying the `restor` task again I finally selected the results obtained for those robust parameter which gave the best compromise between sensitivity and resolution. Usually this was `2.0`.

7.4 Data reduction: optical photometry

Optical bands: The basic steps that were performed before performing the photometry are (i) removing bias and dark current, (ii) flat-fielding.

NIR bands: NIR images were reduced using `jitter`, a task that belongs to `eclipse`[4] which is a software package developed by ESO. `jitter` calculates the background sky flux of a set of images that have been taken at different sky positions (mosaicing), then corrects for the sky contribution and applies the standard bias, dark subtraction and flat-fielding. It finally shifts and adds the images obtained at different telescope positions.

The GROND Pipeline (GP) is a code that has been developed by the GROND team at MPE. It is written in python[5] and uses pyraf[6], which allows to run IRAF (Tody 1993) under the flexibility of python. Once the master bias and master flats are created, GP invokes the IRAF task `ccdproc` which subtracts the bias and dark images from the science image and thereupon divides it by the master flat. This procedure is applied individually to each single optical image inside an observing block (OB). The final image is then the sum of the individual images and it is obtained via the IRAF task `imcombine`.

[4] http://www.eso.org/sci/software/eclipse/faq/faq-jitter.html
[5] www.python.org
[6] www.stsci.edu/resources/software_hardware/pyraf

Astrometry: GP performs the astrometric correction using `daofind` which identifies the objects in an image by fitting a gaussian with a specific FWHM. To safe computing time, the number of objects that are used by the GP are reduced to the brightest stars in the field selected by the `pstselect` IRAF task. Then a specific algorithm is applied to match between the coordinates of the image and the catalog objects using `xyxymatch`. Finally the correction in the astrometry is performed by `ccmap`.

Photometry: In GP, all optical/NIR data are analysed through point spread function (PSF) photometry using the `daophot` and `allstar` tasks of IRAF as described in Krühler et al. (2008) and Küpcü Yoldaş et al. (2008). PSF fitting is also used to measure the magnitudes of an optical transient.

The optical data are calibrated against the Sloan Digital Sky Survey (SDSS DR7; Abazajian et al. 2009), if available. Otherwise a standard star field is observed under photometric conditions. For the NIR bands, photometric calibration is always performed against the 2MASS catalogue (Skrutskie et al. 2006). This procedure results in a typical absolute accuracy of 0.04 mag in $g'r'i'z'$, 0.06 mag in JH, and 0.08 mag in K_s.

Observed magnitudes were corrected for Galactic reddening based on Schlegel et al. (1998), assuming a Milky Way extinction curve with a ratio of total-to-selective extinction of $R_V = 3.1$.

Throughout the Thesis, if not otherwise stated all reported magnitudes are in the AB photometric system. For GROND the Vega-to-AB conversion is

- $g'_{\rm AB} = g'_{\rm Vega} - 0.06$ mag,
- $r'_{\rm AB} = r'_{\rm Vega} + 0.18$ mag
- $i'_{\rm AB} = i'_{\rm Vega} + 0.41$ mag
- $z'_{\rm AB} = z'_{\rm Vega} + 0.54$ mag
- $J_{\rm AB} = J_{\rm Vega} + 0.93$ mag
- $H_{\rm AB} = H_{\rm Vega} + 1.39$ mag
- $K_{s,\rm AB} = K_{s,\rm Vega} + 1.80$ mag

except for observations after an intervention on the instrument on March 2008, for which $K_{\rm AB} = K_{s,\rm Vega} + 1.86$ mag. Extinction corrections for the GROND filters are

- $A(g') = 1.253\,A_V$
- $A(r') = 0.799\,A_V$
- $A(i') = 0.615\,A_V$
- $A(z') = 0.454\,A_V$

- $A(J) = 0.292\,A_V$
- $A(H) = 0.184\,A_V$
- $A(K_s) = 0.136\,A_V$.

7.5 Data reduction: optical spectroscopy

The data was reduced in a standard fashion using IRAF, i.e.:

- **Removal of cosmic rays.** This was done using the IRAF task `crmedian`. Here a standard deviation is calculated for all pixels in the complete image. Then, those pixels that have a value which is statistically larger than a fixed threshold (e.g., 5σ) are identified as pixels affected by cosmic rays. Once they are identified, the value of this pixel is replaced by the median value of the neighbored pixels.
- **Bias and flatfield correction.** Similar to the case of the photometrical data (see above), I applied the corresponding bias and flatfield correction. The package `ccdproc` is able to correct and calibrate for the electronic effects of the detector. The tasks `zerocombine` corrects for the bias contribution while the task `flatcombine` does it for the flatfield effect.
- **Wavelength calibration.** This was done by fitting a dispersion function for the arc-lamp calibration spectra with the IRAF task `identify`. In my case the HgCdHe or the HgCdHe+Ar calibration lamps were used. Naturally, the solution found has to be applied to the scientific images.
- **Extract the one-dimensional spectra.** The trace of my objects were usually faint. Before extracting the one-dimensional spectra of my object, I removed the sky lines. Once this was done, I used the IRAF task `apall` to extract the one-dimensional spectra of my object. Sometimes the trace was not visible along the complete wavelength range of the image and this was causing problems. In those cases I just extracted from the image those parts on which the trace was visible.
- **Flux calibrating the one-dimensional spectra.** The final step is to flux calibrate the one-dimensional wavelength-calibrated spectra using the flux known for a photometric standard star.

Bibliography

Aasi, J., Abbott, B. P., Abbott, R., et al. 2015, Physical Review D., 91, 062008

Abazajian, K. N., Adelman-McCarthy, J. K., Agüeros, M. A., et al. 2009, Astroph. J. Suppl, 182, 543

Acernese, F., Agathos, M., Agatsuma, K., et al. 2015, Classical and Quantum Gravity, 32, 024001

Adams, S. M., Kochanek, C. S., Gerke, J. R., Stanek, K. Z., & Dai, X. 2017, Mon. Not. R. Astron. Soc., 468, 4968

Alatalo, K., Cales, S. L., Rich, J. A., et al. 2016, Astroph. J. Suppl, 224, 38

Aloy, M. A., Janka, H.-T., & Müller, E. 2005, Astron. Astroph., 436, 273

Amati, L., Frontera, F., Tavani, M., et al. 2002, Astron. Astroph., 390, 81

Amati, L., Guidorzi, C., Frontera, F., et al. 2008, Mon. Not. R. Astron. Soc., 391, 577

Antonelli, L. A., D'Avanzo, P., Perna, R., et al. 2009, Astron. Astroph., 507, L45

Antonelli, L. A., Maund, J. R., Palazzi, E., et al. 2010, GRB Coordinates Network, 10620, 1

Arnouts, S., Cristiani, S., Moscardini, L., et al. 1999, Mon. Not. R. Astron. Soc., 310, 540

Aso, Y., Michimura, Y., Somiya, K., et al. 2013, Physical Review D., 88, 043007

Baldwin, J. A., Phillips, M. M., & Terlevich, R. 1981, Publ. Astron. Soc. Pac., 93, 5

Barthelmy, S. 2008, Astronomische Nachrichten, 329, 340

Barthelmy, S. D., Barbier, L. M., Cummings, J. R., et al. 2005a, Space Sci. Rev., 120, 143

Barthelmy, S. D., Butterworth, P., Cline, T. L., et al. 1995, Astroph. Space Sc., 231, 235

Barthelmy, S. D., Chincarini, G., Burrows, D. N., et al. 2005b, Nature, 438, 994

Barthelmy, S. D., Sakamoto, T., Norris, J., & Gehrels, N. 2007, GRB Coordinates Network, 6788

Bauswein, A., Goriely, S., & Janka, H.-T. 2013, Astroph. J., 773, 78

Beardmore, A. P., Page, K. L., Palmer, D. M., & Ukwatta, T. N. 2015, GRB Coordinates Network, 17743

Beckmann, V., Beck, M., Ferrigno, C., et al. 2010, GRB Coordinates Network, 10898, 1

Belczynski, K., Perna, R., Bulik, T., et al. 2006, Astroph. J., 648, 1110

Bell, E. F. 2003, Astroph. J., 586, 794

Berger, E. 2006, GRB Coordinates Network, 5952, 1

Berger, E. 2009, Astroph. J., 690, 231

Berger, E. 2010a, Astroph. J., 722, 1946

Berger, E. 2010b, GRB Coordinates Network, 10943, 1

Berger, E. 2014, Ann. Rev. Astron. Astroph., 52, 43

Berger, E., Cenko, S. B., Fox, D. B., & Cucchiara, A. 2009, Astroph. J., 704, 877

Berger, E., Cowie, L. L., Kulkarni, S. R., et al. 2003, Astroph. J., 588, 99

Berger, E., Fong, W., & Chornock, R. 2013a, Astroph. J. Lett., 774, L23

Berger, E., Fox, D. B., Price, P. A., et al. 2007a, Astroph. J., 664, 1000

Berger, E., Guver, T., & Fong, W. 2010a, GRB Coordinates Network, 10911, 1

Berger, E., Guver, T., Fong, W., & Chornock, R. 2010b, GRB Coordinates Network, 10902, 1

Berger, E. & Kaplan, D. L. 2007, GRB Coordinates Network, 6680, 1

Berger, E., Morrell, N., & Roth, M. 2007b, GRB Coordinates Network, 7151, 1

Berger, E., Price, P. A., Cenko, S. B., et al. 2005, Nature, 438, 988

Berger, E., Zauderer, B. A., Levan, A., et al. 2013b, Astroph. J., 765, 121

Bernardini, M. G., Ghirlanda, G., Campana, S., et al. 2015, Mon. Not. R. Astron. Soc., 446, 1129

Bianco, C. L., Amati, L., Bernardini, M. G., et al. 2012, Memorie della Societa Astronomica Italiana Supplementi, 21, 139

Bissaldi, E., McBreen, S., Connaughton, V., & von Kienlin, A. 2008, GRB Coordinates Network, 8204, 1

Bloom, J. S., Kulkarni, S. R., & Djorgovski, S. G. 2002, Astron. J., 123, 1111

Bloom, J. S., Prochaska, J. X., Pooley, D., et al. 2006, Astroph. J., 638, 354

Boer, M., Ricker, G., Atteia, J.-L., et al. 2005, GRB Coordinates Network, 3653, 1

Briggs, D. S. 1995, in Bulletin of the American Astronomical Society, Vol. 27, American Astronomical Society Meeting Abstracts, 1444

Burenin, R., Khorunzhev, G., Sazonov, S., et al. 2010, GRB Coordinates Network, 10900, 1

Burgay, M., D'Amico, N., Possenti, A., et al. 2003, Nature, 426, 531

Burrows, D. N., Hill, J. E., Nousek, J. A., et al. 2005, Space Sci. Rev., 120, 165

Butler, N., Ricker, G., Atteia, J.-L., et al. 2005, GRB Coordinates Network, 3570, 1

Caito, L., Amati, L., Bernardini, M. G., et al. 2010, Astron. Astroph., 521, A80

Cameron, P. B., Harrison, F. A., & Frail, D. A. 2005, GRB Coordinates Network, 3688, 1

Cano, Z., Wang, S.-Q., Dai, Z.-G., & Wu, X.-F. 2017, Advances in Astronomy, 2017, 8929054

Casey, C. M., Narayanan, D., & Cooray, A. 2014, Physics Reports, 541, 45

Castelvecchi, D. 2017, Nature, 549

Castro Cerón, J. M., Michałowski, M. J., Hjorth, J., et al. 2006, Astroph. J. Lett., 653, L85

Castro-Tirado, A. J., Sanchez-Ramirez, R., Lombardi, G., & Rivero, M. A. 2015, GRB Coordinates Network, 17758

Castro-Tirado, A. J., Soldán, J., Bernas, M., et al. 1999a, Astron. Astroph. Suppl. Ser., 138, 583

Castro-Tirado, A. J., Zapatero-Osorio, M. R., Caon, N., et al. 1999b, Science, 283, 2069

Cenko, S. B. & Cucchiara, A. 2013, GRB Coordinates Network, 14670

Cenko, S. B., Perley, D. A., Bloom, J. S., Morgan, A. N., & Cucchiara, A. 2010, GRB Coordinates Network, 10946, 1

Chandra, P. & Frail, D. A. 2007, GRB Coordinates Network, 6742, 1

Chandra, P. & Frail, D. A. 2012, Astroph. J., 746, 156

Christensen, L., Vreeswijk, P. M., Sollerman, J., et al. 2008, Astron. Astroph., 490, 45

Church, R. P., Levan, A. J., Davies, M. B., & Tanvir, N. 2012, Memorie della Societa Astronomica Italiana Supplementi, 21, 104

Condon, J. J. 1992, Ann. Rev. Astron. Astroph., 30, 575

Condon, J. J., Helou, G., Sanders, D. B., & Soifer, B. T. 1993, Astron. J., 105, 1730

Condon, J. J. & Ransom, S. M. 2016, Essential Radio Astronomy
Costa, E., Frontera, F., Heise, J., et al. 1997, Nature, 387, 783
Covino, S., Antonelli, L. A., Romano, P., et al. 2005, GRB Coordinates Network, 3665
Covino, S., Malesani, D., Israel, G. L., et al. 2006, Astron. Astroph., 447, L5
Crowther, P. 2012, Astronomy and Geophysics, 53, 4.30
Cucchiara, A. & Fox, D. B. 2010, GRB Coordinates Network, 10624, 1
Cucchiara, A., Levan, A. J., Fox, D. B., et al. 2011, Astroph. J., 736, 7
Cucchiara, A., Prochaska, J. X., Perley, D., et al. 2013, Astroph. J., 777, 94
Cucchiara, A. & Sakamoto, T. 2007, GRB Coordinates Network, 7150, 1
Cummings, J., Barthelmy, S. D., Baumgartner, W., et al. 2008, GRB Coordinates Network, 8187, 1
D'Avanzo, P. 2015, Journal of High Energy Astrophysics, 7, 73
D'Avanzo, P., Fiore, F., Piranomonte, S., et al. 2007, GRB Coordinates Network, 7152, 1
D'Avanzo, P., Malesani, D., Covino, S., et al. 2009, Astron. Astroph., 498, 711
D'Avanzo, P. & Piranomonte, S. 2006, GRB Coordinates Network, 5896, 1
D'Avanzo, P., Piranomonte, S., Chincarini, G., & Stella, L. 2006, GRB Coordinates Network, 5884, 1
de Ugarte Postigo, A. 2015, IAU General Assembly, 22, 2257336
de Ugarte Postigo, A., Horváth, I., Veres, P., et al. 2011, Astron. Astroph., 525, A109
de Ugarte Postigo, A., Malesani, D., Levan, A. J., Hjorth, J., & Tanvir, N. R. 2008, GRB Coordinates Network, 8195, 1
de Ugarte Postigo, A., Thöne, C. C., Rowlinson, A., et al. 2014, Astron. Astroph., 563, A62
Domínguez, A., Siana, B., Henry, A. L., et al. 2013, Astroph. J., 763, 145
Donevski, D. & Prodanović, T. 2015, Mon. Not. R. Astron. Soc., 453, 638
Eldridge, J. J., Langer, N., & Tout, C. A. 2011, Mon. Not. R. Astron. Soc., 414, 3501
Elliott, J., Krühler, T., Greiner, J., et al. 2013, Astron. Astroph., 556, A23
Evans, P. 2011a, GRB Coordinates Network, 12273, 1
Evans, P. A. 2011b, GRB Coordinates Network, 12250, 1
Evans, P. A., Beardmore, A. P., Page, K. L., et al. 2009, Mon. Not. R. Astron. Soc., 397, 1177
Fensch, J., Duc, P.-A., Weilbacher, P. M., Boquien, M., & Zackrisson, E. 2016, Astron. Astroph., 585, A79
Ferrero, P., Kann, D. A., Zeh, A., et al. 2006, Astron. Astroph., 457, 857
Ferrero, P., Sanchez, S. F., Kann, D. A., et al. 2007, Astron. J., 134, 2118
Fishman, G. J., Meegan, C. A., Wilson, R. B., et al. 1994, Astroph. J. Suppl, 92, 229
Fomalont, E. B. & Perley, R. A. 1999, in Astronomical Society of the Pacific Conference Series, Vol. 180, Synthesis Imaging in Radio Astronomy II, ed. G. B. Taylor, C. L. Carilli, & R. A. Perley, 79
Fong, W. 2015, GRB Coordinates Network, 17804
Fong, W. & Berger, E. 2013, Astroph. J., 776, 18
Fong, W., Berger, E., Chornock, R., et al. 2013, Astroph. J., 769, 56
Fong, W., Berger, E., Chornock, R., et al. 2011, Astroph. J., 730, 26
Fong, W., Berger, E., Margutti, R., & Zauderer, B. A. 2015, Astroph. J., 815, 102
Fong, W., Metzger, B. D., Berger, E., & Özel, F. 2016, Astroph. J., 831, 141

Fox, D. B., Frail, D. A., Price, P. A., et al. 2005, Nature, 437, 845
Frail, D. A., Kulkarni, S. R., Nicastro, L., Feroci, M., & Taylor, G. B. 1997, Nature, 389, 261
Frater, R. H., Brooks, J. W., & Whiteoak, J. B. 1992, Journal of Electrical and Electronics Engineering Australia, 12, 103
Fruchter, A. S., Levan, A. J., Strolger, L., et al. 2006, Nature, 441, 463
Fynbo, J. P. U., Watson, D., Thöne, C. C., et al. 2006, Nature, 444, 1047
Galama, T. J., Vreeswijk, P. M., van Paradijs, J., et al. 1998, Nature, 395, 670
Gehrels, N., Chincarini, G., Giommi, P., et al. 2004, Astroph. J., 611, 1005
Gehrels, N., Sarazin, C. L., O'Brien, P. T., et al. 2005, Nature, 437, 851
Gerke, J. R., Kochanek, C. S., & Stanek, K. Z. 2015, Mon. Not. R. Astron. Soc., 450, 3289
Golenetskii, S., Aptekar, R., Frederiks, D., et al. 2015, GRB Coordinates Network, 17752
Golenetskii, S., Aptekar, R., Mazets, E., et al. 2006, GRB Coordinates Network, 5890, 1
Golenetskii, S., Aptekar, R., Mazets, E., et al. 2007a, GRB Coordinates Network, 7155, 1
Golenetskii, S., Aptekar, R., Mazets, E., et al. 2007b, GRB Coordinates Network, 6690, 1
Gorosabel, J., Castro-Tirado, A. J., Guziy, S., et al. 2006, Astron. Astroph., 450, 87
Gorosabel, J. & de Ugarte Postigo, A. 2010, in Proc. High Time Resolution Astrophysics - The Era of Extremely Large Telescopes (HTRA-IV). May 5 - 7, 2010, 36
Greiner, J., Bornemann, W., Clemens, C., et al. 2008, Publ. Astron. Soc. Pac., 120, 405
Greiner, J., Krühler, T., Klose, S., et al. 2011, Astron. Astroph., 526, A30
Greiner, J., Mazzali, P. A., Kann, D. A., et al. 2015, Nature, 523, 189
Greiner, J., Michałowski, M. J., Klose, S., et al. 2016, Astron. Astroph., 593, A17
Grupe, D., Gronwall, C., Wang, X.-Y., et al. 2007, Astroph. J., 662, 443
Güdel, M. 1992, Astron. Astroph., 264, L31
Güdel, M. 2002, Ann. Rev. Astron. Astroph., 40, 217
Guidorzi, C., Barbier, L. M., Barthelmy, S. D., et al. 2007a, GRB Coordinates Network, 6678, 1
Guidorzi, C., Romano, P., & Moretti, A. 2007b, GRB Coordinates Network, 6682, 1
Guidorzi, C., Sato, G., Cucciara, A., et al. 2007c, GCN Report, 77, 2
Haarsma, D. B., Partridge, R. B., Windhorst, R. A., & Richards, E. A. 2000, Astroph. J., 544, 641
Haislip, J., Lacluyze, A., Reichart, D., et al. 2006, GRB Coordinates Network, 5895, 1
Hammer, F., Flores, H., Schaerer, D., et al. 2006, Astron. Astroph., 454, 103
Hatsukade, B., Hashimoto, T., Ohta, K., et al. 2012, Astroph. J., 748, 108
Henriques, B. M. B., White, S. D. M., Lemson, G., et al. 2012, Mon. Not. R. Astron. Soc., 421, 2904
Hjorth, J., Malesani, D., Jakobsson, P., et al. 2012, Astroph. J., 756, 187
Hjorth, J., Sollerman, J., Gorosabel, J., et al. 2005a, Astroph. J. Lett., 630, L117
Hjorth, J., Sollerman, J., Møller, P., et al. 2003, Nature, 423, 847
Hjorth, J., Watson, D., Fynbo, J. P. U., et al. 2005b, Nature, 437, 859
Hogg, D. W., Pahre, M. A., McCarthy, J. K., et al. 1997, Mon. Not. R. Astron. Soc., 288, 404
Holland, S. T. & Marshall, F. 2006, GRB Coordinates Network, 5883, 1
Horváth, I., Balázs, L. G., Bagoly, Z., & Veres, P. 2008, Astron. Astroph., 489, L1
Hunt, L. K., Palazzi, E., Michałowski, M. J., et al. 2014, Astron. Astroph., 565, A112

Hunt, L. K., Palazzi, E., Rossi, A., et al. 2011, Astroph. J. Lett., 736, L36

Hurley, K., Golenetskii, S., Aptekar, R., et al. 2011, in American Institute of Physics Conference Series, Vol. 1358, American Institute of Physics Conference Series, ed. J. E. McEnery, J. L. Racusin, & N. Gehrels, 385–388

Ibar, E., Ivison, R. J., Best, P. N., et al. 2010, Mon. Not. R. Astron. Soc., 401, L53

Iglesias-Páramo, J., Buat, V., Hernández-Fernández, J., et al. 2007, Astroph. J., 670, 279

Ilbert, O., Arnouts, S., McCracken, H. J., et al. 2006, Astron. Astroph., 457, 841

Immler, S. 2010, GRB Coordinates Network, 10901, 1

Immler, S., Starling, R. L. C., Evans, P. A., Barthelmy, S. D., & Sakamoto, T. 2010, GCN Report, 290, 1

Izzo, L., Thöne, C. C., Schulze, S., et al. 2017, ArXiv e-prints

Jakobsson, P., Hjorth, J., Fynbo, J. P. U., et al. 2004, ApJ, 617, L21

Jakobsson, P., Hjorth, J., Malesani, D., et al. 2012, 279, 187

Jelínek, M., Castro-Tirado, A. J., Cunniffe, R., et al. 2016, Advances in Astronomy, 2016, 192846

Just, O., Obergaulinger, M., & Janka, H.-T. 2015, Mon. Not. R. Astron. Soc., 453, 3386

Kann, D. A., Klose, S., & Zeh, A. 2006, Astroph. J., 641, 993

Kann, D. A., Klose, S., Zhang, B., et al. 2011, Astroph. J., 734, 96

Kann, D. A., Klose, S., Zhang, B., et al. 2010, Astroph. J., 720, 1513

Kann, D. A., Schady, P., Olivares E., F., et al. 2016, ArXiv e-prints

Kann, D. A., Tanga, M., & Greiner, J. 2015, GRB Coordinates Network, 17757

Kasen, D., Fernández, R., & Metzger, B. D. 2015, Mon. Not. R. Astron. Soc., 450, 1777

Kawabata, K. S., Deng, J., Wang, L., et al. 2003, Astroph. J. Lett., 593, L19

Kennicutt, Jr., R. C. 1998, Ann. Rev. Astron. Astroph., 36, 189

Klebesadel, R. W., Strong, I. B., & Olson, R. A. 1973, Astroph. J., 182, L85

Klose, S. 2000, in Reviews in Modern Astronomy, Vol. 13, Reviews in Modern Astronomy, ed. R. E. Schielicke, 129

Klose, S., Eisloeffel, J., & Richter, S. 1996, Astroph. J. Lett., 470, L93

Klose, S., Greiner, J., Rau, A., et al. 2004, Astron. J., 128, 1942

Klose, S., Schmidl, S., Kann, D. A., Nicuesa Guelbenzu, A., & et a, l. 2017, subm. to A&A, 601

Kochanek, C. S., Pahre, M. A., Falco, E. E., et al. 2001, Astroph. J., 560, 566

Kouveliotou, C., Meegan, C. A., Fishman, G. J., et al. 1993, Astroph. J. Lett., 413, L101

Kramer, M., Stairs, I. H., Manchester, R. N., et al. 2006, Science, 314, 97

Krimm, H., Barbier, L., Barthelmy, S., et al. 2006, GRB Coordinates Network, 5704, 1

Krimm, H., Barbier, L., Barthelmy, S. D., et al. 2007, GRB Coordinates Network, 6732, 1

Krühler, T., Fynbo, J. P. U., Geier, S., et al. 2012, Astron. Astroph., 546, A8

Krühler, T., Greiner, J., Schady, P., et al. 2011, Astron. Astroph., 534, A108

Krühler, T., Kuncarayakti, H., Schady, P., et al. 2017, Astron. Astroph., 602, A85

Krühler, T., Küpcü Yoldaş, A., Greiner, J., et al. 2008, Astroph. J., 685, 376

Krühler, T., Malesani, D., Fynbo, J. P. U., et al. 2015, Astron. Astroph., 581, A125

Kulkarni, S. & Desai, S. 2017, Astroph. Space Sc., 362, 70

Kulkarni, S. R., Frail, D. A., Wieringa, M. H., et al. 1998, Nature, 395

Küpcü Yoldaş, A., Krühler, T., Greiner, J., et al. 2008, in American Institute of Physics Conference Series, Vol. 1000, American Institute of Physics Conference Series, ed. M. Galassi, D. Palmer, & E. Fenimore, 227–231

Le Floc'h, E., Charmandaris, V., Forrest, W. J., et al. 2006, Astroph. J., 642, 636

Le Floc'h, E., Duc, P.-A., Mirabel, I. F., et al. 2003, Astron. Astroph., 400, 499

Le Floc'h, E., Duc, P.-A., Mirabel, I. F., et al. 2002, Astroph. J. Lett., 581, L81

Leibler, C. N. & Berger, E. 2010, Astroph. J., 725, 1202

Levan, A. J. & Tanvir, N. R. 2013, GRB Coordinates Network, 14667

Levan, A. J., Tanvir, N. R., Fruchter, A. S., et al. 2006, Astroph. J. Lett., 648, L9

Levan, A. J., Tanvir, N. R., Wiersema, K., & Cenko, S. B. 2010, GRB Coordinates Network, 10909, 1

Levan, A. J., Tanvir, N. R., Wiersema, K., & O'Brien, P. T. 2011, GRB Coordinates Network, 12414

Levesque, E. M., Bloom, J. S., Butler, N. R., et al. 2010a, Mon. Not. R. Astron. Soc., 401, 963

Levesque, E. M., Kewley, L. J., Berger, E., & Zahid, H. J. 2010b, Astron. J., 140, 1557

Li, L.-X. & Paczyński, B. 1998, Astroph. J. Lett., 507, L59

Lithwick, Y. & Sari, R. 2001, Astroph. J., 555, 540

Lu, R.-J., Wei, J.-J., Qin, S.-F., & Liang, E.-W. 2012, Astroph. J., 745, 168

MacFadyen, A. I. & Woosley, S. E. 1999, Astroph. J., 524, 262

Malesani, D., Barthelmy, S. D., Gehrels, N., et al. 2013, GRB Coordinates Network, 14650

Malesani, D., Covino, S., D'Avanzo, P., et al. 2007, Astron. Astroph., 473, 77

Malesani, D., de Ugarte Postigo, A., Fynbo, J. P. U., et al. 2008, GRB Coordinates Network, 8190, 1

Malesani, D., Stella, L., Covino, S., et al. 2006a, GRB Coordinates Network, 5705, 1

Malesani, D., Stella, L., D'Avanzo, P., et al. 2006b, GRB Coordinates Network, 5718, 1

Malesani, D., Xu, D., Watson, D. J., & Blay, P. 2015, GRB Coordinates Network, 17756

Manthey, E., Hüttemeister, S., Aalto, S., Horellou, C., & Bjerkeli, P. 2008, Astron. Astroph., 490, 975

Margalit, B. & Piran, T. 2015, Mon. Not. R. Astron. Soc., 452, 3419

Marshall, F. E., Barthelmy, S. D., Burrows, D. N., et al. 2007, GCN Report, 80, 1

Marshall, F. E. & Beardmore, A. P. 2015, GRB Coordinates Network, 17751

Martinez Aviles, G., Ferrari, C., Johnston-Hollitt, M., et al. 2016, Astron. Astroph., 595, A116

Matheson, T., Garnavich, P. M., Stanek, K. Z., et al. 2003, Astroph. J., 599, 394

Mazzali, P. A., Deng, J., Nomoto, K., et al. 2006, Nature, 442, 1018

McBreen, S., Krühler, T., Rau, A., et al. 2010, Astron. Astroph., 516, A71

McGuire, J. T. W., Tanvir, N. R., Levan, A. J., et al. 2016, Astroph. J., 825, 135

Meegan, C., Lichti, G., Bhat, P. N., et al. 2009, Astroph. J., 702, 791

Mészáros, P. 2006, Rep. Prog. Phys., 69, 2259

Michałowski, M. J., Hjorth, J., Castro Cerón, J. M., & Watson, D. 2008, Astroph. J., 672, 817

Michałowski, M. J., Hunt, L. K., Palazzi, E., et al. 2014, Astron. Astroph., 562, A70

Michałowski, M. J., Kamble, A., Hjorth, J., et al. 2012, Astroph. J., 755, 85

Michałowski, M. J., Xu, D., Stevens, J., et al. 2016, ArXiv e-prints

Modjaz, M., Kewley, L., Kirshner, R. P., et al. 2008, Astron. J., 135, 1136

Moin, A., Chandra, P., Miller-Jones, J. C. A., et al. 2013, Astroph. J., 779, 105

Moorey, G. G., Bolton, R. J., & Bowen, M. A. 2008, 38th European Microwave Conference, 12, 155
Murphy, E. J., Condon, J. J., Schinnerer, E., et al. 2011, Astroph. J., 737, 67
Narayana Bhat, P., Meegan, C. A., von Kienlin, A., et al. 2016, Astroph. J. Suppl, 223, 28
Nemiroff, R. J. 1994, Comments on Astrophysics, 17, 189
Nicuesa Guelbenzu, A., Klose, S., Greiner, J., et al. 2012, Astron. Astroph., 548, A101
Nicuesa Guelbenzu, A., Klose, S., Michałowski, M. J., et al. 2014, Astroph. J., 789, 45
Nicuesa Guelbenzu, A., Klose, S., Palazzi, E., et al. 2015, Astron. Astroph., 583, A88
Nicuesa Guelbenzu, A., Klose, S., Rossi, A., et al. 2011, Astron. Astroph., 531, L6
Niino, Y., Aoki, K., Hashimoto, T., et al. 2017, Publ. Astron. Soc. Japan
Norris, J. P. & Bonnell, J. T. 2006, Astroph. J., 643, 266
Onda, K., Tashiro, M., Terada, Y., et al. 2008, GRB Coordinates Network, 7158, 1
Paczynski, B. 1986, Astroph. J. Lett., 308, L43
Pagani, C., Baumgartner, W. H., Beardmore, A. P., et al. 2008, GRB Coordinates Network, 8180, 1
Panaitescu, A., Kumar, P., & Narayan, R. 2001, Astroph. J. Lett., 561, L171
Pedersen, K., Elíasdóttir, Á., Hjorth, J., et al. 2005, Astroph. J. Lett., 634, L17
Perley, D. A., Bloom, J. S., Modjaz, M., et al. 2008, GRB Coordinates Network, 7889, 1
Perley, D. A., Cenko, S. B., Bloom, J. S., et al. 2009, Astron. J., 138, 1690
Perley, D. A., Krühler, T., Schulze, S., et al. 2016a, Astroph. J., 817, 7
Perley, D. A. & McConnell, N. J. 2015, GRB Coordinates Network, 17745
Perley, D. A., Modjaz, M., Morgan, A. N., et al. 2012, Astroph. J., 758, 122
Perley, D. A. & Perley, R. A. 2013, Astroph. J., 778, 172
Perley, D. A., Perley, R. A., Hjorth, J., et al. 2015, Astroph. J., 801, 102
Perley, D. A., Tanvir, N. R., Hjorth, J., et al. 2016b, Astroph. J., 817, 8
Perley, D. A., Thoene, C. C., & Bloom, J. S. 2007, GRB Coordinates Network, 6774, 1
Perri, M., Stratta, G., Conciatore, M. L., Burrows, D. N., & Marshall, F. E. 2006, GRB Coordinates Network, 5885, 1
Pian, E., Mazzali, P. A., Masetti, N., et al. 2006, Nature, 442, 1011
Piran, T. 2004, Reviews of Modern Physics, 76, 1143
Piro, L. & BeppoSAX Team. 1997, in ESA Special Publication, Vol. 382, The Transparent Universe, ed. C. Winkler, T. J.-L. Courvoisier, & P. Durouchoux, 179
Planck Collaboration, Ade, P. A. R., Aghanim, N., et al. 2016, Astron. Astroph., 594, A13
Price, P. A., Roth, K., & Fox, D. W. 2005, GRB Coordinates Network, 3605, 1
Prieto, J. L., Krühler, T., Anderson, J. P., et al. 2016, Astroph. J. Lett., 830, L32
Prochaska, J. X., Bloom, J. S., Chen, H.-W., et al. 2006, Astroph. J., 642, 989
Prochaska, J. X., Bloom, J. S., Chen, H.-W., et al. 2005, GRB Coordinates Network, 3700, 1
Rau, A., Savaglio, S., Krühler, T., et al. 2010, Astroph. J., 720, 862
Renaud, F., Bournaud, F., & Duc, P.-A. 2015, Mon. Not. R. Astron. Soc., 446, 2038
Rezzolla, L., Giacomazzo, B., Baiotti, L., et al. 2011, Astroph. J. Lett., 732, L6
Rhoads, J. E. 1999, Astroph. J., 525, 737
Rich, J. A., Kewley, L. J., & Dopita, M. A. 2015, Astroph. J. Suppl, 221, 28

Ricker, G. R. 1997, in All-Sky X-Ray Observations in the Next Decade, ed. M. Matsuoka & N. Kawai, 366

Ricker, G. R., Atteia, J.-L., Crew, G. B., et al. 2003, in American Institute of Physics Conference Series, Vol. 662, Gamma-Ray Burst and Afterglow Astronomy 2001: A Workshop Celebrating the First Year of the HETE Mission, ed. G. R. Ricker & R. K. Vanderspek, 3–16

Robitaille, T. P. & Whitney, B. A. 2010, Astroph. J. Lett., 710, L11

Roming, P. W. A., Kennedy, T. E., Mason, K. O., et al. 2005, Space Sci. Rev., 120, 95

Rossi, A., Klose, S., Ferrero, P., et al. 2012, Astron. Astroph., 545, A77

Rossi, A., Piranomonte, S., Savaglio, S., et al. 2014, Astron. Astroph., 572, A47

Rowlinson, A., Wiersema, K., Levan, A. J., et al. 2010, Mon. Not. R. Astron. Soc., 408, 383

Ruderman, M. 1975, in Annals of the New York Academy of Sciences, Vol. 262, Seventh Texas Symposium on Relativistic Astrophysics, ed. P. G. Bergman, E. J. Fenyves, & L. Motz, 164–180

Sadler, E. M., Ekers, R. D., Mahony, E. K., Mauch, T., & Murphy, T. 2014, Mon. Not. R. Astron. Soc., 438, 796

Sakamoto, T., Barthelmy, S. D., Baumgartner, W. H., et al. 2011, Astroph. J. Suppl, 195, 2

Sakamoto, T., Baumgartner, W. H., Beardmore, A. P., et al. 2007a, GRB Coordinates Network, 7147, 1

Sakamoto, T., Norris, J., Ukwatta, T., et al. 2007b, GRB Coordinates Network, 7156, 1

Salvaterra, R., Devecchi, B., Colpi, M., & D'Avanzo, P. 2010, Mon. Not. R. Astron. Soc., 406, 1248

Sánchez-Ramírez, R., Hancock, P. J., Jóhannesson, G., et al. 2016, ArXiv e-prints

Sanders, N. E., Caldwell, N., McDowell, J., & Harding, P. 2012, Astroph. J., 758, 133

Sari, R., Piran, T., & Halpern, J. P. 1999, Astroph. J. Lett., 519, L17

Sato, G., Barbier, L., Barthelmy, S. D., et al. 2007, GRB Coordinates Network, 7148, 1

Sault, R. J., Teuben, P. J., & Wright, M. C. H. 1995, in Astronomical Society of the Pacific Conference Series, Vol. 77, Astronomical Data Analysis Software and Systems IV, ed. R. A. Shaw, H. E. Payne, & J. J. E. Hayes, 433

Savaglio, S., Glazebrook, K., & Le Borgne, D. 2009, Astroph. J., 691, 182

Savaglio, S., Rau, A., Greiner, J., et al. 2012, Mon. Not. R. Astron. Soc., 420, 627

Schady, P., Burrows, D. N., Cummings, J. R., et al. 2006, GRB Coordinates Network, 5699, 1

Schady, P., Krühler, T., Greiner, J., et al. 2015, Astron. Astroph., 579, A126

Schlegel, D. J., Finkbeiner, D. P., & Davis, M. 1998, Astroph. J., 500, 525

Schmidl, S., Kann, D. A., & Greiner, J. 2013, GRB Coordinates Network, 14655

Schulze, S., Chapman, R., Hjorth, J., et al. 2015, Astroph. J., 808, 73

Schulze, S., Klose, S., Björnsson, G., et al. 2011, Astron. Astroph., 526, A23

Schulze, S., Krühler, T., Leloudas, G., et al. 2016, ArXiv e-prints

Schulze, S., Malesani, D., Cucchiara, A., et al. 2014, Astron. Astroph., 566, A102

Siegel, M. H., Barthelmy, S. D., Burrows, D. N., et al. 2010, GRB Coordinates Network, Circular Service, 10916, 1 (2010), 916, 1

Silva, L., Granato, G. L., Bressan, A., & Danese, L. 1998, Astroph. J., 509, 103

Skiff, B. 2002, The Astronomer, 39, 215

Skrutskie, M. F., Cutri, R. M., Stiening, R., et al. 2006, Astron. J., 131, 1163
Soderberg, A. M., Berger, E., Kasliwal, M., et al. 2006, Astroph. J., 650, 261
Stanek, K. Z., Gnedin, O. Y., Beacom, J. F., et al. 2006, Acta Astron., 56, 333
Stanek, K. Z., Matheson, T., Garnavich, P. M., et al. 2003, Astroph. J. Lett., 591, L17
Stanway, E. R., Davies, L. J. M., & Levan, A. J. 2010, Mon. Not. R. Astron. Soc., 409, L74
Stanway, E. R., Levan, A. J., & Davies, L. J. M. 2014, Mon. Not. R. Astron. Soc., 444, 2133
Starling, R. L. C., Evans, P. A., & Immler, S. 2010, GRB Coordinates Network, 10941, 1
Stratta, G., D'Avanzo, P., Piranomonte, S., et al. 2007, Astron. Astroph., 474, 827
Suzuki, D., Omori, K., Hayashi, F., et al. 2010, GRB Coordinates Network, 10904, 1
Svensson, K. M., Levan, A. J., Tanvir, N. R., Fruchter, A. S., & Strolger, L.-G. 2010, Mon. Not. R. Astron. Soc., 405, 57
Tanaka, M. & Hotokezaka, K. 2013, Astroph. J., 775, 113
Tanvir, N. R., Levan, A. J., Fruchter, A. S., et al. 2012, Astroph. J., 754, 46
Tanvir, N. R., Levan, A. J., Fruchter, A. S., et al. 2013, Nature, 500, 547
Tanvir, N. R., Levan, A. J., Fruchter, A. S., et al. 2015, GRB Coordinates Network, 18100
Thöne, C. C., Campana, S., Lazzati, D., et al. 2011, Mon. Not. R. Astron. Soc., arXiv:1101.3488
Thöne, C. C., Christensen, L., Prochaska, J. X., et al. 2014, Mon. Not. R. Astron. Soc., 441, 2034
Thöne, C. C., Fynbo, J. P. U., Sollerman, J., et al. 2006, GRB Coordinates Network, 5161
Thöne, C. C., Wiersema, K., Ledoux, C., et al. 2008, Astron. Astroph., 489, 37
Tinney, C., Stathakis, R., Cannon, R., et al. 1998, IAU Circ., 6896, 3
Tody, D. 1993, ASP Conf. Ser., 52, 173
Tomsick, J. A., Bodaghee, A., Rodriguez, J., et al. 2012, Astroph. J. Lett., 750, L39
Troja, E., Page, K. L., Burrows, D. N., & Schady, P. 2006, GRB Coordinates Network, 5703, 1
Troja, E., Sakamoto, T., Cenko, S. B., et al. 2016, Astroph. J., 827, 102
Tunnicliffe, R. L., Levan, A. J., Tanvir, N. R., et al. 2014, Mon. Not. R. Astron. Soc., 437, 1495
Uhm, Z. L. & Zhang, B. 2016, Astroph. J., 825, 97
Ukwatta, T. N., Baumgartner, W. H., Chester, M. M., et al. 2008a, GRB Coordinates Network, 7203, 1
Ukwatta, T. N., Tueller, J., Mangano, V., et al. 2008b, GCN Report, 111, 1
Updike, A., Nardini, M., Afonso, P., et al. 2010, GRB Coordinates Network, 10910, 1
Urata, Y., Tashiro, M., Abe, K., et al. 2006, GRB Coordinates Network, 5717
Usov, V. V. 1992, Nature, 357, 472
Řípa, J., Mészáros, A., Veres, P., & Park, I. H. 2012, Astroph. J., 756, 44
van den Heuvel, E. P. J. & Portegies Zwart, S. F. 2013, Astroph. J., 779, 114
van der Horst, A. J., Kamble, A., Resmi, L., et al. 2008, Astron. Astroph., 480, 35
van Paradijs, J., Groot, P. J., Galama, T., et al. 1997, Nature, 386, 686
van Paradijs, J., Kouveliotou, C., & Wijers, R. A. M. J. 2000, Ann. Rev. Astron. Astroph., 38, 379
Varela, K., van Eerten, H., Greiner, J., et al. 2016, Astron. Astroph., 589, A37
Vergani, S. D. & Chassande-Mottin, E. 2015, in SF2A-2015: Proceedings of the Annual meeting of the French Society of Astronomy and Astrophysics, ed. F. Martins, S. Boissier, V. Buat, L. Cambrésy, & P. Petit, 253–256

Vergani, S. D., D'Avanzo, P., Levan, A. J., et al. 2010, GRB Coordinates Network, 10512
Vernet, J., Dekker, H., D'Odorico, S., et al. 2011, Astron. Astroph., 536, A105
Villasenor, J. S., Lamb, D. Q., Ricker, G. R., et al. 2005, Nature, 437, 855
Voss, R. & Tauris, T. M. 2003, Mon. Not. R. Astron. Soc., 342, 1169
Vrba, F. J., Hartmann, D. H., & Jennings, M. C. 1995, Astroph. J., 446, 115
Wiersema, K., Savaglio, S., Vreeswijk, P. M., et al. 2007, Astron. Astroph., 464, 529
Wilson, W. E., Ferris, R. H., Axtens, P., et al. 2011, Mon. Not. R. Astron. Soc., 416, 832
Wong, T.-W., Willems, B., & Kalogera, V. 2010, Astroph. J., 721, 1689
Woosley, S. E. 1993, Astroph. J., 405, 273
Woosley, S. E. & Bloom, J. S. 2006, Ann. Rev. Astron. Astroph., 44, 507
Woosley, S. E. & Heger, A. 2006, Astroph. J., 637, 914
Woosley, S. E. & Heger, A. 2012, Astroph. J., 752, 32
Wright, E. L., Eisenhardt, P. R. M., Mainzer, A. K., et al. 2010, Astron. J., 140, 1868
Xin, L., Liang, E., Wei, J., et al. 2010, Mon. Not. R. Astron. Soc., 1404
Xu, D., Levan, A. J., Tanvir, N. R., et al. 2013, GRB Coordinates Network, 14653
Yang, B., Jin, Z.-P., Li, X., et al. 2015, Nature Communications, 6, 7323
Yoon, S.-C. & Langer, N. 2005, Astron. Astroph., 443, 643
Zeh, A., Klose, S., & Hartmann, D. H. 2004, Astroph. J., 609, 952
Zeh, A., Klose, S., & Kann, D. A. 2006, Astroph. J., 637, 889
Zhang, B. & Mészáros, P. 2004, Int. J. Mod. Phys. A, 19, 2385
Zhang, W., Woosley, S. E., & Heger, A. 2004, Astroph. J., 608, 365
Zhang, Z., Xie, G. Z., Deng, J. G., & Jin, W. 2006, Mon. Not. R. Astron. Soc., 373, 729
Zvyagina, E. V. 1968, Soviet Astron., 12, 406

List of abbreviations

- *AB mags:* AB magnitude system
- *ACS:* Hubble Space Telescope, Advanced Camera for Surveys
- *ATCA:* Australia Telescope Compact Array
- *BACODINE:* BAtse COordinates DIstribution NEtwork (electronic system for GRB trigger data)
- *BAT:* Burst Alert Telescope (Swift satellite)
- *BATSE:* Burst And Transient Source Experiment
- *BeppoSAX:* Italian/Dutch satellite mission
- *BOOTES:* Burst Observer and Optical Transient Exploring System
- *CABB:* Compact Array Broadband Backend (CABB) correlator (ATCA radio telescope)
- *CGRO:* Compton Gamma-Ray Observatory
- *Fermi:* high-energy satellite (launched in 2008)
- *FRED:* fast rise and exponential decay (GRB profile)
- *GCN:* Gamma-ray Burst Coordinates Network (electronic GRB circulars)
- *GMRT:* Giant Metrewave Radio Telescope
- *GRASIL:* software package used to fit SEDs of galaxies from radio to the UV domain
- *GRB:* Gamma-Ray Burst; naming convention yy/mm/dd
- *GROND:* Gamma-Ray Burst Optical/Near-Infrared Detector
- *HETE:* High Energy Transient explorer (satellite)
- *HST:* Hubble Space Telescope
- *IPN:* Interplanetary Network
- *IRAF:* collection of software written at the National Optical Astronomy Observatory for the reduction of astronomical data
- *ISM:* interstellar medium
- *KAGRA:* Kamioka Gravitational Wave Detector
- *Le PHARE:* Photometric Analysis for Redshift Estimate
- *LIGO:* Laser Interferometer Gravitational Wave Observatory
- *Miriad:* Data analysis software for radio interferometry
- *MPE:* Max Planck Institute for Extraterrestrial Physics
- *MPG:* Max-Planck-Gesellschaft
- *MUSE:* Multi Unit Spectroscopic Explorer
- *NIR:* near infrared
- *NS:* neutron star
- *OT:* optical transient
- *PSF:* point spread function
- *PSR:* pulsating source of radio emission

- *RFI:* radio-frequency interference
- *SDSS:* Sloan Digital Sky Survey
- *SED:* spectral energy distribution ($F_\nu(\nu)$)
- *SFR:* star formation rate
- *SN:* supernova
- *sSFR:* specific star formation rate (SFR per stellar mass)
- *SVOM:* Space Variable Objects Monitor (planned satellite mission)
- *Swift:* GRB satellite, the name is not an acronym
- *T90:* the interval (burst duration) between the observed times where the measured gamma-ray fluence has reached 5% and 95% of its total fluence
- *TLS:* Thüringer Landessternwarte Tautenburg, Germany
- *TOUGH sample:* The Optically Unbiased GRB Host (GRB host galaxy survey)
- *UVOT:* Ultraviolet/Optical Telescope (Swift satellite)
- *UV:* ultraviolet
- *VIRGO:* European Laser Interferometer designed to detect gravitational waves
- *VLT:* Very Large Telescope (ESO, Chile, Paranal)
- *WISE:* Wide-field Infrared Survey Explorer (satellite)
- *WSRT:* Westerbork Synthesis Radio Telescope
- *XRT:* X-ray Telescope (Swift satellite)

Acknowledgements

I thank Prof. Dr. Artie P. Hatzes for giving me the opportunity to work on my PhD Thesis at the Thüringer Landessternwarte (TLS) Tautenburg, Germany.

I thank Prof. Dr. Katharina Schreyer, FSU Jena, for her advice during this work was done.

I thank my colleagues Dr. Andrea Rossi, Dr. David Alexander Kann, and Dipl.-Phys. Sebastian Schmidl for many useful discussions and general help. I thank Dr. Andrea Rossi for his excellent knowledge in *GROND* photometry and SED modelling of galaxies. In addition, I also thank the colleagues at the TLS for a friendly working atmosphere.

I thank the *GROND* team at MPE Garching, led by Dr. habil. J. Greiner, for a productive time together. In particular, I thank Dr. Thomas Krühler, MPE Garching, for valuable help in many aspects concerning the operation of *GROND* and the *GROND* data reduction.

I thank the staff at CSIRO in Sydney and in Narrabri, Australia, for their support in the operation of *ATCA*. In particular, I thank Prof. Dr. Sarah Maddison, Swinburne University (Australia) for helping me with *ATCA* remote observations in Lyon (France).

I thank the late Dr. Javier Gorosabel Urkía, IAA Granada (Spain) for working together in several GRB projects. I thank Dr. Rubén Sánchez Ramírez, IAA Granada (Spain) for helping me with 10-m GTC data reduction.

I am deeply indepted to Dr. Eliana Palazzi, INAF, Bologna (Italy), who explained me the secrets of FORS2 long-slit spectroscopy. I thank Dr. Steve Schulze, Universita Católica (Chile), for his help in python programming and FORS2 spectroscopy data reduction.

I thank Dr. Michal Michałowski, University of Edinburth (UK), and Prof. Dieter H. Hartmann, Clemson, Sc, USA, for very fruitful communications concerning several observing proposals and publications.

My special thank is devoted to Dr. habil. Sylvio Klose, TLS, for his continuous help during this work.

En lo personal, me gustaría terminar agradeciendo a mi familia y a mis amigos por todo su apoyo a lo largo de estos años en esta aventura del doctorado. Sin su ayuda este camino tan interesante hubiera sido mucho más áspero y adusto. En especial mi madre siempre positiva en sus mensajes y en sus consejos, animando cuando las dificultades llegaban.

Tautenburg, den 9. Oktober 2017 Ana Maria Nicuesa Guelbenzu

Ehrenwörtliche Erklärung

Ich erkläre hiermit ehrenwörtlich, dass ich die vorliegende Arbeit selbstständig, ohne unzulässige Hilfe Dritter und ohne Benutzung anderer als der angegebenen Hilfsmittel und Literatur angefertigt habe. Die aus anderen Quellen direkt oder indirekt übernommenen Daten und Konzepte sind unter Angabe der Quelle gekennzeichnet.

Bei der Auswahl und Auswertung folgenden Materials haben mir die nachstehend aufgeführten Personen in der jeweils beschriebenen Weise unentgeltlich geholfen:

- Dr. Sylvio Klose in der Erstellung von Abb. 1.2, 2.3, 5.1, und in der Berechnung der Wahrscheinlichkeiten gemäß Eq. (1.1)
- Dr. Mark Wieringa, Australia Telescope National Facility, CSIRO, Sydney, Australia, in der Auswertung der *ATCA*-Daten zu GRB 050709
- Dipl.-Phys. Sebastian Schmidl für die Erstellung der Abb. 1.4
- Dr. Steve Schulze in der Erstellung von Abb. 3.9 via Python
- Dr. Andrea Rossi und Dr. Thomas Krühler für die Installation der GROND data analysis software auf meinen Arbeitscomputern
- Prof. Dr. K. Schreyer und Prof. Dr. A. P. Hatzes für eine Durchsicht des finalen Manuskripts dieser Arbeit

Weitere Personen waren an der inhaltlich-materiellen Erstellung der vorliegenden Arbeit nicht beteiligt. Insbesondere habe ich hierfür nicht die entgeltliche Hilfe von Vermittlungs- bzw. Beratungsdiensten (Promotionsberater oder andere Personen) in Anspruch genommen.

Niemand hat von mir unmittelbar oder mittelbar geldwerte Leistungen für Arbeiten erhalten, die im Zusammenhang mit dem Inhalt der vorgelegten Dissertation stehen.

Diese Arbeit wurde bisher weder im In- noch im Ausland in gleicher oder ähnlicher Form einer anderen Prüfungsbehörde vorgelegt.

Die geltende Promotionsordnung der Physikalisch-Astronomischen Fakultät der Friedrich-Schiller-Universität Jena ist mir bekannt.

Ich versichere ehrenwörtlich, dass ich nach bestem Wissen die reine Wahrheit gesagt und nichts verschwiegen habe.

Tautenburg, den 9. Oktober 2017 Ana Maria Nicuesa Guelbenzu